2019•2020

Faculteit Industriële ingenieurswetenschappen

master in de industriële wetenschappen: elektromechanica

Masterthesis

Design and development of printed, stretchable antennas for 3D integration

PROMOTOR :

Prof. dr. ir. Wim DEFERME

BEGELEIDER :

De heer Indranil BASAK

Jan Claes, Ivo Dekker

Scriptie ingediend tot het behalen van de graad van master in de industriële wetenschappen: elektromechanica

Gezamenlijke opleiding UHasselt en KU Leuven

2019•2020

Faculteit Industriële ingenieurswetenschappen

master in de industriële wetenschappen: elektromechanica

Masterthesis

Design and development of printed, stretchable antennas for 3D integration

PROMOTOR :

Prof. dr. ir. Wim DEFERME

BEGELEIDER :

De heer Indranil BASAK

Jan Claes, Ivo Dekker

Scriptie ingediend tot het behalen van de graad van master in de industriële wetenschappen: elektromechanica

UHASSELT KU LEUVEN

Deze masterproef werd geschreven tijdens de COVID-19 crisis in 2020. Deze wereldwijde gezondheidscrisis heeft mogelijk een impact gehad op de opdracht, de onderzoekshandelingen en de onderzoeksresultaten.

Preface

Dear Reader
The thesis *Design and development of printed stretchable antennas for 3D integration* presented to you here, is the result of months of research within the framework of the master's thesis. It also forms the final part of the four-year course in Engineering Technology at UHasselt and KULeuven.

The set-up of this master's thesis was created by a request from Fremach, a company specialized in the injection moulding of car interiors. The question was whether it was possible to obtain a working antenna by printing it and vacuum or thermoforming it on a 3D object, such as car interiors. This seemed a very challenging but interesting question to investigate. Our shared interest in design and materials science strengthened our motivation even more. An obstacle in this research was our limited knowledge about antenna systems. Their complex shapes, working and properties took us several days of work to understand just the basics.

However, this master's thesis did not come about by us alone. We have received a lot of advice and assistance from a few people. We would like to thank them for the influence they had on this result. First of all, we would like to thank Prof. Dr. Ir. Deferme. He gave us the opportunity to investigate a subject where the question specifically came from the industry, what makes it an interesting experience for future industrial engineers. Furthermore, the countless times that he advised us on the approach and communication involved in carrying out such a project has led us to grow as engineers.

Our thanks also go to Indranil Basak and Ing. Jarne Machiels. Both always assisted us in the lab and during our trials with practical tips and inspired us with ideas for our research. Their contribution has helped shape this master's thesis into what it is now.

A special thanks goes out to Prof. Dr. Ir. Sam Lemey and Ir. Igor Lima de Paula from the university of Ghent for giving us the much needed information on measurement and design of antennas. Because of our limited knowledge on this subject, this part of the thesis would have been a lot harder without their help. Furthermore, we would like to thank Dr. Ir. John Bijnens for giving us extra knowledge on the process of virtual testing using finite element analyses.

Jan Claes & Ivo Dekker

Table of contents

Preface ... 3
List of tables ... 9
List of figures ... 11
Abstract ... 13
Abstract in Dutch ... 15

1 **Introduction** ... 17
1.1 Problem statement ... 18
1.2 Requirements ... 19
1.3 Materials and methods ... 19
1.4 Content and structure ... 20

2 **Literature study** ... 21
2.1 Introduction ... 21
2.2 Stretchable Electronic Structures ... 21
2.2.1 Buckling structures ... 22
2.2.2 Percolating structures ... 23
2.2.3 2D serpentine interconnects ... 24
2.3 Materials ... 25
2.3.1 Substrates ... 25
2.3.2 Inks ... 26
2.3.3 Manufacturers ... 27
2.4 Printing techniques ... 29
2.4.1 Screen printing ... 29
2.4.2 Inkjet printing ... 30
2.5 Shaping process ... 32
2.6 Applications ... 34
2.6.1 Haptic Feedback in structural electronics ... 34
2.6.2 Antennas in structural electronics ... 37
2.7 Discussion ... 41

3 **Antenna theory** ... 43
3.1 Overview of Antenna parameters ... 43
3.2 Inset fed patch antenna ... 46
3.2.1 Design ... 46
3.2.2 Theory and remarks ... 47
3.3 Dipole antenna ... 48

3.3.1 Design ... 48
3.3.2 Theory and remarks ... 49
3.4 RFID antenna ... 50
3.4.1 Design ... 50
3.4.2 Theory and remarks ... 51
3.5 Connectors ... 52
3.6 Conclusion ... 52

4 **Antenna development steps** ... 55
4.1 Determine antenna design ... 55
4.2 Determine the choice of materials ... 58
4.2.1 Wettability of substrate ... 58
4.2.2 Structure of ink particles ... 61
4.3 Determine pre-stretch shape ... 62
4.3.1 Physical test ... 63
4.3.2 Virtual test ... 63
4.4 Final characterisation ... 64
4.4.1 Reflection coefficient characterization ... 64
4.4.2 Efficiency, gain and radiation pattern measurement. ... 65
4.5 Conclusion ... 67

5 **Material configuration for stretchable antenna development** ... 69
5.1 Influence of ink and substrate on resistance without elongation ... 69
5.1.1 Influence of the substrate on the resistivity of the RFID with silver inks ... 71
5.1.2 Influence of the number of layers on the resistivity of the RFID with silver inks ... 75
5.1.3 PEDOT:PSS printed RFID ... 76
5.2 Influence of ink and substrate on the resistance under elongation ... 77
5.3 Conclusion ... 79

6 **Antenna simulation in Sonnet Lite** ... 81
6.1 Simulation setup ... 82
6.1.1 Inset fed patch antenna ... 82
6.1.2 RFID antenna ... 93
6.2 Inset fed patch antenna simulations ... 99
6.2.1 Elongation in vertical direction ... 99
6.2.2 Elongation in horizontal direction ... 104
6.2.3 Elongation in both directions ... 109
6.3 RFID antenna simulations ... 113
6.3.1 Elongation in vertical direction ... 114

6.3.2 Elongation in horizontal direction 116
6.3.3 Elongation in both directions 119
6.4 Conclusion 121

7 **Conclusion** 124
Bibliography 126

List of tables

Table 1: Properties of common polymer materials 39
Table 2: Non-resonant antenna dimensions in mm 40
Table 3: Dimensions inset fed patch antenna 46
Table 4: Dimensions dipole antenna 48
Table 5: Resistance ME602 RFID on different substrates 71
Table 6: Resistance of Orgacon ink on different substrates 73
Table 7: Resistance of ME602 on TPU1 with multiple layers 75
Table 8: Sheet resistance in function of elongation of ME602 on TPU1 77
Table 9: sheet resistance in function of elongation of ME602 on TPU2 78
Table 10: Average values of important dielectric parameters of TPU 81
Table 11: values of important dielectric parameters of PET as given by Sonnet 81
Table 12: Influence of ink layer thickness on inset fed patch 82
Table 13: Varying substrate thickness on resonant frequency and reflected power on TPU for patch 83
Table 14: Varying substrate thickness on resonant frequency and reflected power on PET for patch 85
Table 15: Influence of conductivity of ink on TPU for patch 87
Table 16: Influence of conductivity of ink on PET for patch 88
Table 17: Influence of ink layer thickness on RFID 93
Table 18: Varying substrate thickness on resonant frequency and reflected power on TPU for RFID 95
Table 19: Varying substrate thickness on resonant frequency and reflected power on PET for RFID 96
Table 20: Influence of conductivity of ink on TPU for RFID 97
Table 21: Influence of conductivity of ink on PET for RFID 97
Table 22: New dimensions of inset fed patch after vertical elongation in mm on TPU 99
Table 23: New dimensions of inset fed patch after vertical elongation in mm on PET 100
Table 24: Results of vertical elongation simulations from 0 % to 30 % on TPU 100
Table 25: Results of vertical elongation simulations from 0 % to 30 % on PET 103
Table 26: New dimensions of inset fed patch after horizontal elongation in mm on TPU 105
Table 27: New dimensions of inset fed patch after horizontal elongation in mm on PET 105
Table 28: Results of horizontal elongation simulations from 0 % to 30 % on TPU 106
Table 29: Results of horizontal elongation simulations from 0 % to 30 % on PET 108
Table 30: New dimensions of inset fed patch after elongation in both directions on TPU and PET 110
Table 31: Results of elongation in both directions simulations from 0 % to 30 % on TPU 110
Table 32: Results of elongation in both directions simulations from 0 % to 30 % on PET 112
Table 33: New dimensions of RFID after vertical elongation in mm on TPU 114
Table 34: Results of vertical elongation simulations from 0 % to 30 % on TPU for RFID 115
Table 35: Results of 2,054 Ω/sq at 0 % and 25 % vertical elongation for RFID 115
Table 36: New dimensions of RFID after horizontal elongation in mm on TPU 117
Table 37: Results of horizontal elongation simulations from 0 % to 30 % on TPU for RFID 117
Table 38: Results of 2,054 Ω/sq at 0 % and 25 % horizontal elongation for RFID 118
Table 39: New dimensions of RFID after elongation in both directions in mm on TPU 119
Table 40: Results of elongation in both directions from 0 % to 30 % on TPU for RFID 119

List of figures

Figure 1: Visual example stretchable electronics 17
Figure 2: Example of control panel in a car 18
Figure 3: Order and construction of the literature study 21
Figure 4: Buckling structures 23
Figure 5: Percolating structures 23
Figure 6: Serpentine structures 24
Figure 7: Schematic depiction of screen printing 29
Figure 8: Simplified schematic of inkjet printing 30
Figure 9: Schematic representation of thermoforming/vacuum forming 32
Figure 10: Schematic representation of thermoforming 32
Figure 11: Working principle DEA 35
Figure 12: Squeeze film effect 35
Figure 13: Squeeze film effect on small and large radius curves 36
Figure 14: Schematics of piezoelectric actuator 37
Figure 15: Pifa antenna 38
Figure 16: Dipole antenna 38
Figure 17: Non-resonant antenna design 40
Figure 18: 2D and 3D plot of the radiation pattern of a dipole antenna 44
Figure 19: Example of reflection coefficient measurement 44
Figure 20: Antenna impedance network 45
Figure 21: Inset fed patch antenna design 46
Figure 22: Inset fed patch antenna design with ground plane on back 47
Figure 23: Inset fed patch antenna design with surrounding ground plane 48
Figure 24: Dipole antenna design 48
Figure 25: Dipole with a balun and a mirrored signal in the lugs inspired by 49
Figure 26: TV with rabbit ears 49
Figure 27: NOKIA 6110 with monopole antenna 50
Figure 28: The monopole is a dipole with one side connected to the ground 50
Figure 29: Paperonics RFID antenna L18_2 51
Figure 30: Example of an impedance measurement on an RFID tag 51
Figure 31: SMA and UFL connector 52
Figure 32: mesh out of triangular or quadrialteral elements and a combination of both 56
Figure 33: user interface of CST Microwave Studio 57
Figure 34: User-interface of Ansys HFSS 57
Figure 35: User-interface of Sonnet Lite 57
Figure 36: Schematic representation wettability 58
Figure 37: Schematic representation of corona treatment 59
Figure 38: Real life example of corona treatment 1 60
Figure 39: Real life example of corona treatment 2 60
Figure 40: SEM image of silver nano-particles 61
Figure 41: SEM image of silver micro flakes 62
Figure 42: SEM images of PEDOT:PSS 62
Figure 43: Principle of deforming mesh 63
Figure 44: Example of a network analyzer by siglent 65
Figure 45: radiation pattern of a dipole antenna 66
Figure 46: Example of the inside of an anechoic chamber 67
Figure 47: Silver micro flake RFID antenna 69
Figure 48: Upper row TPU1, TPU2, TPU3, Lower row TPU4, TPU5, PET 70
Figure 49: Mean resistance for ME602 single layer on different substrate materials 72
Figure 50: Crack formation on conductive paths; Orgacon ink on TPU1 73
Figure 51: Crack formation on conductive paths; Orgacon ink on TPU5 74
Figure 52: Mean resistance of ME602 on TPU1 with multiple printing layers 75
Figure 53: PEDOT:PSS RFID antenna 76
Figure 54: Left: unstretched right: 30 % stretched patch antenna 77

Figure 55: Average sheet resistance in function of elongation of ME602 on TPU1 78
Figure 56: Average sheet resistance in function of elongation of ME602 on TPU2 79
Figure 57: Mesh of inset fed patch design in Sonnet 82
Figure 58: S11 in function of frequency for a 5 µm ink layer and 100 µm dielectric layer for patch 83
Figure 59: Resonant frequency in function of substrate thickness on TPU for patch 84
Figure 60: Reflected power in function of the substrate thickness on TPU for patch 84
Figure 61: Resonant frequency in function of substrate thickness on PET for patch 85
Figure 62: Reflected power in function of substrate thickness on PET for patch 86
Figure 63: Resonant frequency in function of the sheet resistance on TPU for patch 87
Figure 64: Reflected power in function of the sheet resistance on TPU for patch 88
Figure 65: Resonant frequency in function of sheet resistance on PET for patch 89
Figure 66: Reflected power in function of sheet resistance on PET for patch 89
Figure 67: S11 in function of the frequency for a PEDOT:PSS inkjet ink for patch 90
Figure 68: S11 in function of the frequency for PEDOT:PSS DuPont ME801 for patch 90
Figure 69: Stress-Strain characteristic of Elastollan C88 A TPU 91
Figure 70: (a) Vertical elongation of inset fed patch (b) Horizontal elongation of inset fed patch 92
Figure 71: Reworked RFID antenna design in sonnet lite 93
Figure 72: S11 in function of frequency for a 5 µm ink layer and 200 µm dielectric layer for RFID 94
Figure 73: S11(blue) and VSWR(pink) for RFID antenna with a 400 µm substrate layer 94
Figure 74: Resonant frequency in function of substrate thickness on TPU for RFID 95
Figure 75: Reflected power in function of substrate thickness on TPU for RFID 96
Figure 76: S11 in function of the frequency for a PEDOT:PSS inkjet ink for RFID 98
Figure 77: Inset fed patch antenna at (a) 0 % vertical elongation (b) 30 % vertical elongation 99
Figure 78: S11 and VSWR in function of the frequency for vertical elongation on TPU 101
Figure 79: Resonant frequency in function of vertical elongation on TPU 102
Figure 80: VSWR in function of vertical elongation on TPU 102
Figure 81: S11 and VSWR in function of the frequency for vertical elongation on PET 103
Figure 82: Resonant frequency in function of vertical elongation on PET 104
Figure 83: VSWR in function of vertical elongation on PET 104
Figure 84: Inset fed patch antenna at (a) 0 % horizontal elongation (b) 30 % horizontal elongation 105
Figure 85: S11 and VSWR in function of the frequency for horizontal elongation on TPU 106
Figure 86: Resonant frequency in function of horizontal elongation on TPU 107
Figure 87: VSWR in function of horizontal elongation on TPU 107
Figure 88: S11 and VSWR in function of the frequency for horizontal elongation on PET 108
Figure 89: Resonant frequency in function of horizontal elongation on PET 109
Figure 90: VSWR in function of horizontal elongation on PET 109
Figure 91: S11 and VSWR in function of the frequency for elongation in both directions on TPU 110
Figure 92: Resonant frequency in function of elongation in both directions on TPU 111
Figure 93: VSWR in function of elongation in both directions on TPU 111
Figure 94: S11 and VSWR in function of the frequency for elongation in both directions on PET 112
Figure 95: Resonant frequency in function of elongation in both directions on PET for patch 113
Figure 96: VSWR in function of elongation in both directions on PET for patch 113
Figure 97: RFID antenna at (a) 0 % vertical elongation (b) 30 % vertical elongation 114
Figure 98: S11 and VSWR in function of the frequency for vertical elongation on TPU for RFID 115
Figure 99: RFID antenna at (a) 0 % horizontal elongation (b) 30 % horizontal elongation 116
Figure 100: S11 and VSWR in function of the frequency for elongation on TPU for RFID 118
Figure 101: S11 and VSWR in function of frequency with 2,054 Ω/sq for RFID 118
Figure 102: S11 and VSWR in function of the frequency for elongation on TPU for RFID 120

Abstract

Printable, stretchable electronics show an increasing importance over traditional electronics as they can be formed and shaped over an existing surface using thermo and vacuum forming techniques. This master's thesis researches the possibility of stretchable, printed antenna applications in collaboration with Fremach and IMO-IMOMEC. The goal is to see how antennas produced from different material combinations react when deformed, and for how long they remain functional.

To achieve this, PEDOT:PSS, silver micro flakes and nanoparticle inks are applied on TPU and PET substrates using screen and inkjet printing. Three different antenna designs are subject to research: an inset fed patch, a dipole and an RFID antenna. Resistivity measurements and antenna simulations (using *Sonnet Lite)* are performed at different levels of stretch to study how elongation affects the antennas' behaviour.

The silver micro flake ink shows great potential on TPU with 0,3 and 2,1 Ω/sq for 0 to 25 % of stretch respectively. Using the proposed inset fed patch design, the optimal TPU thickness was found to be 320 µm. The antenna remains functional from 0 to 20 % of horizontal and 0 to 10 % of vertical elongation. For PET, the optimal thickness was determined to be 170 µm. However, the antenna appears to be non-functional at 10 % of horizontal or 5 % of vertical elongation. The RFID antenna is not affected by elongation, only by its sheet resistance.

Abstract in Dutch

Printbare, rekbare elektronica wordt alsmaar belangrijker ten opzichte van traditionele elektronica doordat ze over bestaande oppervlakten gevormd kunnen worden met thermo- en vacuümformtechnieken. Deze masterproef onderzoekt de mogelijkheid van rekbare, printbare antenneapplicaties in samenwerking met Fremach en IMO-IMOMEC. Het doel is te analyseren hoe de antennes gemaakt met verschillende materiaalcombinaties reageren als ze vervormd worden, en hoelang ze functioneel blijven.

Dit gebeurt door het verschil bij gebruik van PEDOT:PSS, zilver micro flakes en zilver nano-particle inkten op TPU en PET substraten gebruik makend van screen- en inkjetprinten te analyseren. Drie antennedesigns worden voorgesteld: een inset fed patch,.dipole en RFID antenne. Door hierop weerstandsmetingen en antennesimulaties (in *Sonnet Lite)* uit te voeren bij verschillende rekhoeveelheden, wordt het gedrag bestudeerd.

Zilver micro flake inkt toont groot potentieel op TPU met 0,3 en 2,1 Ω/sq van 0 tot 25 % rek respectievelijk. Bij simulaties met de voorgestelde inset fed patch antenne wordt een optimale TPU dikte van 320 µm gevonden. De antenne blijft functioneel van 0 tot 20 % horizontale en van 0 tot 10 % verticale rek. Voor PET is een optimale dikte van 170 µm gevonden. Echter blijkt de antenne bij 10 % horizontale en 5 % verticale rek al niet meer functioneel te zijn. De RFID antenne wordt niet beïnvloed door vervorming, maar enkel door de weerstand.

1 Introduction

This master's thesis will be focused on research into the practical use of printed stretchable antennas in 3D applications. This is an application of stretchable electronics. Stretchable electronics are conductive circuits that can be bended and (slightly) stretched. This has the advantage that the electronics do not have to be on a straight surface. Printing these kinds of electronics directly onto a curved object is difficult, therefore the printing is done on a flat substrate material which can be wrapped around the desired object later. However, there are multiple possible materials that can be used as ink and as a substrate. Furthermore, there are a couple of different printing techniques to apply the ink onto the substrate material. The goal of this study is to find out which combination is the most effective to produce an antenna system using this technology. Figure 1 shows an example of an electronic stretchable circuit.

Figure 1: Visual example stretchable electronics [1]

Stretchable electronics could be used in various fields of application. There are many companies that are looking for a method to implement this technology in their products as this could be added value for their product. The biomedical sector is looking for practical implementations on post-operative bandages to check the healing of a wound for example. In the textile sector, they are looking for printed solar cells and heart rhythm visualization on t-shirts. A last example can be found in the development of flexible displays, also the electronics herein must be flexible. All these examples have a common need. When the goal is to transfer data from or to the application (for example a Bluetooth antenna in a curved dashboard), an antenna that is also flexible and stretchable is required.

The research will be done in collaboration with Fremach, a company focused on injection molded parts for the automotive industry like dashboard and interior control panels. For this industry and Fremach, the technology is interesting as electronics (and specifically antennas) could possibly be attached to complex parts directly in the molding process and thereby eliminating an additional step of applying the film on the object. This ensures an optimized production process. Furthermore, Fremach hopes to gain additional knowledge about printed stretchable haptic feedback and antenna applications. They are specifically interested in what should be taken into account when developing and implementing this in their production process.

1.1 Problem statement

While research into stretchable antennas is making great progress, it remains unclear how these can be developed and which design aspects should be taken into account. A great deal of knowledge has already been acquired on substrates and printable conductive inks that are suitable for making antennas. However, the question which combination of substrates, conductive inks, printing techniques and designs result in the best combination remains. This taking into account the application in which it is to be implemented.

An example of the industrial sector can be found at Fremach: To open a storage space or to control the settings of the car, a button or lever and antenna is often required. This sometimes disturbs the appearance of the interior, or has less aesthetic value than a continuously smooth surface. An internally mounted sensor and antenna that takes up as little space as possible and follows the curved surfaces of the interior would offer added value. Not only the aesthetics are important. The current way in which the electronics are mounted requires a lot of time, which increases the production cost. Another problem with the current electronics is that buttons and cabling are relatively heavy and take up a lot of space. This increases the fuel consumption of cars and limits the manufacturer's design. A research of IDtechex [2] explains that in-mold electronics can save up to 70 % in weight on the electronics. Furthermore, this new method could be 30 % cheaper and reduce the assembly time by 40 %.

Fremach already developed touch sensors and sliders. However, it is more difficult to develop haptic systems and antennas with this technology. For example, a haptic system needs an actuator to produce feedback to the user. For antennas it is important that the antenna parameters have their desired values after the antenna is formed over the object. This difficulty means that it is unclear to Fremach how they should approach the development of a haptic feedback system or antenna system, what influencing factors are involved and what materials are suitable.

Figure 2 shows an example of the implementation of touch sensors and lighting in the interior of a car, made with in-molded stretchable electronics.

Figure 2: Example of control panel in a car [3]

1.2 Requirements

The purpose of this thesis is to research the antenna development process and the behaviour of different antennas under elongation. In this research, only silver based and PEDOT:PSS inks will be used. These will be printed using screen printing and inkjet printing. Fremach obtained the best results with screen printing in the past and they would like to continue with this, but inkjet printing can be useful because of its shorter changeover time as it only requires a digital drawing. The process can therefore be adjusted very easily and quickly. An adjustment in screen printing is much more difficult as when the design changes, a new screen has to be purchased. This can take up to several weeks.

For Fremach, both an antenna or a haptic feedback application is interesting to investigate. In the case of an antenna, the objective is to obtain a working antenna even after it has been thermoformed. The bandwidth is defined by the type of antenna application. Fremach does not consider it important which frequency or antenna is tested. As the usefulness for the industry is central, it is stated that the frequencies should be between the High-Frequency range and C-band of the electromagnetic spectrum because these are often used in automotive applications. This comes down to 3 MHz to 8 GHz. The dimensions are subordinate but the aim is to be as small as possible. The requirements for a haptic feedback system are that the actuator must produce a minimum of 0,5 g acceleration and must be able to deliver a force of 2 N, so that it can be sufficiently detected by a human being. After a literature study and a consultation with Fremach, it was ultimately decided that the focus of this thesis would be put on antennas.

This research has to show how the substrate and ink materials can be determined for a specific antenna design. It must also show how the antennas behaviour changes and if it continues to work after deformation. Furthermore, the most important steps and choices that occur in the development process should be indicated so that Fremach has a basis on which they can further develop the application.

1.3 Materials and methods

The first step is a literature study. The aim is to gain insight and knowledge about the various sub-topics involved in the practical implementation of stretchable electronics and the development of antennas. the literature study is divided into four stages: first, structural electronics and more specifically, how they can be implemented and shaped will be discussed. In-mold techniques are very interesting for this. After this, possible or commonly used materials and printing techniques that are utilised in this research will be investigated.

The printing technique will influence the choice of ink. This is the logical next step in the literature study. Finally, applications for these stretchable electronics will be examined. Specific focus will be on the development of an antenna or a haptic feedback system with all the information gathered previously.

After the literature review, the information and development methods found are discussed with Fremach to discuss which application will eventually be further developed and would be the most useful for them. Then, these methods are tested in a practical study. This means that prototypes are made using various inks and substrates. Thereafter, tests are carried out on the conductivity, elasticity, and comparison of the used materials. Data acquired from these tests can then be utilised for virtual testing in *Sonnet Lite* to study the behaviour of the antennas.

For the tests, the screen printers that are available in the lab and screens, produced by Meka screen will be used. The used inks will be also already available in the lab, supplemented with inks from the DuPont range (as Fremach works with these). The substrate materials will be provided by *grafityp,* a company which is involved in other projects at the IMO-IMOMEC.

1.4 Content and structure

This thesis is structured as follows: chapter 2 shows the literature study, then Chapter 3 provides more specific information on antennas that may be useful in the development of stretchable and printable antennas. Thereafter chapter 4 discusses a theoretical step-by-step plan if Fremach wants to develop a stretchable antenna itself and what the stumbling blocks would be. Chapter 5 gives the results of some practical tests on material configuration. Next, simulations are performed on the antennas in chapter 6. Finally, chapter 7 gives a summary of the entire thesis.

2 Literature study

2.1 Introduction

Structural electronics involves implementing electric circuitry into or onto regular structures. By doing this, computing and energy transferring components can be integrated into load bearing structures. Not only does this make objects more intelligent and aesthetically pleasing as the electrical components are removed from the consumer's view, it also reduces material cost as space that was originally purely structural can now be used to transfer and compute data or electricity [4].

The focus of this literature study is only on the design of printable electronics. As Fremach showed interest in both haptic feedback and antenna applications, both will be looked at to see which one will be the focus of the thesis. At the end, the antenna system was chosen in collaboration with Fremach.

This literature study is structured according to the sequence of processes to design in-mold printable electronics. First, ways to give printed electronics stretchable properties are discussed. Next, the in-mold production technique is described. This is followed by an investigation of the materials involved in the printing of electronics, in which a distinction is made between the materials that can be used as inks and those that can serve as carriers or substrates for these inks. The ways to print are discussed in chapter 2.4. Here, the principle of inkjet printing and screen printing is explained. Finally, the haptic feedback and antenna applications will be discussed. Figure 3 shows the construction of the literature study in a schematic form.

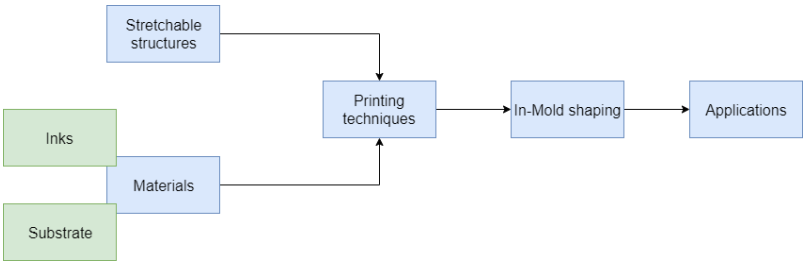

Figure 3: Order and construction of the literature study

2.2 Stretchable Electronic Structures

Traditional additive manufacturing and prototyping techniques fill in the need for quick manufacturing to test a form or fit of a piece, but are lacking for applications where complex electronics systems need to be implemented [5]. These still need to be bread boarded, bug tested and implemented. This can take up to weeks or even months of testing. Traditional automated printing electronics processes operate on the assumption of a predefined, flat 2D surface. According to [5], 3D printed designs have been performed manually. Stretchable electronics could be the answer for these 3D implementations, as the circuitry could be printed in 2D as it is being done already, and later applied over the desired 3D object without the need of manual 3D design of the electronics in CAD software. but as stated, it is important that the electronics are elastic so that they are not damaged during the forming process.

Making electronics stretchable can be achieved in two different ways. The first is by making stretchable structures like buckling structures, percolating networks, arc shaped interconnects and serpentine shaped interconnects [6]. The second approach consists of using novel materials that are inherently stretchable.

Any material can be somewhat flexible when it is sufficiently thin. When in this form they are not inherently stretchable however. Stretchability can be achieved by creating structures that allow the flexibility of the thin materials to be 'converted' into stretching. These structures are generally described as wavy patterns, like arc or serpentine interconnects or mesh shapes.

2.2.1 Buckling structures

One of the most common ways to create a 'wavy' or buckling structure is by pre stretching the substrate, coating it and then releasing the strain [6]. When released, highly periodic structures with well-defined wavelengths will be formed (Figure 4). The achieved wavelength and amplitude is linear with the thickness of the coating and relies on the material properties of the coating and the applied pre-strain. The wavelength can be defined with the following formula:

$$\lambda_0 = 2\pi h_f \left[\bar{E}_f / (3\bar{E}_s) \right]^{1/3} \tag{1}$$

With

$$\bar{E}_s = E_s / \left(1 - \nu_s^2\right) \tag{2}$$

The amplitude can be expressed by:

$$A_0 = h_f \sqrt{\frac{\varepsilon_{pre}}{\varepsilon_c} - 1} \tag{3}$$

with ε_c the buckling strain or the minimal strain to induce the buckling effect

$$\varepsilon_c = \frac{1}{4}\left(\frac{3\bar{E}_s}{\bar{E}_f} \right)^{2/3} \tag{4}$$

Both the wavelength and the amplitude of the wave can be augmented by applying more strain:

$$\lambda = \lambda_0 / \left[\left(1 + \varepsilon_{pre}\right)\left(1 + \xi\right)^{1/3} \right] \tag{5}$$

$$A = A_0 / \left[\left(\sqrt{1 + \varepsilon_{pre}}\right)\left(1 + \xi\right)^{1/3} \right] \tag{6}$$

with

$$\xi = \frac{5}{32}\varepsilon_{pre}\left(1 + \varepsilon_{pre}\right) \tag{7}$$

This kind of structure is similar to the working of an accordion. When a stretching or compressing strain is induced the wavelength and amplitude of the waveshape change, involving high strain in the substrate but not in the conductive layer itself. This gives a highly stretchable structure that doesn't lose its conductivity when stretched. This shape can further be expanded by applying a biaxial pre-strain, creating a herringbone structure when released. The herringbone enables stretching in both directions.
This technique comes with its downsides too. As the generated waves are a 3D structure, the surface roughness of the object is generally high. furthermore, the adhesion of the ink to the substrate is poor, meaning the object has poor durability.

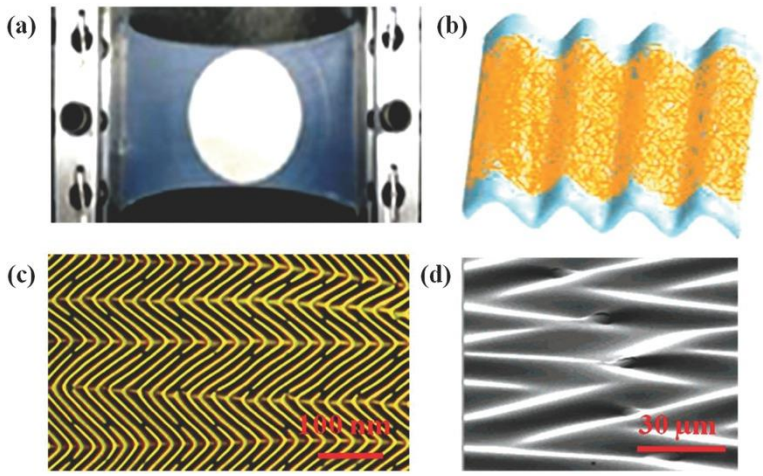

Figure 4: Buckling structures [6, p. 3]

2.2.2 Percolating structures

Electrodes which are made of percolating structures are created by depositing a conductive ink onto a substrate with a pre-strain applied. The ink consists of small conductive particles such as nanowires, microsheets or other nano-particles. This results in a conductive path because the nanostructures overlap with each other (Figure 5). When the object is stretched, the particles in the percolating structure are able to reconfigure and slightly move or hinge over each other without breaking connection. This results in a reconfigurable, conductive path. First [6], the ink is placed on top of a glass substrate making sure the network is fully interconnecting. Next, a polymer top layer is applied over the network and cured. When fully cured the film is peeled off of the glass substrate. The stretchability of these electrodes is highly dependent on the level of the entangled particles to reconfigure themselves to accommodate the applied strain.

Films made using this technique achieve lower stretchability than the films made using the buckling wave technique, but have higher adhesion resulting in high durability. These films also show very low surface roughness because the conductive particles are imbedded inside the polymer substrate, instead of lying on top of it.

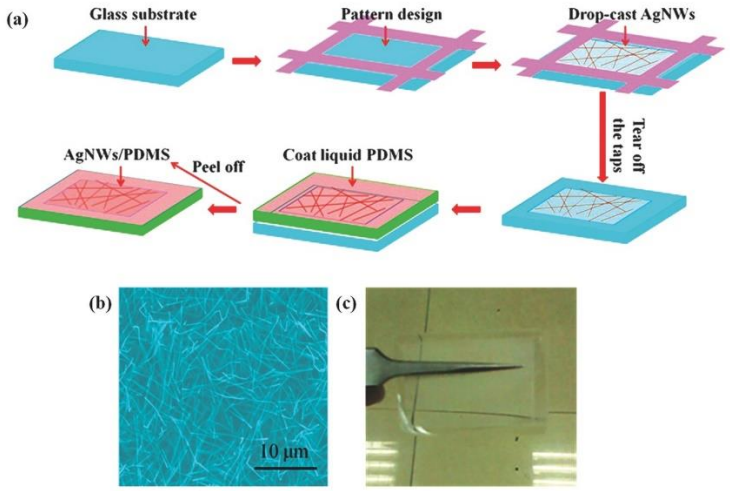

Figure 5: Percolating structures [6, p. 4]

2.2.3 2D serpentine interconnects

2D serpentine interconnects means that the interconnects are printed on the substrate with in a wavelike pattern with a specific amplitude to wavelength ratio (Figure 6) [6]. When stretched or compressed, these interconnects react like a spring. The level of stretchability is correlated to the amplitude-wavelength ratio, with higher ratios generally resulting in higher levels of stretchability. Where the buckling shape accommodates applied strain by shifting out of plane, these patterns undergo in-plane amplitude and wavelength changes. When strain is applied, the wavelength increases while the amplitude decreases until the wire is fully stretched. The opposite reaction occurs when the structure is compressed.

[7] states that the maximum achievable strain is 50 % for a gold pattern with a linewidth and line thickness of 5 µm, The amplitude in this experiment was 40 µm while the “period” or wavelength was 80 µm. Further writes [7] that it is also possible to print extra waves in a "wave" of the serpentine, this results in a fractal shape and can stretch higher.

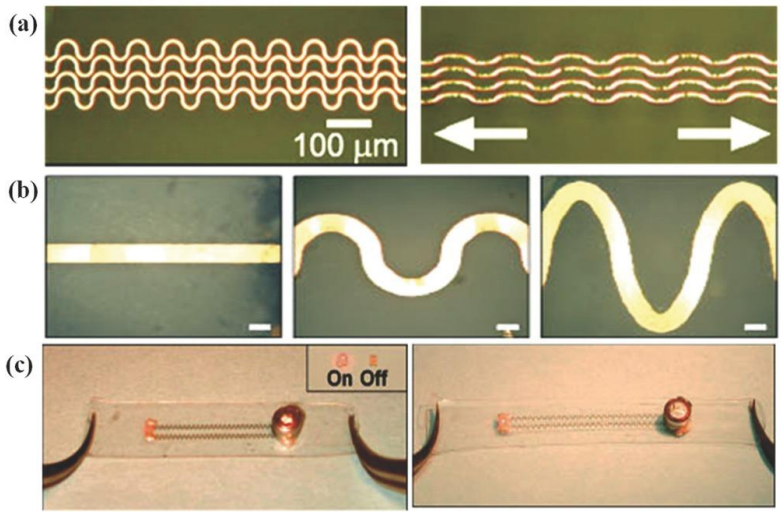

Figure 6: Serpentine structures [6, p. 5]

2.3 Materials

When looking into the design of printed electronics, the material selection for the used inks and substrates is an important element. Different materials have different properties that determine the printing techniques that can be used, the mechanical design and the electrical and mechanical properties of the components. First, different substrate materials will be researched and discussed. Next, the different possible inks will be listed. Finally, some large scale manufacturers will be shown.

2.3.1 Substrates

The choice of substrate material will affect the outcome that can be achieved. Therefore depending on the desired application, different materials can be of interest. It is also important to look at how the substrate interacts with the ink. The ink needs to adhere properly to the substrate to get a durable product. Here, different available substrate materials will be studied and discussed.

PDMS poly(dimethylsiloxane) is a common used substrate. The reason for this is that it is a durable material which is not hazardous for humans and thus could be used in biomedical devices [8]. PDMS is described as a colourless and odourless silicone [9]. The structure is built out of $(CH_3)_2SiO$ monomers with on both sides a $(CH_3)_3SiO$ group. Due to its low E-modulus ($2{,}05*10^{-4}$ - $2{,}15*10^{-4}$ GPa) it is easy to stretch and clamp for printing conductive circuits. An obstacle is the fact that PDMS is hydrophobic. For a good adhesion between the ink and sublayer, it is important that the ink disperses on the surface instead of forming separate drops. This makes it difficult to apply water-based inks. Furthermore, metals do not adhere well [10]. The PDMS will try to repel them under normal circumstances. This means that the ink does not adhere properly to the substrate. When it is stretched or a voltage is applied, the ink will come loose easily. However, this disadvantage can be reduced by treating the substrate surface. A possible example of a suitable surface treating is plasma barrel etching [8]. Another technique that can be used is adding (3-Mercaptopropyl)trimethoxysilane (MPTMS) to increase the surface wettability, which leads to less water rejection and a better bonding between a conductive metal and the PDMS [9].

Polyurethane (PU) has the advantage of not being hydrophobic, Its Young's-modulus is between 0,0025 and 0,0030 GPa, this shows that more force is needed to stretch the substrate then when PDMS is used. Not only the material but also the thickness of the substrate is important [11]. An elongation to failure test showed that the conductivity of printed ink on a substrate of 0,2 mm, decreases faster than on a substrate of 0,4 mm. one can therefore impose a higher elongation on a substrate of 0,4 mm than one of 0,2 mm. PU is often used in biomedical devices with stretchable electronics because it matches the behaviour of human skin.

PET and PI share a common disadvantage. Both have a high young's modulus. For stretchable electronics this is usually too high. PET and PI are therefore considered as non-stretchable. However, these materials can be used in flexible electronics. PET is an interesting material when looking at thermoforming, as it is a very common material for this technique (ex: PET bottles).

Ecoflex has the ability to be very elastic. It's E-modulus is 60 kPa and thereby much more stretchable than PDMS [12]. Ecoflex can be used as a substrate and covered with SBS Poly(styrene-b-butadiene-b-styrene), which acts as an elastic separator between the Ecoflex and the conductive parts. An advantage of Ecoflex is its high tear strength (6,6 N/mm) compared to that of PDMS (2,6 N/mm) [13]. Combined with its high elongation at break (900 %) makes this an interesting substrate for stretchable electronics.

2.3.2 Inks

When talking about printable and stretchable electronics, the big question is finding materials for inks that are not only conductive but also stretchable and flexible. This can be approached in two ways.

The first strategy is printing the pattern in a wavy or buckling shape, creating a system that is stretchable although the ink material might not be stretchable by itself. By printing silicon for example in a specific wavy pattern [14], this can reduce strain in the silicon up 20 times the strain that exists in the PDMS substrate. This achieves a flexible and stretchable silicon layer. These techniques are discussed in section 2.2.

A second approach is searching conductive materials that are inherently stretchable. A good example of this is a conductive rubber like an elastomer loaded with carbon black. One popular combination is using single walled carbon nanotubes (SWCN) as a dopant in a rubber matrix creating a so called *bucky gel*. When using this material on a PDMS substrate, it can yield up to 100 % stretchability while not losing conductivity [14].

There are a couple of interesting materials that are popular in the printable (and stretchable) electronics industry:

- Indium Tin Oxide (ITO)
- Silver Nanowires (AgNW)/ Silver microstructures - microplates
- Carbon Nanotubes (SWCNT)
- PEDOT:PSS nanocomposite
- Gold
- Graphene

First off, ITO is the most accepted material when it comes to printing transparent electrodes [15]. It has become the industry standard because of its good resistance values and high optical transparency. This material however requires a lot of energy to be produced. Furthermore, when looking at flexible applications, ITO loses its appeal. The process temperatures of up to 400 °C is too high for most flexible substrate materials. The material is also too brittle to be useful for stretchable or flexible purposes.

AgNW is an interesting alternative to ITO as it is easy to fabricate and has inherently high conductivity and ductility [16]. When it comes to electrical conductivity, silver is the most conductive material in the world. It also requires lower processing temperatures than ITO. Silver Nanowire can be coated on a film with a required process temperature of around 100 °C, which most polymer substrate films can withstand. An added bonus is that AgNW films are generally lighter and thinner than glass based ITO sensors. According to [17] silver nanowire inks can be stretched to at least 40 % tensile strain stretching without any significant changes in sheet resistance.

SWCNT are a very interesting dopant material [18], But also as a main material it shows great promise. The nanotubes have a high aspect ratio (Thickness compared to length). This makes them curved and entangled in their microstructure by nature. Much like AgNW, they also show high optical transparency, making them appealing for the use of stretchable display technology for example. SWCNT is also a very interesting material for the use of stretchable electrodes, but not so much when used for the interconnects. When looking at this application, composites of carbon nanotubes and suitable polymeric binders show great promise. The use of this material has already been proven and demonstrated with several stretchable functional devices, like strain gauges, pressure sensors, OLED and supercaps. Especially the strain gauges far outperformed the conventional metal foil type gauges.

Gold is often used in the biomedical industry. The problem with silver for these kinds of applications is that it reacts with bodily fluids, making it unsuitable for biomedical devices. Gold is inert and solves this problem [19]. Organic-conductor polymers like PEDOT:PSS can be used for these purposes as well, but gold remains the material of choice because of its superior stability, inertness to aqueous media, biological fluids and living tissue, and its mechanical robustness.

The next material is the first organic-conductor polymer material. PEDOT:PSS is already a material heavily used for flexible purposes. It can be engineered to be applicable for greater forms of deformability (stretching). A freestanding sheet made of PEDOT can achieve stretching up to 175 %, whereas a PEDOT pattern on a support material can stretch up to 800 %. This is another material with great optical transparency for the use of OLED,… PEDOT also shows high resistance to degradation by oxygen and water [20]. PEDOT:PSS films are stable to temperatures up to 150° Celsius, anything above this will degrade the material rapidly, with full decomposition at 390°. Its maximum conductivity can be achieved by annealing the ink in air at 160°. By adding dimethylsulfoxide (DMSO) the annealing can be done at room temperature, but anything above room temperature will decrease the conductivity of the film. PEDOT cannot be used in situations with prolonged exposure to temperatures higher than 55 °C. This would degrade the material too rapidly. Finally, [20] determined a Young's modulus of 0.9 to 2,9 GPa at 55 % and 23 % relative humidity respectively. This shows that the humidity level is an important parameter to take into account. When the humidity became higher than 55 %, the PEDOT lost its level of cohesion.

Graphene is a material with high promise due to its excellent mechanical properties. It has a 25 % fracture strain and a Young's modulus of 1 TPa, making it highly suitable for flexible electronic devices [21]. Furthermore, graphene has good optical transmittance, high conductivity, good piezoresistive aspects and is easy to implement with existing technology. Graphene can also be assembled onto flexible and stretchable substrates under ambient conditions. Because graphene can be printed at very low temperatures, printing on unusual substrates becomes possible.

When looking at the different materials, ITO drops off as a possibility as it is too brittle to use in flexible or stretchable applications. Gold is also eliminated as it is primarily 'printed' using CVD or PVD techniques. These will not be applied in this thesis. As a conclusion, Two inks will be researched. Silver based inks and PEDOT:PSS will be utilised for inkjet and screen printing purposes.

2.3.3 Manufacturers

When searching for inks, it is also wise to look at which inks are on offer and which manufacturers are available. The most important manufacturers are listed below.

DuPont developed a series of inks, especially for in-mold electronics. ME101 for example is a silver conductive ink, developed for antenna applications and interconnecting circuitry. This ink requires a substrate of PC or surface treated polyester. This ink is compatible with the thermoforming processes and must be printed with screen printing. It is important to dry the ink after printing so the solvent is removed to eliminate further interaction of the ink with the substrate. This process imposes thermal material requirements on all the materials involved, because they must be resistant to the heat used for curing the ink [22]. For other inks in their range, DuPont also provides a clear manual in which you can quickly find out how to use the ink and its functional properties.

Agfa is a Belgian company in the industrial printing sector. In addition to the standard printing techniques, they developed a series of silver inks under the name ORGACON to be used in the stretchable electronics industry. Their Orgacon SI-P1000x is a screen-printable ink consisting of dissolved silver nano-particles. In the online datasheet [23] they explain that the required amount of ink is minimised by its low resistance (3 mΩ/sq/mil). The ink is usable for high resolution printing. A resolution of 75 µm would be possible according to Agfa which allows this ink to be used in space-limited places and reduces the line width which results in further ink savings. Another advantage is that this ink is compatible with the Orgacon PEDOT:PSS ink. This gives the possibility to use different types of ink for different parts of an electronic circuit, which work best for each part. The ink adheres well to (pretreated) PET, PI, and the Orgacon PEDOT:PSS coated substrates [23].

Like DuPont, Henkel is one of the largest players in the printable inks market. For these materials, the brand Henkel is better known as Loctite [24]. For the automotive sector, Henkel presents their silver inks: 'loctite M4100 E&C' and 'loctite EDAG PM 46OA E&C'. They also make proposals for the production of RFID applications. These inks have good permeability so that they interact well on RF waves (which means that they can receive and transmit waves with radio frequencies). Furthermore, they also have a high surface roughness and low impedance. Henkel has developed the inks 'Loctite ECI 1005 E&C', 'loctite EDAG PF 050 E&C' and 'loctite EDAG PM 406 E&C' especially for RFID applications.

2.4 Printing techniques

Depending on the materials chosen for the ink and substrate, a fitting printing technique can be chosen to realise the desired product. The printing technique is more dependent on the chosen ink material than the substrate. As an example, the particles of silver micro flake ink are too large for an inkjet printer and might clog up the nozzle of the cartridge. For this reason, this ink is used for screen printing. In this literature study, the technique of screen printing and inkjet printing will be discussed as these are also the methods that will be used during the practical phases of the thesis.

2.4.1 Screen printing

One common technique to print the electronic paths onto the desired substrate is by using the method of screen printing.

First, a stencil is made of the desired print. In [25], silicon is used as the stencil material as it yielded a high resolution. This stencil is placed over the substrate material. The conductive ink is spread over the stencil and substrate with a squeegee. Only the areas on the substrate that are not covered by silicon will be covered by the ink.

Using screen printing as a technique is appealing as it is simple in execution and relatively quick for mass production. The downside however is that the print is highly dependent on the resolution of the used stencil. Normally, these stencils are made by using a photochemically defined emulsion coating on a screen mesh. The lithography resolution of the emulsion and the mesh size make it hard to improve on these stencils quality. The working principle of screen printing is shown in Figure 7.

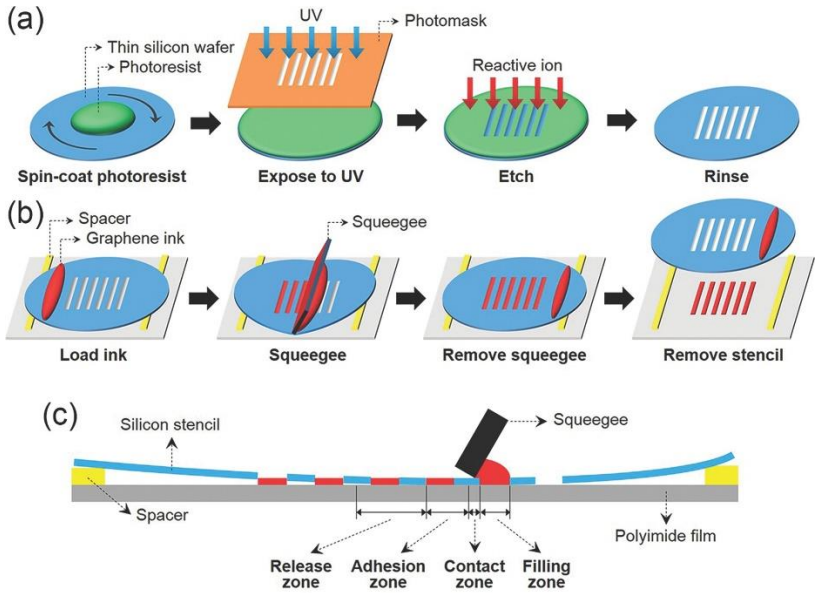

Figure 7: Schematic depiction of screen printing [25, p. 2]

The thickness of the mask is an important parameter [25]. It should be thick enough to withstand the applied mechanical forces during printing, but thinner masks provide better results for fine line printing. This is because with a thin stencil, it's easier for the ink to pass through the stencil onto the substrate.

Different printing orientations can give different results. The printing orientation is defined as the movement of the squeegee compared to the orientation of the pattern lines. The best results can be achieved by printing perpendicular to the lines. The reasoning behind this is that when going over the pattern perpendicularly, the squeegee can deform more, creating higher pressure on the ink. This in turn forces the ink down on the substrate more causing it to contact better.

When it comes to viscosity, lower viscosity inks can achieve finer print thicknesses. However, When printing a thickness that can be achieved with both low and high viscosity ink, the ink with the higher viscosity turns out to be superior. When looking at the printed width of the line compared to the actual width of the stencil, a higher viscosity ink gives results more true to the dimension of the stencil. Low viscosity inks can run out more easily creating pathways that are wider than desired. Furthermore, a more viscous ink results in a thicker printed line, giving it a higher aspect ratio. Given all this, a more viscous ink turns out to be preferable.

The inks used for screen printing generally contain three parts: conductive particles like conductive nanowires, nano-particles or micro sheets, an organic binder/additive and a solvent [25]. The problem when screen printing silver inks for example, is the low viscosity of these inks. As discussed above, a higher viscosity is preferable for screen printing. It is possible to make the inks more viscous with thickening agents like solutions with cellulose nanofibrils [26], but these could dramatically increase the inter-particle contact resistance in the resulting coating, making the result less conductive.

2.4.2 Inkjet printing

Inkjet printing has some advantages over other technologies for the construction of stretchable conductive tracks. Inkjet printing is a simple technique that is not time consuming for the operator and is largely self-sufficient, because of the digital control of the printer. Another advantage is its low energy requirement [27]. It is possible to produce conductive patterns, even consisting of metals without melting it like other transform techniques. A schematic working principle is shown in Figure 8.

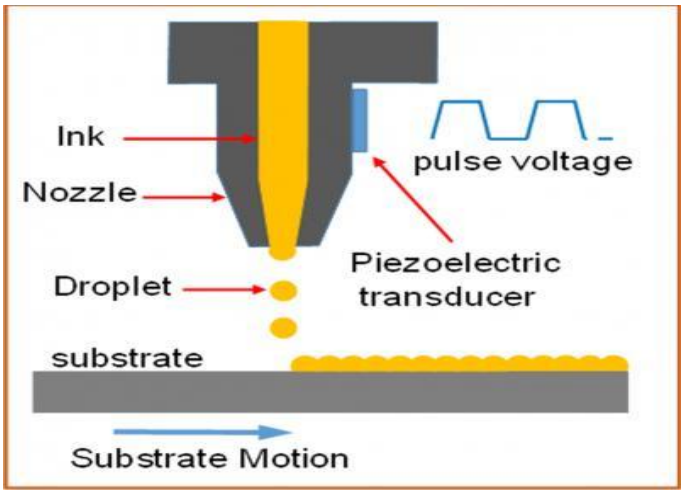

Figure 8: Simplified schematic of inkjet printing [28]

Due to the use an inkjet process the printed tracks are more porous than standard electronics [27]. This results in better results in bending tests.

One major advantage of inkjet printing over screen printing is its more economic use of ink material. In screen printing, a lot of material is lost by the use of a mask. The conductive material is applied over the screen, but the ink at the edges does not end up on the substrate. With inkjet, this is not the case, every dispensed drop is digitally controlled by the computer, this leads to the advantage that no expensive ink is wasted.

For inkjet printing, a substrate is placed inside the printer, this substrate is what paper is for a normal inkjet printer at an office or at home. However, for printing on flexible substrates the substrate should be clamped down or held down via vacuum while printing, so it will not curl up or warp during the printing process. The ink consists largely of solvent, in which conductive particles, such as silver micro sheets for example, are dispensed. When applied upon the substrate, the solvent can hereby be absorbed. This causes a swelling and increasing of the dimensions of the substrate as discussed in [27]. The volume increase can on its turn cause a warping, the non-flat surface does not yield correct results, so the process will fail. By stretching the substrate lightly, a slight tension is created. This keeps the print surface flat. When the ink is drying after the printing process, the solvent evaporates and the swollen state of the substrate decreases. This could give a problem during the printing process. The problem of warping is not only caused by a temporarily absorption of the solvent. Thermal changes could also influence the volume of the substrate, and thereby introduce the same problem.

The printer contains a printhead. This is the part that will move above the substrate and dispense the ink on the substrate. The top of the print head contains a reservoir in which the ink is stored. Before the ink is injected into the reservoir, it is prepared completely outside the printer. The bottom of the printhead consists of multiple ink drop generators. On the surface of the drop generator are rows of small holes. These holes are the nozzles that drop the ink in droplets on the substrate. The control of these nozzles is usually accomplished by piezoelectric pieces that push a droplet out of the hole. After a drop has fallen, the surface tension of the ink ensures that only one drop can fall per push of the piezoelectric crystal.

2.5 Shaping process

Stretchable, printed electronics allow for products with clean aesthetics. The electronical leads and components are either completely invisible or can blend in with the shape and form of the object. Integrating these kind of electronics directly into the molding step is the logical next step to make the production step quicker and more efficient.

The construction process of in-mold electronics consists of 3 stages [29]. In the first stage, an electronic circuit is printed on a flat polymer substrate with the previously discussed print techniques. The second stage consists of the shaping of the printed circuit. This can be done by thermoforming or vacuum forming. For this purpose, the substrate on which the electronic circuit was printed is clamped in the device. Then this sheet is heated by a heat element. The heating element can make contact with the sheet but usually is kept at a distance to heat up the sheet with heated air. This provides a more uniform temperature and avoids degradation of the plastic. Another heating technique uses infrared radiation. This radiation is absorbed by the plastic, causing it to heat up. During this step, the sheet will sag lightly.

forming the plastic can be done in two ways. In the first method, the sheet is moved down over a mold, where a vacuum ensures that the atmospheric pressure forms the sheet inside or over the mold, possibly accompanied by an extra stamp or air pressure during its movement downwards for internal shapes. This method is shown in Figure 9. A second approach means that the sheet does not move but the mold moves upwards into the sheet like is shown by Figure 10, also here a vacuum is created so that the environmental pressure forms the sheet around the mold. A schematic representation of thermoforming and vacuum forming are shown in Figure 9 and Figure 10 respectively.

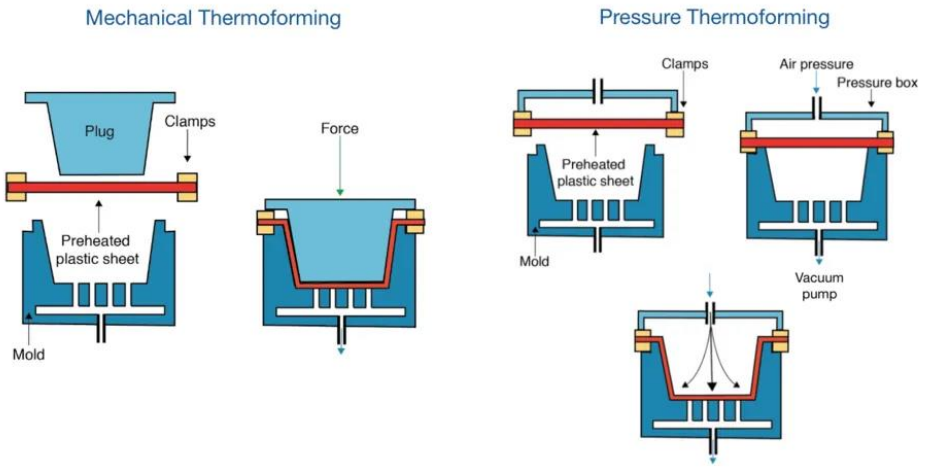

Figure 9: Schematic representation of thermoforming/vacuum forming [30]

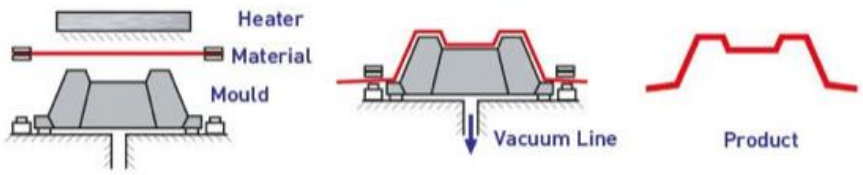

Figure 10: Schematic representation of thermoforming [31]

It is important to be aware that the wall thickness of the sheet is not constant after the thermoforming process.

When using a mold that moves upwards, the wall thickness will be thickest at the place where the mold hits the sheet first [32]. On vertical or highly inclined surfaces, the sheet is stretched the most, making the wall thickness thinner in these places. For thermoforming of internal shapes, the sheet retains its wall thickness at the point of clamping, but it decreases further towards the centre. The use of an additional stamp that accompanies the sheet results in a less pronounced thickness reduction of the sheet.

After forming, It is important to cool the workpiece slowly. Fast cooling traps the molecular chains in the plastic in their condition, also called freezing. This causes more internal stresses in the material which could lead to cracks, and could deform or warp the work piece [29].

The third and last stage is placing the formed substrate with the printed electronic circuit in the desired object by the in-mold decorating or labelling process. In the previous step, the sheet (which consists of the substrate with the printed electronic circuit on it) was formed as a mirror image of where the electronics will eventually be inserted. The sheet has now been turned into a 3D shell-like object. This shell is placed inside the mold for the injection molding phase. When the polymer gets injected into the mold, it takes the shape of the mold, enveloping the label, melting it and making it an inseparable, integral part of the final piece. The same principle can be applied to in-mold electronics. By injecting the molten polymer, the substrate material that holds the electronic interconnects and sensors will be melted and bonded with the piece. The stretchability aspect of the electronics comes into play in the vacuum forming step. As the patterns are initially printed on a flat surface, the electronics that are printed on the substrate should not break connections, lose conductivity or change in characteristics when the shape is deformed to fit the mold. Tactotek currently is the leader in producing in-mold structural electronics applications. How it is done is by first printing decorations onto an in-mold labeling film, then printing the electronic interconnects on top of this using a conductive ink. After this, components like LEDs etc are placed. This sheet is then vacuum or thermoformed into the desired shape. Finally this formed film is used as an insert in the injection molding process, creating the desired shape with electronics seamlessly integrated into it [33].

2.6 Applications

2.6.1 Haptic Feedback in structural electronics

Dielectric elastomer actuators

One possible solution for creating stretchable haptic feedback implementations is by using so called Dielectric elastomer actuators (DEA). These elastomeric materials are also known as artificial muscles as they behave similar to organic muscle tissue. They are made by making a sandwich construction of two electrodes with the elastomer in the centre (Figure 11) [34]. When a voltage is applied over the electrodes, the induced electrostatic field causes the DEA to deform. This electrostatic field is known as the Maxwell stress which is characterised by:

$$s_z = -\frac{\epsilon_r \epsilon_0 V^2}{Y z^2} \tag{8}$$

Although the material is very promising, it comes with its own set of challenges to overcome. At this point, it is difficult to use it in small applications with low voltages.

[34] shows that it is possible to make use of the material without the use of electrodes. This has the advantage that the deformation of the elastomer is not limited to the stiffness of the electrodes, and it avoids complicated manufacturing for compliant electrodes. However, while spraying charges onto the DEA turned out to be relatively easy, removing them appears to be difficult. This makes electrodes appealing as they can bring and remove charges quickly and easily. Also, when properly designed, they can bring charges to precise locations. This allows for more complex circuitry with several independent zones on one substrate.

The biggest downside of this material is the requirement of high voltage source signals. In [34], driving voltages of up to 1,1 kV were required to make the actuators function accordingly. These high voltages could lead to safety concerns for consumer applications. The necessary electronics to drive the actuators is also large and bulky with a size larger than regular consumer grade media players. There are certain consumer grade applications made for use in for example an Ipod Touch as haptic feedback. This might make the technology usable as a solution for haptic feedback in in-mold electronics.

While the characteristics of DEA and stretchable electronics differ, there are also a lot of aspects they share. They use similar materials, deposition methods and patterning solutions. This could make it appealing to try and combine both technologies.

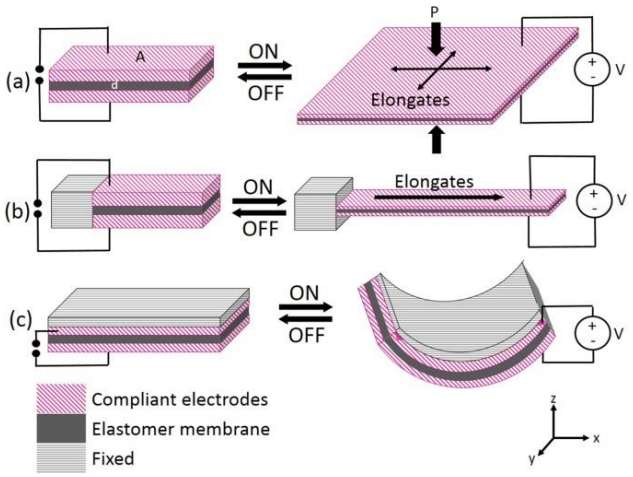

Figure 11: Working principle DEA [35, p. 3]

Squeeze film effect

By applying ultrasonic vibrations between two solid surfaces, a squeeze film effect is induced. This effect can drastically reduce the friction between these plates, making it possible to develop variable friction applications. By doing this, different textures and feels can be achieved, creating a haptic interface [36]. By altering the amplitude of the driving vibration, different haptic sensations can be achieved as the lateral friction coefficient changes.

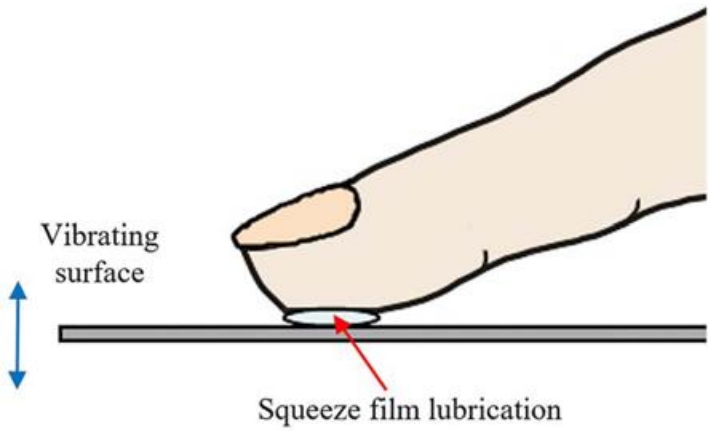

Figure 12: Squeeze film effect [36, p. 1]

The surface of a human finger isn't flat. It has ridges forming fingerprints. When a finger is pressed onto a solid surface, a small film of air is trapped in between these ridges and the surface (Figure 12) [36]. If the surface is then vibrated at ultrasonic speeds, the squeeze film effect can be induced. The vibration uses amplitudes in the order of 1 μm, and frequencies greater than 25 kHz. When these parameters are set, the trapped airfilm acts as a lubricant between the finger and the surface. In [36], a voltage amplitude of 100V was used for all simulations.

The squeeze film effect is dependent on the curvature of the surface the haptic interface is placed on [36]. If the surface is rounded with a small radius, the contact area with the finger is smaller (Figure 13). This may result in less effective squeeze film effects and loss of haptic sensation.

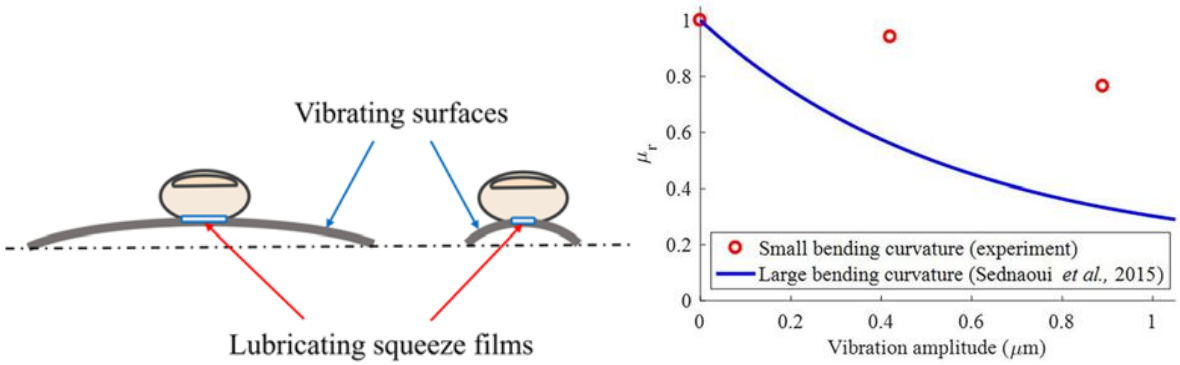

Figure 13: Squeeze film effect on small and large radius curves [36, p. 7]

Piezoelectric

An eccentric rotating mass (ERM) is the oldest and first form of haptic feedback and consists of a motor rotating an eccentric mass, as the name implies. This eccentric motion will cause the unit to vibrate. This system is very simple but slow in response and speed [37]. The linear response actuator is very similar, but shows more efficient power consumption. Both however are motor based-systems. Second, piezoelectric systems were developed. They can respond fast with a wider field of frequencies, but they often require a high driving voltage to operate properly. Third, a system using shape memory alloys. They have significant operating force, but take a long time to relax and are too big for smaller applications.

A thin-film membrane haptic feedback system can be made by coating a substrate material with an electrode on one side [37]. These membranes are stacked atop of each other with a small air gap in between. This acts as a capacitor with two different dielectrics in the centre: the substrate material and air. When more layers are stacked, this can be described as a parallel circuit of capacitors with altering polarities on each layer (Figure 14).

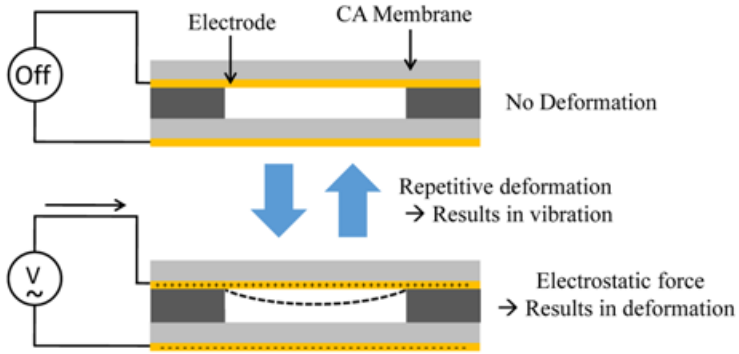

Figure 14: Schematics of piezoelectric actuator [37, p. 2]

Looking at a two-layer capacitor, when voltage is applied over the two electrodes, an electrostatic field is generated perpendicular to the electrodes and substrate material in between the electrodes. This causes the electrodes to gain significant charge. Close to the electrodes in the dielectric substrate, an opposite charge is generated as compensation. When an altering voltage is applied over the electrodes, the attraction forces between the electrodes and the substrate material cause vibration. An example of this can be found in [37], with a driving voltage ranging from 500 to 1500 V. By doing this a vibration acceleration of 1,7 g was achieved.

2.6.2 Antennas in structural electronics

When looking at antennas, the main problem when it comes to making the technology deformable, is the frequency at which the antenna operates. Normal antennas are tuned to specific frequencies which they can detect to enable communication. This frequency is dependent on the design and geometry of the antenna. For a dipole antenna, when an electromagnetic wave crosses a conductive lug, this lug can intercept it. When the frequency of the wave and the resonant frequency of the lug match, an electric current is generated in the antenna, which can be measured and interpreted. The strength of this signal is known as the gain of the antenna.

The main problem lies in this resonant frequency, because this parameter is highly dependent on the geometry of the antenna. When stretched, the length and geometry are changed, in turn altering the resonant frequency of the antenna. This means the antenna will not pick up the frequencies it was designed for.

[38] focusses on two types of stretchable antennas, a pifa (Figure 15) and a dipole antenna (Figure 16). First the pifa is examined. This antenna was made using an evaporation printing technique, creating a thin (<100 μm) layer. It was found that this design and technique lends itself to good stretchability and reproducibility. When the antenna is relaxed back to its original state and restretched, the measured results remained constant. The biggest downside of this antenna is that when stretched, it lost up to 10 dB gain when stretched to 10 %.

Figure 15: Pifa antenna [38, p. 1]

Second, a dipole was tested [38]. This antenna was printed using the inkjet printing method using a silver based stretchable ink. This method lies more in line with the procedure that will be used in this master's thesis. When tested it was found that this design shows better efficiency than the pifa antenna. When stretched to the same 10 %, it showed a significantly lower 1,7 dB loss. The downside however is that when relaxed, this antenna does not regain its original properties. If it is stretched again the results will differ and be worse than those of the initial stretch. Furthermore, the stretchability until resonance is lost is lower than this of the pifa, meaning it is less stretchable.

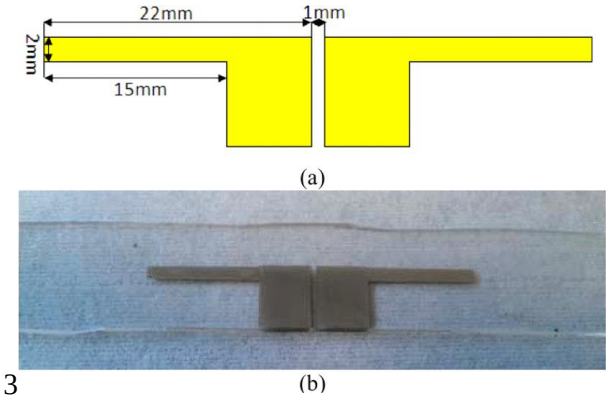

3

Figure 16: Dipole antenna [38, p. 2]

The conclusion is that the pifa design is better when stretchability over multiple stretching cycles is desired. The dipole is the better option when it is only stretched once to get it in the final shape, and a better accuracy to the original resonance frequency is needed [38].

Antennas made out of a conductive polymer have two main problems. They have lower conductivity than their metal counterparts, and they have a process-limited thickness [39]. Both these aspects result in a relatively low efficiency. Because both thickness and conductivity are important, both should be taken into account for estimating their electrical properties. This leads to the parameter of sheet resistance defined by.

$$R_s = \frac{1}{\sigma d} \tag{9}$$

With σ being the conductivity and d the thickness of the film. In Table 1, the properties of some common polymer materials are given.

Table 1: Properties of common polymer materials [39]

Materials	σ (S/m)	d (μm)	δ (μm)	R_s ($\Omega/\square$)	Efficiency
PPy [7]	2000	140	167.8	3.6	64.8%
PPy [6]	2000	120	251.6	4.2	62.0%
PPy [8]	2000	90	145.3	5.6	48.2%
PEDOT [8]	10000	7	65	14.3	33.6%

When the sheet resistance of the material is lower, a higher antenna efficiency is anticipated as the ohmic losses in the conductor will be less. The results found in [39] showed to be unsatisfactory for practical purposes. However, there are strategies to improve the efficiency of these polymer antennas. The first of which is by implementing a non-resonant design (Figure 17). By utilising such a design, the ohmic losses in the antenna are lowered because the current build up in resonant antennas is higher. A second approach to increase the efficiency of the antennas is by applying a chemical treatment to the material. These methods will not be used in this research. A third and last proposed method is increasing the thickness of the film. Looking at formula 9, by increasing the thickness the sheet resistance will in turn decrease. This could be achieved by applying a multilayer structure.

Using a polymer based ink also has significant upsides compared to metal based counterparts. The mechanical flexibility and stretchability are highly desired traits when looking at more flexible design of products.

In [39], an average radiation efficiency of 85 % was realised across the frequency band of the antenna by exploiting the non-resonant antenna design as stated above. The antenna has an operating frequency of 3 to 20 GHz. In [39], a thickness of 70 μm was realised for the PEDOT film with a DC conductivity of 9532 S/m. The design of the antenna used in [39] is given in Figure 17 and Table 2.

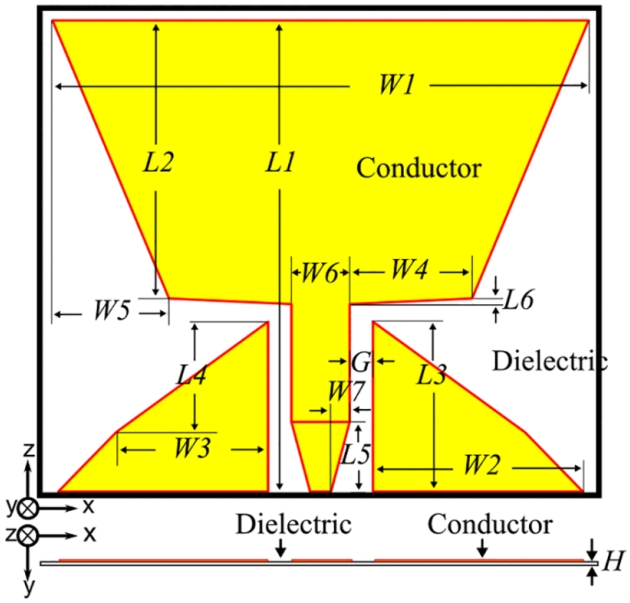

Figure 17: Non-resonant antenna design [39, p. 2]

Table 2: Non-resonant antenna dimensions in mm [39, p. 2]

$L1$	$L2$	$L3$	$L4$	$L5$	$L6$	G
20.25	11.95	7.30	5.00	3.05	0.24	0.85
$W1$	$W2$	$W3$	$W4$	$W5$	$W6$	$W7$
23.00	9.00	6.30	5.25	5.00	2.50	0.80

This antenna was printed on regular sticky tape with a thickness of 150 µm [39]. Because of this the relative permittivity and tangent loss were $\varepsilon_r = 3$ and $\tan\delta = 0{,}01$ respectively. These parameters are not critical for the design. The manufactured antenna turned out to have excellent flexibility and robustness. It was bent to angles of 90 to 180° without any mechanical damage. Furthermore, when bent at 90°, the antenna does not show dramatic decreases in performance. When bent at 180°, a more drastic decrease is observed in the lower region of the spectrum as the length of the antenna is significantly reduced. However, a 180° bend does not have many real world applications.

2.7 Discussion

From the literature review and after consultation with Fremach it is concluded that printable haptic feedback is difficult to realize due to the many-layer construction with interconnecting parts and the different materials that are required. It is therefore decided to investigate how an antenna can be printed and how it can be made so that it still functions after deformation. Fremach is more interested in what is possible, not so much in the kind of antenna that is tried and tested. This gives freedom to provide appropriate designs that may be useful for their industry.

From the literature it is decided to print the antennas with both screen and inkjet printing. After all, the inkjet printer is more flexible in use because for screen printing new screens have to be made after each design revision. This does not only cost money, but also time. Inkjet only requires a design loaded into the printer. This flexibility can be useful for industrial purposes.

Various silver inks will be used, including for example the micro flake silver ink ME602 from DuPont. PEDOT:PSS will also be used because of its interesting advantages such as its transparent properties and high stretchability. PEDOT is also more environmentally friendly because it is soluble in water whereas silver inks are more difficult to break down at the end of their life.

As a substrate material it is decided that TPU is interesting because a manufacturer of this material, namely *Grafityp* is also involved in a project at IMO-IMOMEC. PET will also be examined further because it is easy and commonly used as a material to thermoform.

3 Antenna theory

The field of antennas is broad and vast. There are many different shapes and sizes available depending on the functionality that is desired. This can range anywhere from monopole design antennas for radio applications with lengths up to tens of meters, to high frequency WIFI antennas only measuring a couple of centimetres. For this thesis, it was decided to look at 3 different antenna designs. These are an inset fed patch antenna [40], the dipole antenna also discussed in the literature study [38] and an RFID antenna also used by the *Paperonics* project [41] from the research group FME at IMO-IMOMEC. In 3.1 some important parameters for the characterisation of antennas are discussed. This is followed by 3.2, 3.3 and 3.4, where each sub-section discusses one of the chosen antennas. In 3.5 a sub-section is devoted to the use of connectors that are obviously needed to measure the parameters discussed earlier.

After a meeting with antenna experts Prof. Dr. ir. Sam Lemey and Ir. Igor Lima de Paula from the UGent, it was concluded that creating a functional antenna would be beyond the scope of this thesis. This would focus heavily on the electronics and electromagnetic aspect of the antenna, instead of the desired material aspect. It is also practically difficult because expertise and test equipment are not present in IMO-IMOMEC, while the research institute is specialized in materials research. Therefore the acquired knowledge of antennas and the improvements of the existing designs will only be discussed theoretically.

The following sections discuss each antenna that is utilised in this thesis. For each antenna, theoretical background and some adjustments and remarks resulting from the discussion with the UGent experts are reviewed.

3.1 Overview of Antenna parameters

When designing and characterising an antenna, there are a couple of important parameters to take into account.

The first parameter is the dielectric constant or the relative permittivity (ε_r). This value is the ratio of how much a material resists the passing of an electromagnetic field compared to the vacuum of space. If this value is high, it will be difficult for the field to pass through. For an antenna, it is mostly desired that the dielectric constant of the substrate material is as low as possible, so the dielectric materials does not impact the field radiating from the antenna. The value of this constant is determined by the material that the dielectric is made of. This value can be consulted in tables. As an example, paper has a relative permittivity of about 2 and polyimide a relative permittivity of 3,4 [42].

The second parameter is the loss tangent. This is directly related to the dielectric constant of the substrate. The loss tangent is a representation of how much energy of the electromagnetic wave is lost due to it passing through a dielectric material. The lost energy is dissipated in the dielectric material as heat.

The third important parameter is the radiation pattern. This is a 3D or 2D plot showing the gain of the radiated waves in all directions. The 3D plot is easily comprehendible, but more difficult to produce. The 2D plot is easier to make but does not show the full radiated pattern. The 2D plot can be seen as a slice of the 3D plot. It is often chosen to take this slice where the gain of the radiated waves is the highest [43]. An example of a radiation pattern plot of a dipole antenna can be seen in Figure 18.

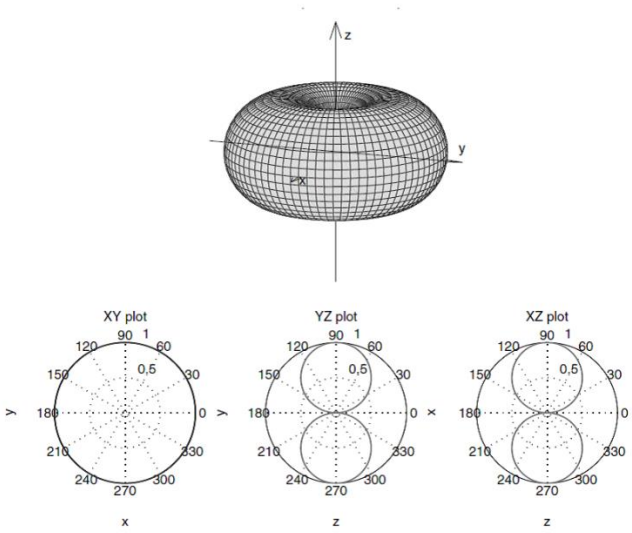

Figure 18: 2D and 3D plot of the radiation pattern of a dipole antenna [44]

The fourth important parameter is the radiation efficiency. While the radiation pattern shows how the antenna radiates, the radiation efficiency shows how much of the input power is converted to the desired radiated output. The higher the efficiency the better [45].

The fifth parameter is the reflection coefficient (commonly referred to as S11). This represents how much of the incoming power is reflected back away from the antenna. S11 is expressed in decibel: when S11 = 0 dB, all incoming power is reflected, so no power can be radiated. According to [46], when S11 = -10 dB, -7 dB is reflected. All the rest is accepted by the antenna and is either radiated or absorbed as losses within the antenna. The example of a measurement shown in Figure 19 indicates that this antenna would resonate most at 2,5 GHz; this is called the resonant frequency of the antenna. At 1,5; 3,5 and 4,5 GHz, all power would be reflected. At any other frequency value, the antenna would resonate, but with much less power than at 2,5 GHz, making these frequencies not desired [46].

It is not possible to decide how well an antenna works purely based on the reflection coefficient, whether its value is high or low. An antenna that reflects a small amount of energy, but with poor efficiency will still not transmit a sufficient amount of energy. The same goes the other way. When an antenna reflects a lot of energy, but has a high enough efficiency, it might still radiate enough energy to be functional.

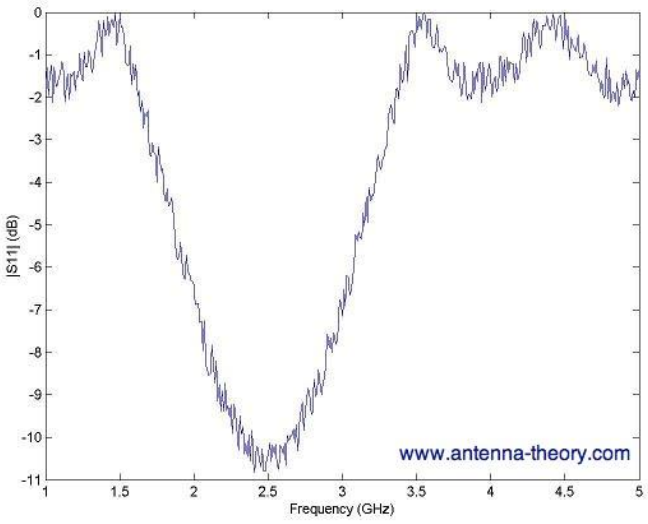

Figure 19: Example of reflection coefficient measurement [46]

From Figure 19 it is also possible to determine the bandwidth of the antenna. The bandwidth of the antenna is the range of frequencies at which the antenna will function as desired. This value is often expressed in function of the voltage standing wave ratio (VSWR). It is a range of frequencies where the VSWR is below a certain chosen value, indicating how much power the antenna reflects in this frequency range. Often, a 2:1 VSWR bandwidth is chosen. This means that the antenna can operate at the range of frequencies where the VSWR is less than 2 [47]. The VSWR is directly related to the return loss and expressed as [48]:

$$VSWR = \frac{1+|S11|}{1-|S11|} \tag{10}$$

When an antenna is not properly matched with its receiver or transmitter, power is reflected causing a reflection coefficient S11 to occur [48]. This reflection interferes with the voltage wave going to the antenna, creating a standing wave. The VSWR is described as the difference between the amplitude of the peaks and the amplitude of the valleys of the standing wave. When the VSWR equals 1, the standing wave form would be a flat line, meaning there is no power reflected. The VSWR always has a value equal to or greater than 1. The smaller the value is, the better the antenna is matched to the receiver.

The last parameter is the antenna impedance. Just as in electricity, it is also important for antennas how voltage and current are related to each other. The antenna impedance can be determined using a network analyser, which determines the capacity, inductance and resistance of the antenna. The impedance consists of a real part and an imaginary part. An antenna is called a “resonant antenna” when the imaginary part is (almost) zero and therefore only has a real impedance. The real part represents the radiated (and received) energy while the imaginary part represents the energy that is lost to the environment. But the impedance depends on the frequency at which the antenna operates. It is therefore also important to match the impedance of the antenna with that of the transmitter that controls the antenna. The following example in Figure 20 illustrates this [49]:

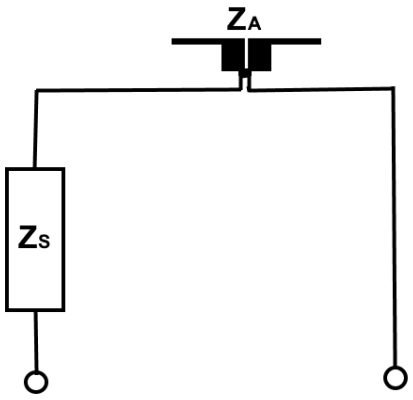

Figure 20: Antenna impedance network

Consider an antenna with impedance Za and a transmitter with impedance Zs. At a low frequency, the influence of the cables may be ignored. In this case, the power absorbed by the antenna applies:

$$P_A = I_A * U_A \tag{11}$$

by applying ohm's law and the voltage divider this becomes:

$$P_A = \frac{U_A}{Z_A+Z_S} * \frac{U_A*Z_A}{Z_A+Z_S} \tag{12}$$

$$P_A = \frac{U_A*{Z_A}^2}{(Z_A+Z_S)^2} \tag{13}$$

(11) shows that when Za and Zs differ too much from each other, no energy reaches the antenna. When the frequency is high (which applies in this thesis), the influence of the cables must also be taken into account. This is much more complex. The impedance of the cables must also be the same as the impedance of the antenna because otherwise the power will be reflected back to the transmitter [49].

An important note is that because of these factors, an antenna design cannot simply be copied and expected to work as desired. When changing the dielectric material, the antenna material and the surrounding area of the antenna, the functionality can change drastically. For this reason, when an antenna is designed, it is first tested virtually with a modelling software like ANSYS HFSS or CST. Then, the antenna is developed physically and tested. The results of the virtual and physical tests are then compared to see if further optimisation is required.

3.2 Inset fed patch antenna

3.2.1 Design

The first antenna design is an inset fed patch antenna. These antennas are commonly used due to their simple geometry, making them easy to produce. This variant is designed to work at 2,4 GHz, making it useful for WIFI and Bluetooth applications. Because of the simple, square geometry, it is expected that this antenna will be less sensitive to deformation and strain (Figure 21). The dimensions used for the inset fed patch antenna are given in Table 3.

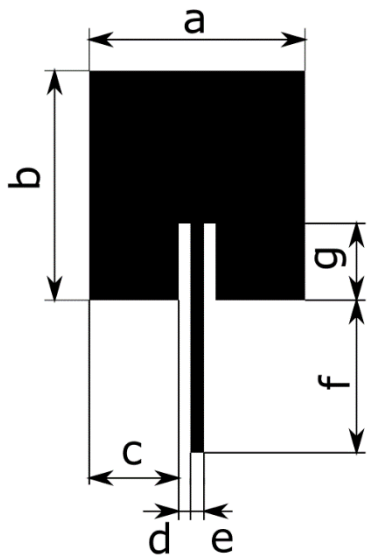

Figure 21: Inset fed patch antenna design

Table 3: Dimensions inset fed patch antenna

a	36,85mm
b	39,15mm
c	15,27mm
d	2,00mm
e	2,30mm
f	26,05mm
g	13,10mm

3.2.2 Theory and remarks

Due to their simple shape, patch antennas are easy to produce. On top of that, this shape also makes them resilient against deformation. The fact that these antennas can be used on many resonant frequencies, impedances and radiation patterns makes it a handy and widely used antenna in current technologies. Usually the rectangular shape is used, but there are also designs utilising a round shape. As shown earlier, a rectangular type is used in this thesis because they are known to be more versatile in the previously mentioned areas such as resonance frequency [50].

Some disadvantages of this antenna are its low efficiency and narrow bandwidth. The narrow bandwidth is preferable if the antenna has to work very well at one specific frequency. When the antenna has to receive and transmit multiple different frequencies, a broad bandwidth is desired (e.g. an FM radio has to be able to receive multiple frequencies). On the other hand, this narrow bandwidth is good in security systems where the antenna is only allowed to work with one specific frequency [50].

In order for the inset fed patch antenna to become functional, it was discussed that a ground layer should be added to the design. This plane could be added on the back of the antenna, or surrounding the antenna on the same printing plane. Depending on this choice, the antenna would radiate hemispherical or spherical respectively. Which choice is the best option, depends on the desired functionality of the antenna. A hemispherical radiation pattern for example is used when the antenna is incorporated in clothing. By applying the ground plane on the back, this ensures that the antenna does not radiate its electromagnetic waves into the human body, therefore shielding the wearer from the radiation produced by the antenna. Figure 22 and Figure 23 shows these two shielding placements. The arrows indicate the direction the antenna can radiate in.

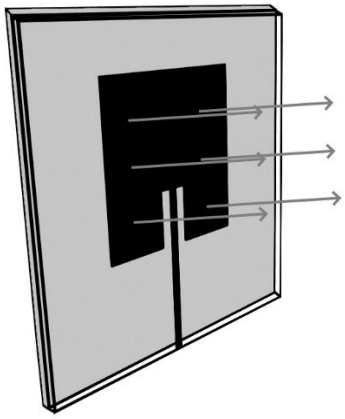

Figure 22: Inset fed patch antenna design with ground plane on back

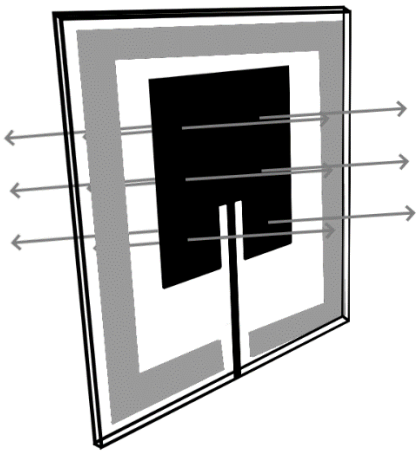

Figure 23: Inset fed patch antenna design with surrounding ground plane

3.3 Dipole antenna

3.3.1 Design

The dipole was also chosen for its simple geometry, much like the inset fed patch antenna. Because the working of this design is highly depended on the length of the antenna arms (dimension “a” on Figure 24), it is suspected that this antenna will be more sensitive to deformation and strain. It might remain in a working condition after forming, but will probably work at a different frequency as the length of the arms is directly related to the resonant frequency of the antenna. The dipole antenna is designed to function at around 3 GHz. Its dimensions are given in Table 4.

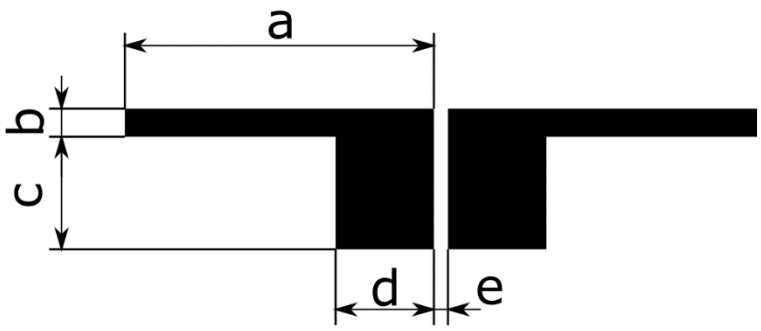

Figure 24: Dipole antenna design

Table 4: Dimensions dipole antenna

a	22mm
b	2mm
c	8mm
d	7mm
e	1mm

3.3.2 Theory and remarks

Although the dipole is expected to work in its current form, a redesign would still be required to power and measure the antenna. A dipole can only work when fed with a differential feed. This means that the left and right lug of the antenna receive a mirrored signal. In a regular setup, this is not the case. A conventional feed is a voltage to ground signal as opposed to the required mirrored signal. In other words, the required signal should be balanced whereas the provided signal is unbalanced. To be able to use a regular unbalanced signal, the addition of a *balun* is required. A balun is an electronical device that is used to 'balance' unbalanced signals. They force an unbalanced signal to be balanced. They are however will not be discussed further than this as this is beyond the scope of this research [51]. Figure 25 shows how the voltage is mirrored between the lugs in red. The blue arrows shows the current direction. The balun converts the incoming signal into two signals with reversed direction.

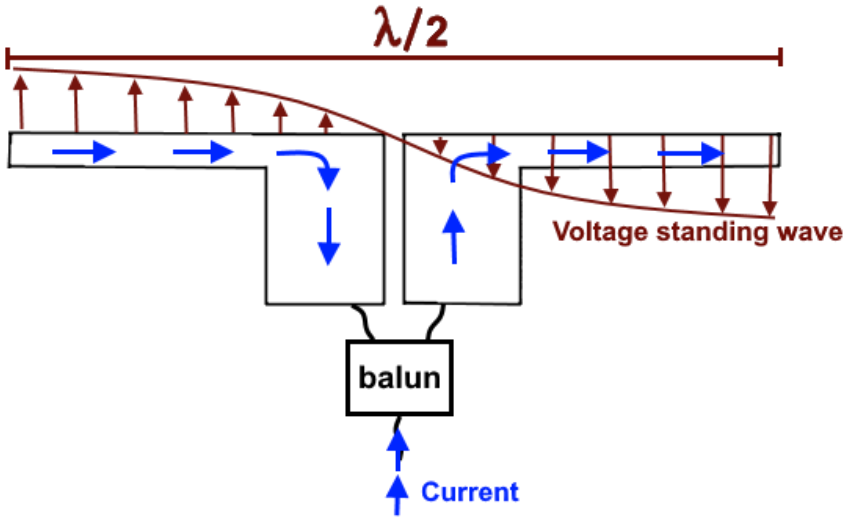

Figure 25: Dipole with a balun and a mirrored signal in the lugs inspired by [52, p. 2]

With a dipole antenna, the length of the antenna arms corresponds to half the wavelength of the electromagnetic radiation emitted by the antenna. The antenna that this thesis considers as an example has a total length of 45 mm. The wavelength of the radiation will therefore be 90 mm, which is equal to a resonant frequency of 3,33 GHz. Dipoles are used in many fields of application, for example in aircraft and ships for radio communication. A visible example of this can be found on old televisions. The so called "rabbit ears" (Figure 26) that pick up the tv-signal, is actually a dipole antenna.

Figure 26: TV with rabbit ears [53]

Another option suggested was to use a monopole antenna design instead of a dipole. The biggest advantage here is that a monopole can be fed with a regular, unbalanced signal, meaning a balun is not required. The monopole is basically one half of the dipole antenna. One of the lugs is now simply a connection to ground, making it functional with a regular unbalanced signal. This is also why monopoles only have half the length of a dipole, which makes them very interesting when the antenna needs to be compact. Because of their shape, the monopoles can only transmit above the ground plane. Contrary to the standard dipoles, they cannot emit in two directions. It is important to note that because of their shape, the impedance is only half of the impedance of the dipole with the same length of lugs. The transmitter connected to the antenna thus has to be adjusted accordingly. Old mobile phones were equipped with a monopole antenna because of their compactness. The housing served as a ground and can be considered as an infinite ground plane [54]. Figure 27 shows an example of a mobile phone with monopole antenna. Figure 28 shows how the monopole is actually the same as a dipole but with one side connected to the ground eliminating the need of a balun.

Figure 27: NOKIA 6110 with monopole antenna [55]

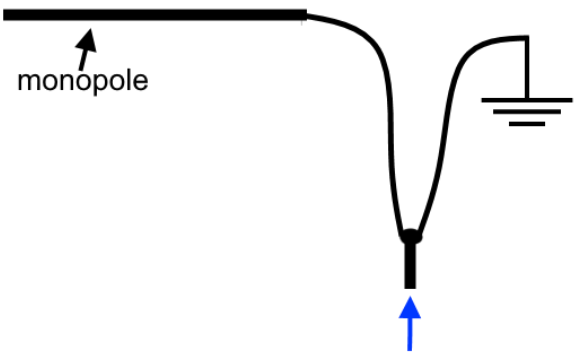

Figure 28: The monopole is a dipole with one side connected to the ground

3.4 RFID antenna

3.4.1 Design

Although the RFID antenna has a more complicated design, this design was chosen as there is in-house knowledge on it thanks to the *Paperonics* project in IMO-IMOMEC. For this antenna, it is known that its DC resistance has to be in the range of 10 to 40 Ω in order for it to function as desired on a paper substrate (Figure 29).

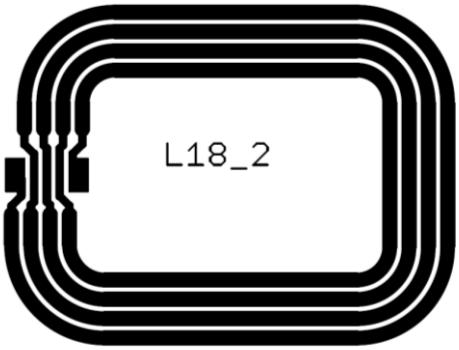

Figure 29: Paperonics RFID antenna L18_2

3.4.2 Theory and remarks

As the RFID antenna is already an optimised design, no suggestions were made to further improve on it. It is expected to be the easiest antenna to characterise as this is an antenna made for near field communication. The dipole as well as the inset fed patch are meant for far field communication. The benefit of being a near field antenna is that the radiation pattern is no longer an important parameter. Often this type of antenna is called an RFID tag. An application of this is, for example, in an identification card to unlock doors in a company building or as a sticker in a library book, allowing the book to be scanned and identified automatically. For logistics this is also a very useful tool. In production processes an RFID tag is often placed on a product, so the product can be found quickly or followed throughout the production process. An RFID antenna can be characterised using an impedance measurement and a reflection coefficient measurement to find the resonant frequency it operates at. This impedance measurement is performed with a vector network analyser [56]. By means of its measurements, the latter will present the RFID tag as an equivalent electrical scheme consisting of virtual resistors, inductances and capacitances. Figure 30 shows an example of an output graph from an impedance measurement of an RFID tag. The resonance frequency of this tag was determined to be at 123 MHz.

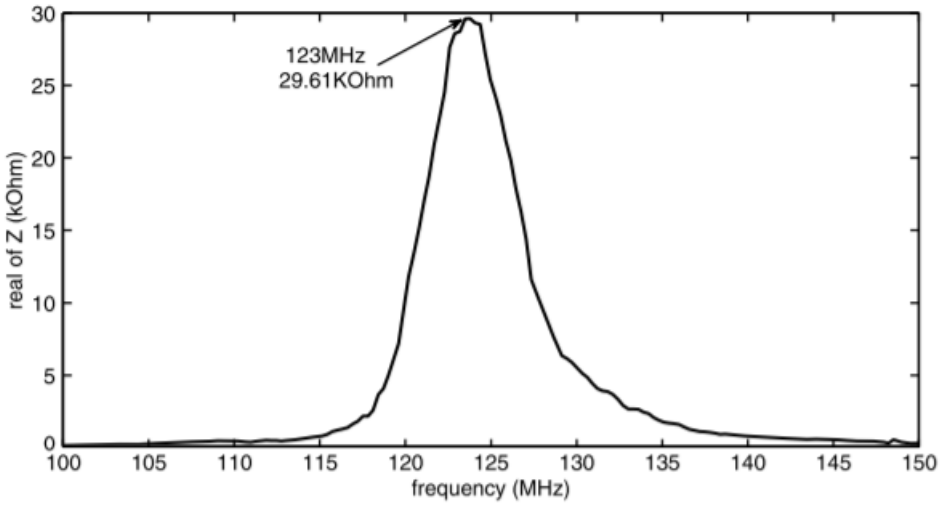

Figure 30: Example of an impedance measurement on an RFID tag [56, p. 3]

The resonance frequency of the RFID tag is highly dependent on many influencing factors. For example when the substrate material changes, the L, R and C components of the equivalent scheme change, and so does the resonance frequency. The RFID tag cannot be compared to other antennas, as its purpose is functionally different. This antenna does not serve to transfer a lot of data over long distances and is not suitable for this purpose. The RFID tag is used for electronic identification. It should be especially

compact. The tags are divided into three groups: active, passive and semi-passive. The active ones need a battery. This is detrimental to the compactness of the tag, but allows it to identify up to several hundred meters because the battery provides the antenna with sufficient energy for this transmission. The passive tags do not have a battery. This makes them more compact. Because of this, they are used the most. This also makes them cheaper than the active or semi-passive variant. They take the energy to transmit from the induced energy in the coil through the incoming flux of the tag reader. They have a range of only a few meters. The semi-passive do have a battery but still need the power of the reader to transmit. Each of these three types of RFID tags still need a chip that contains the data of the identification [57]. The design also functions as a coil creating an inductance. Therefore it is expected that a demonstrator could be made by making an inductively coupled pair. This could be an interesting topic for future research.

3.5 Connectors

Apart from the antennas themselves, the connector elements for connecting the antenna to a feed line and measuring equipment turn out to be more important than initially expected. There are two types of connectors that are commonly used. The first being an SMA connector. This type would be preferable as the measuring and feeding equipment also makes use of it. The second type is a UFL connector. These have the benefit of being smaller than the SMA, making them the only option in certain situations. The downside is that because the rest of the equipment uses the SMA connector, a UFL-to-SMA convertor is required. This causes inaccuracies on the measurement because the device measures the impedance of the antenna, the connector and the converter. With the SMA connector, it would only measure the impedance of the antenna and the connector yielding a more accurate result. Both connector types are shown in Figure 31.

Figure 31: SMA and UFL connector [58]

There is also an option in how the connector is attached to the antenna. This can either be done by soldering the connector directly onto the antenna, or by using a conductive glue to glue it down. In this thesis, TPU and PET will be used as the substrate material. This means that soldering would not be an option as this would melt the substrate. A conductive glue would hereby be the only option.

3.6 Conclusion

This chapter shows the important parameters and design decisions that should be taken into account when designing an antenna. It is concluded that an antenna design is not a “plug-and-play” solution, and

that the parameters should always be optimised for a specific scenario. For example, the voltage standing wave ratio of the antenna should be below 2 in its range of operating frequencies.

To get the dipole working and to be able to test it, a balun should be added. The choice, connection and power supply of this balun will not be easy due to the limited time available and therefore it is decided not to focus on this antenna type further. The next chapters will only discuss the inset fed patch and RFID antenna. Physical demonstrators and antenna testing will not take place as the required measuring equipment (ex: anechoic chamber) is not available. It is therefore decided to change the focus on how the materials and elongation influence the antenna. This eliminates many practical problems and allows more interesting data to be obtained.

4 Antenna development steps

The previous chapter already explained some theory and important aspects to take into account. Because Fremach wants to know what is involved in the development of an antenna for an in-mold production process, this chapter will present a step-by-step plan. Each sub-section explains which step has to be taken, what is important and what theoretical knowledge will come up and is required during these steps. When choices have to be made they will also be explained, but the decisions will have to be made during the process or with the knowledge from the previous steps.

The first step is of course to choose what kind of antenna will be developed. Here, various software to simulate antennas will be discussed. Sub-section 4.2 shows the step of the material selection of the ink and substrate. Aspects like stretchability of the ink and wettability are the major topics here. Next in 4.3, two methods are explained to determine the shape that has to be printed to eventually obtain the desired antenna shape after it has been stretched. Finally, sub-section 4.4 lists the measurements and tests that the antenna has to undergo to characterize it. If these tests show that the antenna is unsatisfactory, it is necessary to go back through the step-by-step plan and make new adjustments.

4.1 Determine antenna design

As mentioned in 3.1, an antenna should not be taken out of literature and expected to work without further adjustments. After all, 5.1 already showed that the substrate and ink materials are influencing the conductivity largely. It is logical that this also influences other antenna parameters (e.g. relative permittivity of the substrate). That is why it is interesting to simulate the antenna in an electromagnetic analysis software or antenna simulation software before making a first physical prototype. Examples of these simulation software packages are: CST microwave studio, Ansys HFSS, FEKO or Sonnet. There are many more antenna simulation software packages available with each their own strengths and weaknesses. The goal is to make the right choice of software for the antenna that should be analysed, what parameters should be analysed and the trade-off between accuracy and speed that should be made.

CST is a software developed by *Dassault Systems*. For its calculations it relies on FIT (Finite Integration technique). The calculations are performed in the time-domain and then converted to the frequency-domain. This makes it useful for wideband analyses because otherwise the calculations would require too much memory and therefore take too long to compute [59].

The main difference with HFSS is that its calculations are performed by means of a FEM analysis in the frequency-domain. This makes it faster if the calculation has to be done on one (or a few) frequencies. The accuracy between these two simulation software packages is about identical when used correctly [60].

FEKO uses yet another method, namely the MoM (Method of Moments). Just like the FEM, MoM performs its calculations in the frequency-domain, but if the upper cut-off frequency increases, this method will take a lot longer. FEKO is ideal for sizing wire and planar antennas. Analysing other antennas is possible but will be slower. However, with the right settings MoM can deliver very accurate results [61].

Not only the solver is important for the calculation speed and accuracy. The mesh build-up also plays a major role. That is why it is always necessary to look at how the software builds its mesh. For example, CST uses PBA (Perfect Boundary Approximation) to better approximate the shape. Another technique that can be applied is for example combining triangular and quadrilateral elements in order to use fewer elements (and thus be able to calculate faster) but still obtain a high accuracy [62]. Figure 39 shows some different meshes consisting of triangular, quadrilateral elements or a combination of both. Notice that the mesh in the middle picture has fewer elements but reaches (almost) the same accuracy of the mesh of only triangular elements.

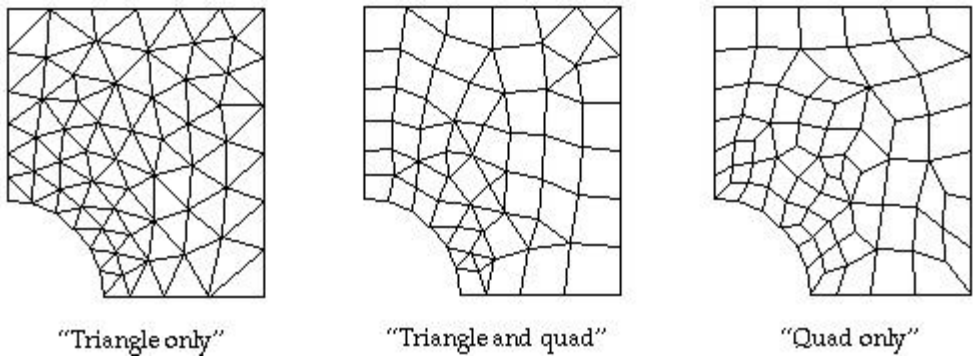

Figure 32: mesh out of triangular or quadrialteral elements and a combination of both [63]

The interface of CST and HFSS are user friendly. This makes it convenient to learn these packages. These are the most used antenna simulation software packages. Not every simulation software is equally suitable for every type of antenna, as mentioned earlier, FEKO is an interesting option for wire and patch antennas, but for others it is not suitable choice. Also CST and HFSS have their areas of expertise in which they work best and others for which they are not ideal.

Next to these specialized antenna simulation software packages, there are even smaller software packages that are often overlooked, but can be very interesting. Often the cost price of the licenses is lower as not all the features that the large specialised companies offer are needed. An example of this is Sonnet. This software is intended for electromagnetic analysis of electronics. It can be used to simulate antennas, but also for electronic filters or the analysis of the electromagnetic influences on a PCB. It can be said that programs like Sonnet are not as powerful as for example CST or HFSS. For example, the radiation patterns they give are not as accurate and are only given in their 2D form. Sonnet is not able to produce a 3D representation which is easier to read and more appealing for use in presentations for example [64]. Figure 33, Figure 34 and Figure 35 show the interfaces of CST, HFSS and Sonnet Lite.

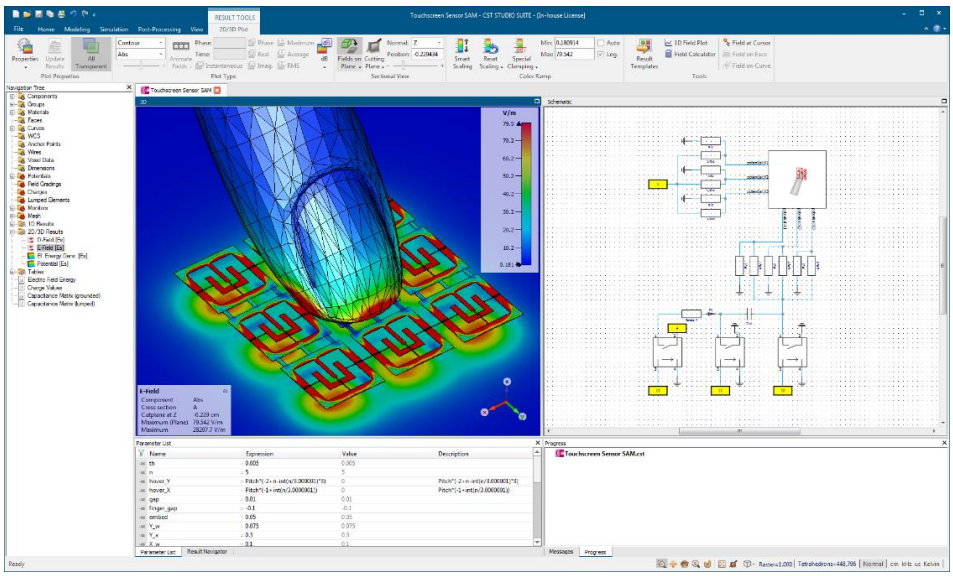

Figure 33: user interface of CST Microwave Studio

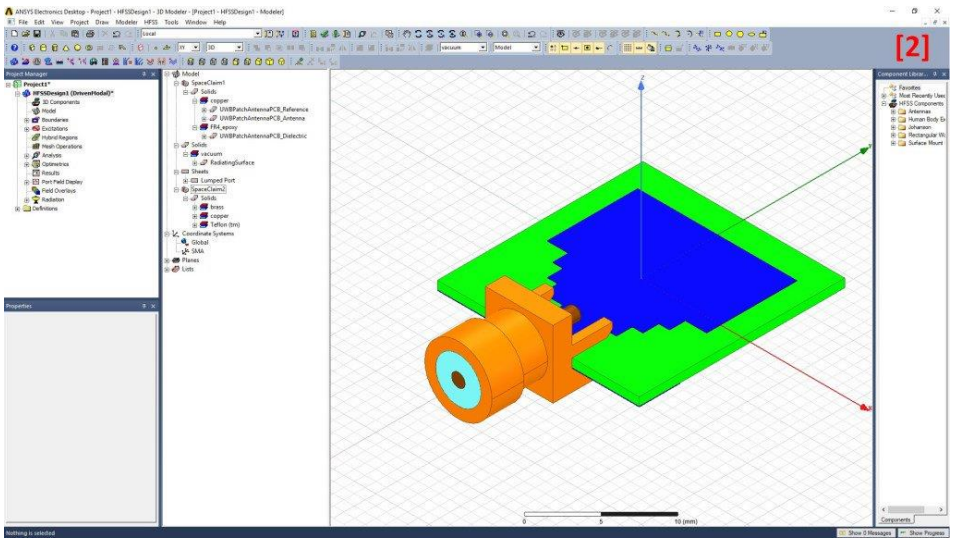

Figure 34: User-interface of Ansys HFSS

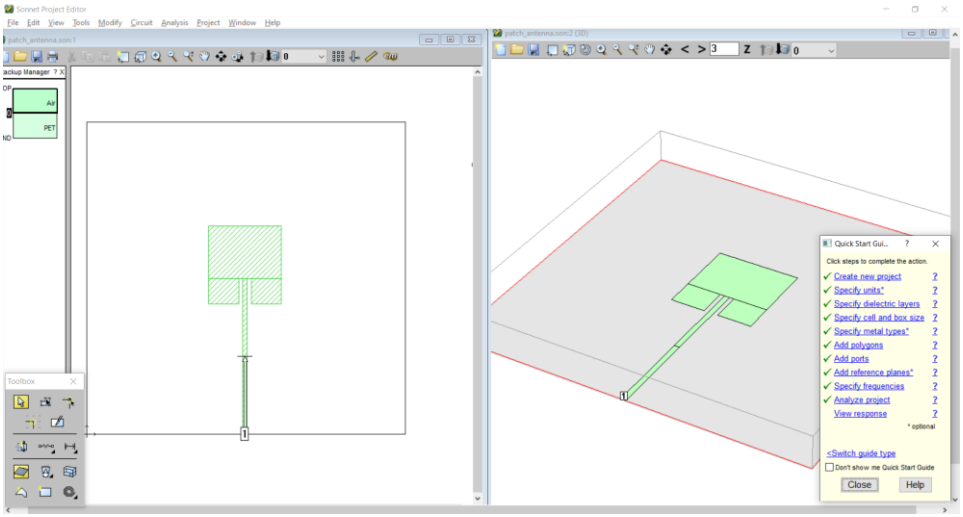

Figure 35: User-interface of Sonnet Lite

Figure 33, Figure 34 and Figure 35 already show that Sonnet Lite belongs to a different category of software than CST or HFSS. For example, less functions are available and less focus is placed on the appearance of the interface.

Before a simulation can be carried out, knowledge of some parameters is required. The dielectric constant from the dielectric substrate, the loss tangent and the thickness of the material need to be known. Note that when specifying the dielectric layers, each layer must be taken into account. For in-mold labelling for example, the injection moulded parts must also be specified, as well as air layers around the antenna. The dielectric parameters of these layers must therefore also be known. For the antenna itself, just like the substrate, some parameters need to be indicated to the software. The thickness and sheet resistance of the ink are the most important. Finally, the range of frequencies over which the antenna has to be simulated will have to be specified. For example, if it is desired to determine the reflection coefficient, it is useful to know at which frequency range the resonant frequency is roughly located so that the calculation time is not too high. Also the size of the mesh has to be determined in advance. The trade-off between accuracy and calculation time is important here. Which additional parameters have to be given for the calculation often depends on the software and how accurate the simulation has to be. For example, it can sometimes be necessary for some substrates to give a conductivity when they are slightly conductive, or a relative magnetic permeability. With the ink, the software can also take into account the current ratio. This is a ratio of the current flowing at the top of the conductive paths to the current flowing at the bottom. However, since the ink is only about 10 µm thick, the influence of this is often negligible.

4.2 Determine the choice of materials

When determining what materials are the best choice, it is important to understand why they behave the way they do. This can be the way the substrate and the ink interact with each other as shown in the experiments in chapter 5. This shows that the same ink behaves differently on different types of substrates.

4.2.1 Wettability of substrate

The first reason this happens is because of the wettability of the substrate surface. The wettability is the ability of a liquid to stick to a solid surface [65]. This is highly dependent of the surface free energy of the solid surface, the surface tension of the liquid and the interfacial free energy between the solid and the liquid. Figure 36 shows a schematic representation of the wettability principle.

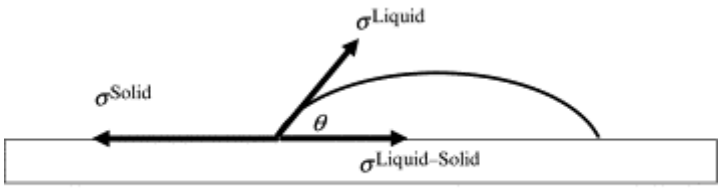

Figure 36: Schematic representation wettability [65]

Here, σ^{Solid} is the surface free energy of the solid surface, σ^{Liquid} is the surface tension of the liquid and $\sigma^{Liquid-Solid}$ is the interfacial free energy. Θ is the contact angle of the droplet to the surface. The wettability of a surface can generally be evaluated by looking at this contact angle. When it is lower than 90°, the wettability is generally seen as good. When the angle is larger than 90°, the wettability is suboptimal [65]. How large this angle is, is determined by the three properties named earlier. This can be expressed by the Young-Laplace equation:

$$\sigma^{Solid} = \sigma^{Liquid} \cdot \cos(\theta) + \sigma^{Liquid-Solid} \quad (15)$$

As the wettability is described as the ratio between the surface energy of the solid surface and the liquid, a high amount of surface free energy for the solid surface is generally desired. The surface energy of the solid should always be higher than the one of the liquid. An example of this would be painting on a greasy surface. The grease on the solid surface lowers the surface free energy making it harder for the paint to properly adhere. The surface roughness also plays a big role in the wettability of a surface. As found in [65], this is described by Wenzel's equation:

$$\cos(\theta') = r \cdot \cos(\theta) \tag{16}$$

Here, θ' is the apparent contact angle of the drop on the rough surface, θ is the contact angle the drop would have on a flat surface of the same material, and r is the roughness factor of the surface. Whether the roughness enhances or decreases the wettability of the surface depends on whether the flat surface is hydrophobic or hydrophilic. When the flat surface is hydrophobic in nature, adding a roughness r would enhance this hydrophobicity. The same goes for a hydrophilic flat surface. Making the surface more rough would further enhance the hydrophilic nature of the surface [65].

When it appears that the resistance of an ink on a substrate is too high, It can sometimes be enhanced by increasing the amount of surface free energy the substrate has. For polymers, this is done by using a so called *Corona treatment*. This treatment will alter the surface free energy of the substrate in an attempt to make it higher than the surface free energy of the ink. The process works by directing a high frequency electric discharge at the surface [66]. These discharges oxidise the long carbon chains that build the polymer splitting the carbon molecules, and ionises the oxygen in the air surrounding it. Some of these oxygen ions bond with the split carbon molecules of the surface creating carbonyl groups which give a higher surface free energy. It should be noted that the remainder of the oxygen ions form ozone, which is toxic and should be extracted. A schematic representation of this process is shown in Figure 37.

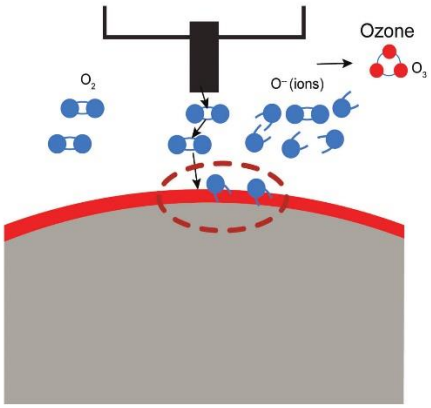

Figure 37: Schematic representation of corona treatment [66]

A corona treatment only effects the surface layer of the material. It can penetrates to a depth of about 0,01 μm [66]. The effect also fades away over time. A surface that is treated will not maintain its high surface free energy. For this reason, the treatment should be applied as close to the printing process as possible.

Figure 38 and Figure 39 show pictures of the corona treatment being used on TPU samples. Unfortunatly it was not possible to use and tests these samples due to reasons discussed earlier.

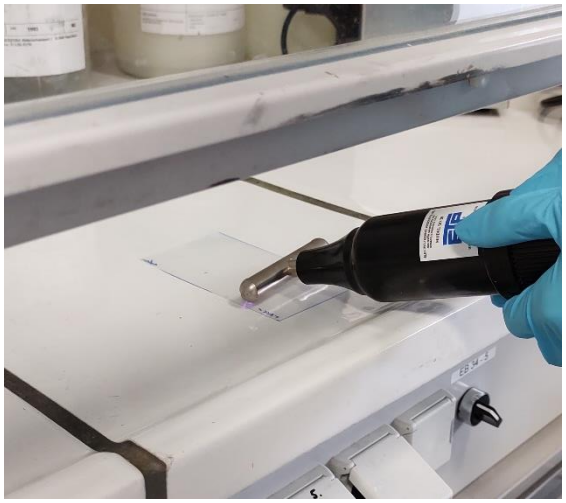

Figure 38: Real life example of corona treatment 1

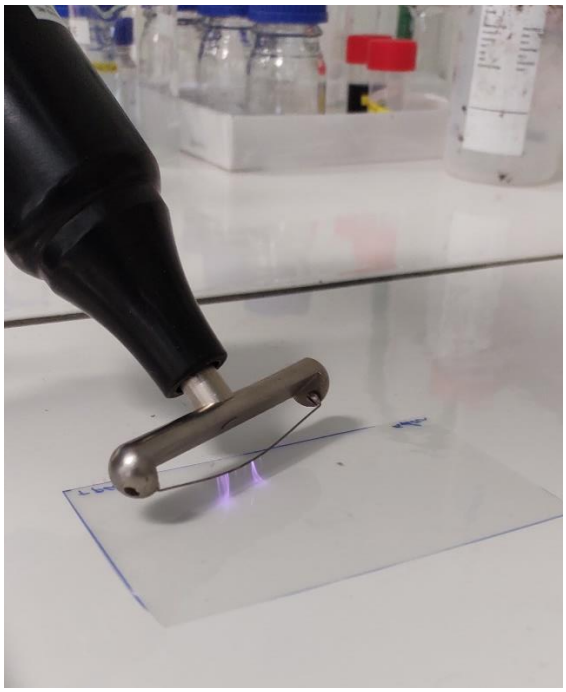

Figure 39: Real life example of corona treatment 2

Apart from the wettability of the substrate, other parameters should also be taken into account. The substrate has to be able to resist the curing temperature of the ink (120 °C for silver micro flake ink). It also goes without saying that for stretchable applications, the substrate also has to be sufficiently stretchable.

4.2.2 Structure of ink particles

Another way to look at how the inks behave is to look inside the ink materials themselves. The types of inks used are silver nano-particles, silver micro flakes and PEDOT:PSS as stated earlier. These have different structures that can also explain why they are (non)stretchable.

When looking at silver nano-particles, the ink is made up of tiny grain-like silver particles with a diameter of about 30 nm [67]. By curing this ink, these particles are sintered together at their point of contact. This is shown in Figure 40. Because these particles are so small, when the ink is cured, it forms a very dense printed silver layer with very little trapped air or other contaminations. The biggest advantage of this is that it reaches a very high conductive value. The downside is shown in its stretchabillity. As the grain-like particles are sintered together at their point of contact with each other, when the ink is stretched, these contacts simply break apart. This means that even with a very small amount of strain the conductive paths will quickly be broken.

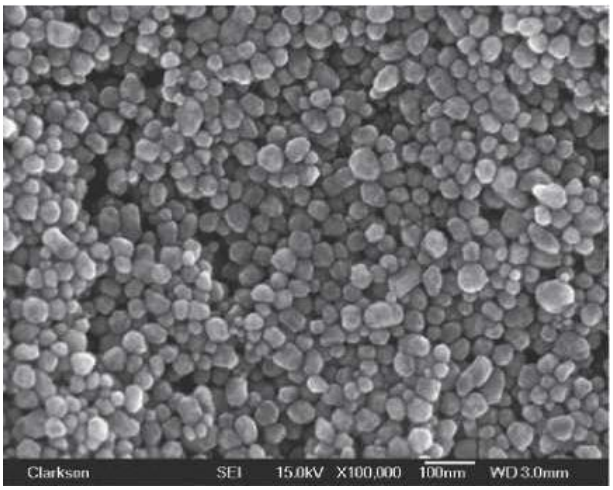

Figure 40: SEM image of silver nano-particles [67, p. 2494]

Silver micro flakes differ from the nano-particles in the shape of the particles found in the ink. Where the nano-particle ink was made up of tiny grain-like particles, the micro flake ink consists of tiny sheets of silver with an area of a few μm² (Figure 41) [68]. As these are bigger than the nano-particles, the layer that is made after curing is less dense with more trapped air and contaminations. This makes the micro flake ink less conductive compared to its nano ink counterpart. The advantage of using this ink over the nano ink is the way the micro flakes interact after the curing process. Whereas the nano-particles were sintered together at the point of contact, these flakes lay on top and over each other. When the ink is stretched, these have the ability to shear over each other remaining in contact. This means that even at higher levels of strain (15-20 %) these flakes can still form a conductive path by sliding and hinging over each other and accommodating a new configuration. This type of ink forms a better compromise between high conductivity and stretchability.

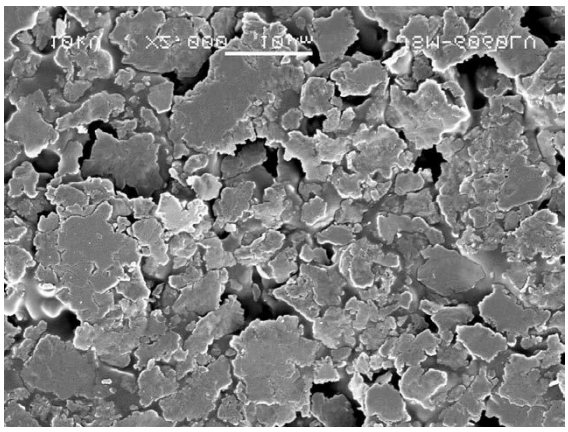

Figure 41: SEM image of silver micro flakes [68, p. 628]

PEDOT:PSS is known for its highly stretchable nature. This can again be explained by looking at the particles that make up the ink. Where the silver inks are made up of grains or flakes, the PEDOT is made up of long, flexible strands of PEDOT:PSS polymer (Figure 42) [69]. These strains can percolate, bend and intertwine with each other much like cooked spaghetti. When this ink is cured and the ink is stretched, the strands can move and relocate themselves while still remaining in contacted as they are tangled together. The conductive path will be broken when the strain becomes so large that the strands are fully straightened out and torn apart. This makes PEDOT:PSS highly stretchable at 100 % strain and above. Although PEDOT is a conductive polymer, its resistance is much greater than this of a silver based ink. Looking at the sheet resistance obtained with the silver micro flake ink this would be as low as 300 mΩ/sq whereas the PEDOT:PSS version of the same sample would reach up to 8 kΩ/sq. These results are found via practical experiments that will further be discussed in detail in chapter 5.

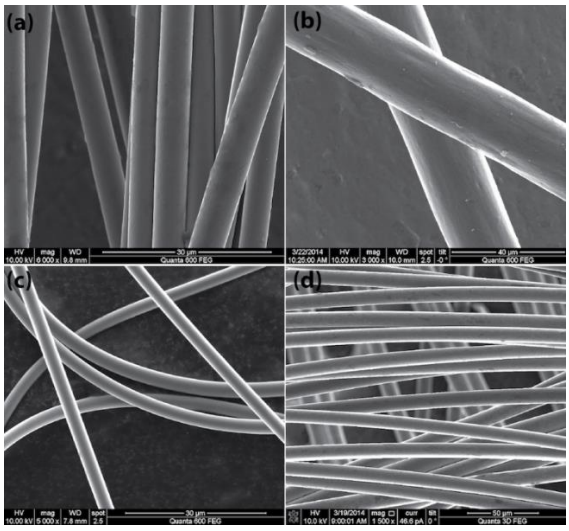

Figure 42: SEM images of PEDOT:PSS [69, p. 4]

4.3 Determine pre-stretch shape

After designing and simulating the antenna virtually and testing it with physical samples, a functioning antenna design is found. If the antenna does not perform satisfactory after deformation, a possible solution could be to print the antenna in an altered design that achieves the desired shape after it is elongated. The printed shape has to be able to compensate the deformation caused by the stretching during the vacuum forming process. To do this, a reverse engineering process is required to calculate this pre-stretched shape. This can be done with a physical or a virtual test. The information needed for the virtual test was obtained via a conversation with Dr. Ir. John Bijnens.

4.3.1 Physical test

The physical test uses a mesh with a large number of simple geometric shapes like squares that is stretched over the same surface that the antenna will be formed over. This causes the simple shapes to deform with it. Every square in the mesh can now be seen as a point of interest with its own deformation in its local X and Y direction. The reason the mesh is made up of simple shapes is because the deformation in the different directions is easy to calculate for each cell individually. This means that the deformation of the entire sample can be approximated by combining the deformation of the individual cells. It goes without saying that the more basic shapes the mesh contains, the better the approximation will be, as more basics shapes means a higher mesh resolution. This means more points of interest and more points with information about the deformation. This principle is shown in Figure 43.

After the forming process is completed, the shape of each cell is compared to its original shape before forming. This gives the information of the deformation of each cell individually. By using the acquired information, and overlaying the deformed mesh with the desired design, the design can be reverse calculated to find the required pre-stretched shape.

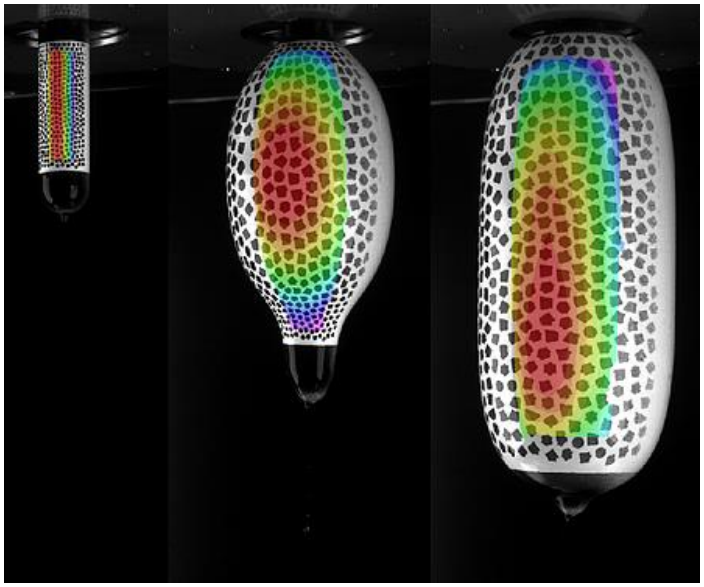

Figure 43: Principle of deforming mesh [70]

4.3.2 Virtual test

The virtual test uses a finite element package to simulate the process used in the physical test. This has the advantage over the physical test that this method does not required the development of samples or a test surface to form over. Fewer material has to be used compared to the physical test. The downside to using this process is that in order to have an accurate simulation, many different aspects have to be taken into account. This makes this technique more complex and difficult to use. If the parameters that are put into the simulation are wrong or missing, the results of the simulation will not be representable.

The first step for this technique after designing the desired shape, is calculating the desired amount of elongation. This value can then be put into the FEA software. When the elongation is known, a couple of different basic shapes are selected on which the FEA calculations will be done. The next step is to determine how the model should be constrained. This step is important as it determines how the model will react to the applied strain. When the chosen constraints are not correct, the outcome of the calculation will also be false. This step is made even more difficult by the different material properties of the ink and the substrate of the sample. These materials will react differently to the applied strain. Because both are connected, the stiffest of the two materials will determine how the other reacts. In some cases, this step can be neglected. When the substrate material has a high elasticity compared to the ink, the impact of the substrate material could be cast aside. This raises the question when the elasticity is high enough for it to be negligible. On the other hand when this parameter is taken into account, another set of questions arises. In this case, it is important to know what the "stickiness" and friction properties between the different materials are.

When these steps are completed successfully, the calculated elongation can be applied to the selected basic shape. At this point, another important question is posed: "Is the elongation applied in a plane, or is it applied over a curved shape?". In the latter, it is possible there are multiple different elongations in different directions.

After going through all of the above with one of the basic shapes, the process has to be redone using the rest of the earlier discussed basic shapes. When all these results are obtained, it is possible to work out an interpolation function between the dimensions of the original shape and the shape after the simulations are completed. With these functions, it is possible to determine the shape required to obtain the desired antenna design after elongation is applied.

4.4 Final characterisation

The last step is to test the antenna and check whether it meets the desired characteristic properties. If this shows that for example the efficiency is too low or that the antenna does not radiate far enough, some adjustments and design changes are required. In the following sub-sections common tests are discussed that are used to characterise antennas.

4.4.1 Reflection coefficient characterization

The reflection coefficient can be determined by connecting the antenna to a network analyser. These devices usually have 2 ports. The antenna is connected to port 1. The network analyser then measures the power that is reflected at port 1 and transmitted to the antenna at a range of frequencies. This is why the reflection coefficient is often referred to as S11. S12 would be the power emitted by port 1 and returned to port 2. Figure 44 shows an example of a network analyser. Notice the 2 ports on the device.

Figure 44: Example of a network analyzer by siglent [71]

If no network analyser is available, a measuring circuit can also be built. This requires a dual log detector, which can measure the forward and the reverse power to and from the antenna [72].

4.4.2 Efficiency, gain and radiation pattern measurement.

As already discussed in 3.1, antenna efficiency is the ratio between the power radiated by the antenna and the power supplied to the antenna. Efficiency decreases when there is a mismatch between the impedance of the transmitter and the antenna or when the power in the antenna is transferred to heat. This means that the efficiency of the antenna is always below 100 %, and the gain below 0 dB [73].

In addition to efficiency, the gain is sometimes also important for an antenna, but this is not discussed further in this thesis. In contrast to efficiency, a gain measurement takes the directional dependency of the antenna into account. Antennas can sometimes have a better efficiency in specific directions than in others and the gain measurement takes this into account. Antennas for GPS tracking, for example, are often direction-dependent and have better efficiency in the direction of the sky [73]. WIFI antennas such as the inset fed patch antenna on the other hand are not directional. Since the antennas on which this thesis focuses are not really specifically designed to have a higher efficiency in one direction (although the RFID does have this characteristic), the gain measurement is not discussed further in this thesis.

To measure the antenna efficiency, the antenna is placed in an anechoic chamber. In this chamber the antenna is activated. At some points of the chamber receivers are placed. These receivers measure the power. By accurately measuring how much power is supplied to the antenna and how much it emits, the ratio can be taken. This ratio is equal to the efficiency.

The anechoic chamber is not only used to characterise the final antenna. During development sometimes a measurement is done without the final transmitter to see how the intermediate design works. Based on the measurements, the designers can clearly see where in the antenna adjustments are needed. In the final measurements the transmitter needs to be brought in however. It has to be studied to identify if it causes interference with the antenna. On average, an efficiency of 50 – 60 % is obtained (which corresponds to approximately -3 to -2,2 dB) [73]. Figure 45 shows a radiation pattern of a dipole.

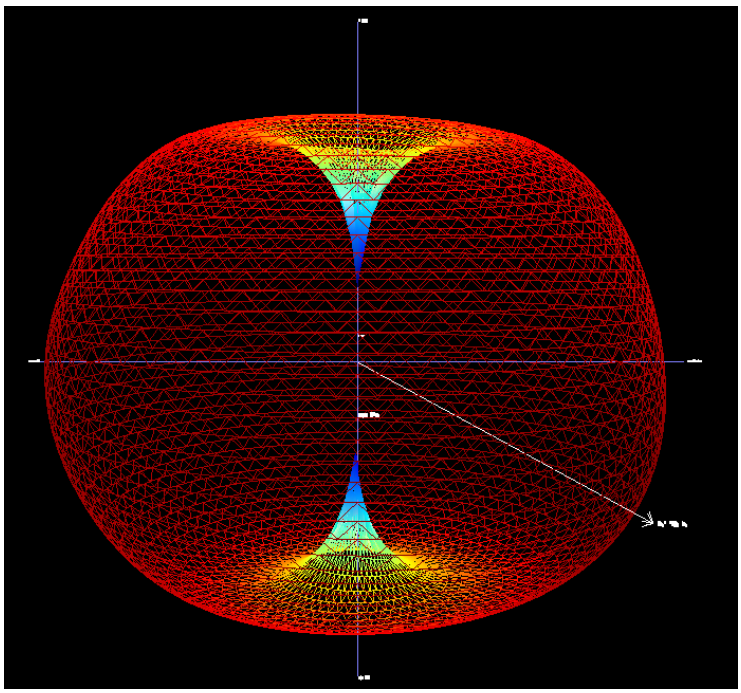

Figure 45: radiation pattern of a dipole antenna [73]

The radiation pattern of Figure 45 shows that the efficiency goes to zero on the vertical axis. However, this is mostly not a problem because this area is very narrow. Therefor it is not important to do a gain measurement but rather just an efficiency measurement.

The anechoic chamber is constructed as follows: a stand is placed in the middle on which the antenna and transmitter are placed and directed. The antenna can be rotated so for the measurement of the gain, the antenna can be measured from all the different angles. The size of the chamber influences what is the lowest possible frequency that can be measured. The lower the frequency, the longer the wavelength. If the wavelength is too large, the receivers cannot detect it properly anymore. For very low frequencies, very large anechoic chambers are necessary [74].

The outside of the chamber is covered with conductive material. This creates a Faraday cage and stops all radiation from the outside world from entering so that it cannot influence the measurement in the chamber. Authors in [74] compare it to measuring a flashlight. If you want to measure the shape of the glow of a flashlight, you must also use light detectors and will perform this measurement in a dark place because otherwise the light from outside sources (the sun for example) will disturb the measurement. On the inside, the anechoic chamber is covered with material that absorbs electromagnetic waves. An often used material for this is carbon loaded foam. When looking at the example of the flashlight again, measuring the shape of the glow is also not possible if the surrounding walls consist of mirrors. These will cause the light to reflect and be detected several times. For the same reason, preventing the reflection of electromagnetic rays against the walls is important for an accurate reading of the antenna. By applying pyramids made of carbon loaded foam, the reflection on the walls decreases to 0,1 – 1 % [74]. Figure 46 shows the inside of an anechoic chamber, notice the foam pyramids on the walls and their black tips from the carbon inside.

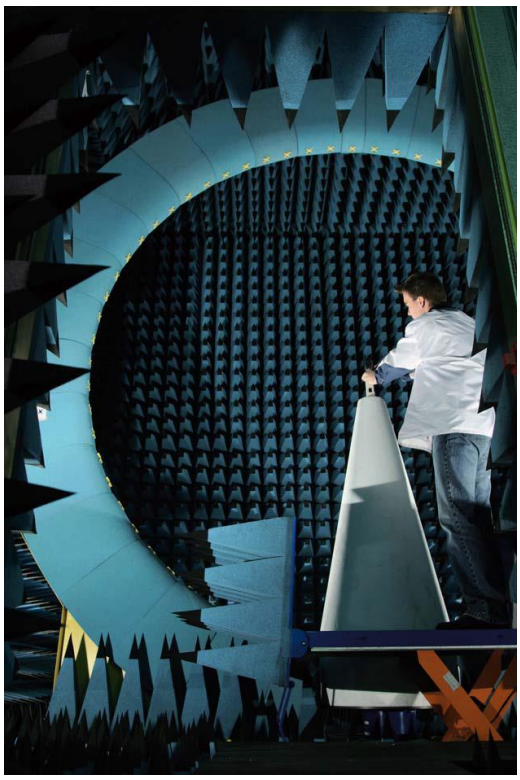

Figure 46: Example of the inside of an anechoic chamber [73]

4.5 Conclusion

Chapter 4 describes the most important steps and choices that need to be taken when developing a stretchable antenna. It can be concluded that sufficient knowledge of the scenario is required before simulations can take place. Often parameters such as the loss tangent of the substrate are not known and require additional measurements.

When choosing the ink, a balance must be made between stretchability and conductivity. PEDOT:PSS is highly stretchable and its conductivity remains quite constant when elongated. But its conductivity is low meaning that for many applications PEDOT:PSS is a difficult material to use. An ink made of silver nano-particles on the other hand has a high conductivity, but is only stretchable for a few percentages at best, so its conductivity decreases drastically even at low elongations. Silver micro flake ink therefore appears to be a promising choice as a combination of high conductivity and relatively good stretchability. The focus will be put on this ink in the further chapters. However, the other inks are not immediately written off yet because it is interesting to compare them and if possible still implement them.

For the selection of the substrate material, the wettability of the surface has proven to be important. Therefore, experiments will be needed to determine how the ink behaves on the surface. If it turns out that the substrate causes the resistance to become too high, perhaps the wettability of the substrate can be increased with a corona treatment. However, when choosing the substrate, some other practical problems that may occur should also be taken into account. For example, the substrate must be able to withstand the temperature at which the ink has to be cured and must be thermo or vacuum formable.

Two ways are also presented to determine the shape that has to be printed so that the antenna has the desired geometry after it is stretched. The first presented method determines the elongation experimentally. This method is the simplest as it takes the influence of the ink and the adhesion into account, but it does not give numerical data and is also less flexible when making adjustments. The second method uses an FEA method and is more difficult. The set-up of the model is cumbersome

because the knowledge of how the ink and substrate will react during stretching and what their influences are on the elongation has to be present. Of course, there must also be a FEA software available and knowledge of how to use it.

Finally, it is listed what properties of the antenna should be characterised. For example, the reflection coefficient and bandwidth should be determined using a network analyser. The radiation pattern is found by using an anechoic chamber. Not all measurements are always necessary, this depends on the type of antenna. The RFID antenna can for example already be fully characterised with a reflection coefficient measurement and impedance measurement so no anechoic chamber is needed for this type.

5 Material configuration for stretchable antenna development

To see how the different combinations of materials for substrates and inks behave when strain is applied, samples are made of the different possible combinations. In 5.1 tests are carried out without stretching, because here the interaction of ink and substrate is studied. In 5.2 the influence of the elongation that will occur during a forming process on the sheet resistance is tested.

Due to the outbreak of the COVID-19 (corona virus), most of the testing phase was cut short. Therefore only limited practical results could be obtained. This results in a more theoretical approach than originally planned.

5.1 Influence of ink and substrate on resistance without elongation

As a first step, it is interesting to look at different possible combinations of substrates and inks to see how these react without applying elongation. The data resulting from these tests can be used as a first method to rule out certain materials. For these tests, the RFID antenna design is chosen. As this design is one long connected pathway, it can be measured using a regular ohm meter as a first test. However, when using a two-point measurement like this, the resistance of the cables is also measured. To obtain more accurate results, a four-point measurement technique like the Van der Pauw method [75] should be used as these measurements are unaffected by the resistance of the cables. Such a sample is shown in Figure 47.

Figure 47: Silver micro flake RFID antenna

First, the influence of the substrate on the DC resistance of the RFID antenna will be examined. The screen printed DuPont's ME602 micro flake ink is used for this as it is expected to have a relatively high conductivity and still be able to withstand a certain elongation. These tests will be repeated with screen printed Orgacon's SI-P2000 silver nano-particle ink. Next, 5.1.2 discusses the influence of multiple layers of ink on the conductivity of the antenna. Finally, in 5.1.3 the same RFID antenna is printed with a screen printed Heraeus Clevios S V4 PEDOT:PSS ink and its conductivity will be examined.

In the following paragraphs, PET and different types of TPU foils are used as substrates. The reason multiple TPU types are used is because the different types differ in surface free energy, meaning the same ink can react differently on the different types of TPU. The different TPU types (numbered from 1 to 5) and PET can be seen in Figure 48

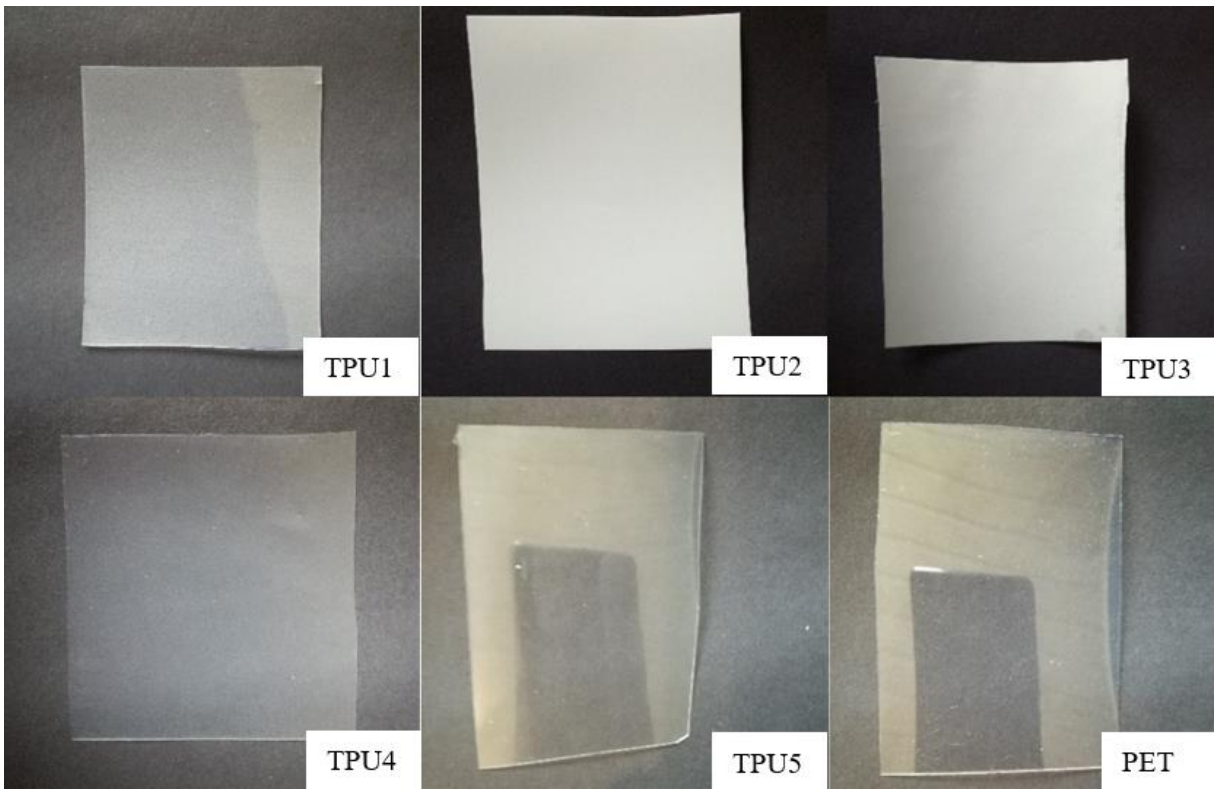

Figure 48: Upper row (from L to R) TPU1, TPU2, TPU3, Lower row (from L to R) TPU4, TPU5, PET

5.1.1 Influence of the substrate on the resistivity of the RFID with silver inks

RFID with ME602

First, DuPont ME602 micro flake silver ink was used on the different types of TPU and on PET substrates. The results of these samples are shown in Table 5. It was later found out that the samples made for TPU2 were printed on the supporting backing material instead of the TPU, making these measurements non-representative. This is why they are included in the measurement results, but are crossed out. These results were obtained using a two-point resistance measurement. The measurement cables play a detrimental role in the obtained results as explained earlier. This is why these results give a first impression. For more accurate results, a four-point measurement should be used.

Table 5: Resistance ME602 RFID on different substrates

TPU1	**Electrical resistance [Ω]**
1	209,1
2	193,7
3	214,0
4	187,1
5	214,0
TPU2	**Electrical resistance [Ω]**
~~1~~	~~495,5~~
~~2~~	~~854,0~~
~~3~~	~~400,9~~
TPU3	**Electrical resistance [Ω]**
1	Overload
2	Overload
3	Overload
TPU4	**Electrical resistance [Ω]**
1	Melted
2	Melted
3	Melted
TPU5	**Electrical resistance [Ω]**
1	159,9
PET	**Electrical resistance [Ω]**
1	793,0

Figure 49 shows the averages of the data from Table 5. This diagram aims to show the influence of the substrate.

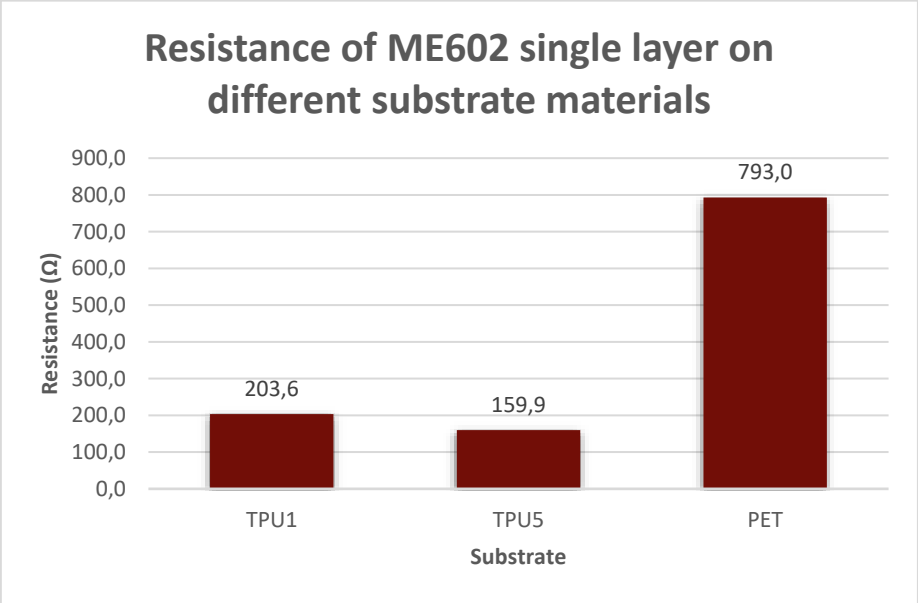

Figure 49: Mean resistance for ME602 single layer on different substrate materials

Four out of the five TPU types have a protective backing that is glued to the TPU which can be removed after printing and curing of the ink is done. TPU4 does not have this backing causing it to melt when trying to cure the ink at the required 120 °C. Therefore TPU4 is eliminated and not discussed further. It can be concluded that the substrate has a significant influence on the resistance of the antenna. It should be noted that these results are used as a first impression. For more exact results, a more accurate and extensive measuring technique is required.

RFID with Orgacon SI-P2000

Lastly, these tests were performed with Orgacon SI-P2000 silver nano-particle ink. TPU4 was left out in these tests as it was already proven that this material would melt when trying to cure the ink, seeing as the curing temperature for the Orgacon ink is even higher at 150°C. Again, the prints for TPU2 were made on the wrong side of the foil, making these results invalid. The results are shown in Table 6. When comparing the results of the Orgacon SI-P2000 on TPU1 with the DuPont ME602 on TPU1, it can be observed that the Orgacon ink achieves higher conductivity. It also shows more overload values than the ME602 ink. Although the achieved resistance values are lower for the Orgacon ink, it appears that it is less compatible with the given TPU substrates. Due to the many overloaded values, a visual representation using the mean values of each TPU sample set would not give an accurate view. Although many of the measured values return as an overload, this ink is not eliminated from further examination, because of the same reasoning as PEDOT. The material might react better when a design with bigger, less complex areas is chosen.

Table 6: Resistance of Orgacon ink on different substrates

TPU1	**Electrical resistance [Ω]**
1	70,2
2	65,3
3	53,1
4	57,6
5	67,9
6	Overload
7	46,5
8	Overload
9	Overload
10	Overload
TPU2	**Electrical resistance [Ω]**
~~1~~	~~52~~
~~2~~	~~46,5~~
~~3~~	~~56,8~~
~~4~~	~~41,7~~
~~5~~	~~40,1~~
TPU3	**Electrical resistance [Ω]**
1	Overload
2	Overload
3	Overload
4	Overload
5	449,2
TPU5	**Electrical resistance [Ω]**
1	Overload
PET	**Electrical resistance [Ω]**
1	35,5

After curing and looking at the samples, it is observed that the TPU1 samples using Orgacon show crack formation along its conductive path, This is also the case for TPU5 with fewer but wider cracks. Figure 50 shows an example of a sample of the Orgacon SI-P2000 ink on a TPU1 substrate. There are many small fractures in the upper and lower paths. Figure 51 shows the cracks on the TPU5 substrate.

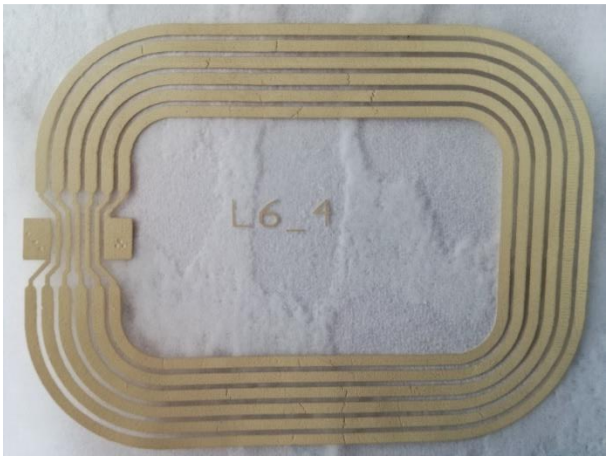

Figure 50: Crack formation on conductive paths; Orgacon ink on TPU1

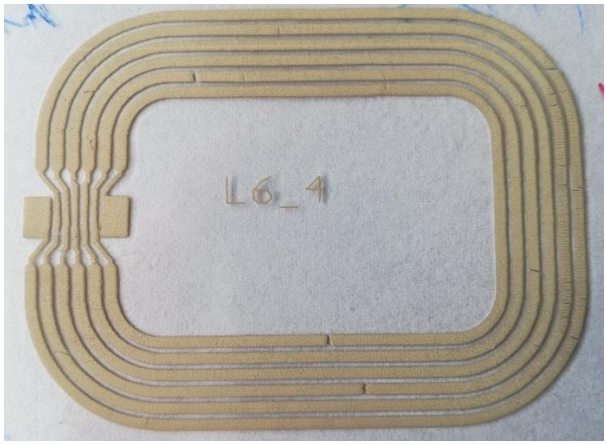

Figure 51: Crack formation on conductive paths; Orgacon ink on TPU5

Although TPU3 does not show any signs of cracking, the combination still does not appear to work. This could be explained with the formation of a lot of tiny microcracks which cannot be seen with the naked eye. Another explanation could be the wettability of the substrate. These explanations are only suggestions and should be examined further.

5.1.2 Influence of the number of layers on the resistivity of the RFID with silver inks

To see what the influence of the layer thickness would be, ME602 was again printed on TPU1 printing multiple layers on top of each other. Here, samples were made with two, three and five layers stacked. The results are shown in Table 7 with a visual representation in Figure 52.

Table 7: Resistance of ME602 on TPU1 with multiple layers

Sample nr.	# Layers	Electrical resistance [Ω]
1	1	209,1
2	1	193,7
3	1	214,0
4	1	187,1
5	1	214,0
6	2	88,0
7	2	106,2
8	2	91,0
9	2	121,3
10	2	81,9
11	3	55,5
12	3	52,8
13	5	50,2

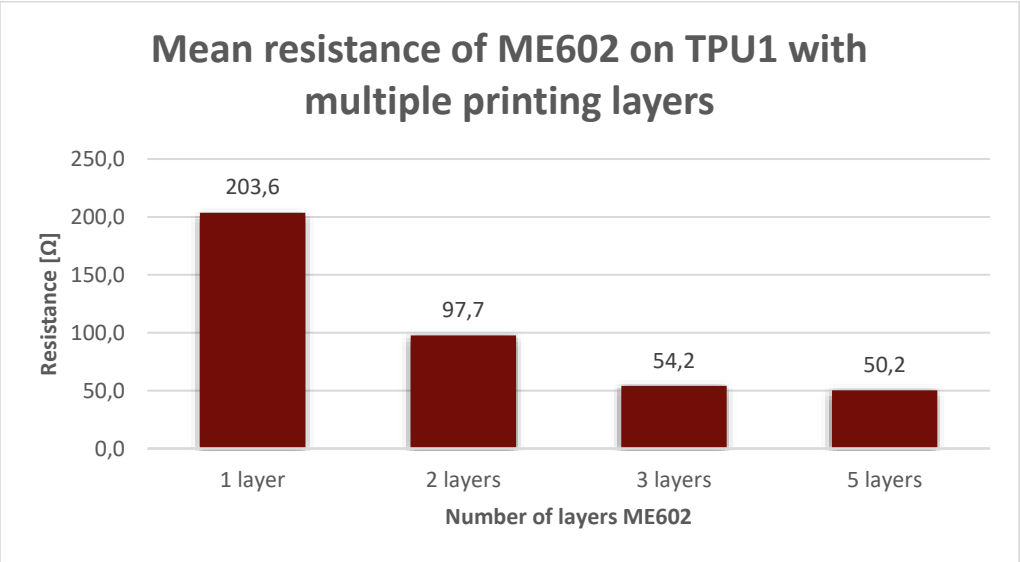

Figure 52: Mean resistance of ME602 on TPU1 with multiple printing layers

Figure 52 shows that increasing the amount of printed layers by one decreases the resistance by ±50 % till three printing layers. Printing more than three layers on top of each other with this ink does not show any further improvement. It is important to note that the layers were applied immediately after each other and not sintered in between because the printer does not allow this.

5.1.3 PEDOT:PSS printed RFID

For the next set of tests, PEDOT:PSS was used. The ink used was the PEDOT:PSS Clevios SV4 screen printing ink from Heraeus. This however always returned an overload value on every substrate. Increasing the number of print layers was not enough to get a readout. This is probably due to the thin and long design of the conductive path for this antenna design. Another reason why the PEDOT:PSS samples are not successful could be because the screen that is used during printing is optimised for silver-based screen printing inks like the ME602 ink. As the viscosity of the Heraeus PEDOT:PSS ink is lower, a different screen with smaller diameter openings could yield better results. PEDOT:PSS ink might still be an interesting option with a different type of antenna or when the antenna is inkjet printed. This is why PEDOT is not ruled out as a material, but it can already be observed that the conductivity of PEDOT:PSS will be low.

Figure 53 shows one of the samples that was printed with PEDOT:PSS. The antenna is barely visible because of the transparency of the PEDOT:PSS as stated before.

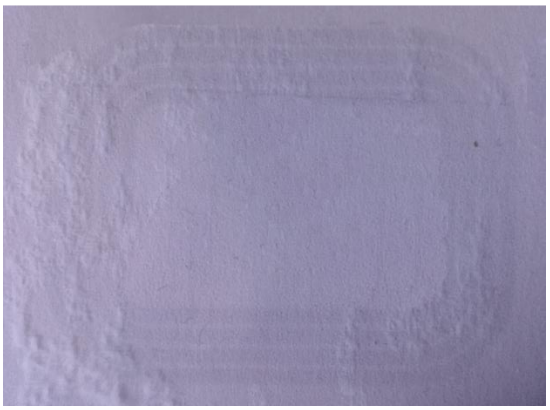

Figure 53: PEDOT:PSS RFID antenna

5.2 Influence of ink and substrate on the resistance under elongation

After the first measurements without stretching the antenna, it is now interesting to see how the samples react to elongation. The inset fed patch antenna is used for these experiments instead of the RFID antenna. The first reason for this is to obtain more accurate results of the sheet resistance by using the four-point Van der Pauw method as explained earlier. These measurements are easier to perform on the large, square surface area of the patch antenna. The second reason is that the screen used for printing this design was not yet available when performing the tests on the RFID antenna design. The last reason is that the different levels of elongation are easier to achieve by hand with the inset fed patch design.

First off, the ME602 ink from DuPont was tested by printing the inset fed patch design on TPU1. Afterwards, samples were stretched up to 10, 15, 20, 25 and 30 % elongation. For all of these samples the sheet resistance was measured (Table 8) using the Van der Pauw measuring method. The averages of these measurements are plotted in Figure 55 to give a better look at the shape of the curve. Figure 54 shows the deformation of the antenna when it is stretched up to 30 %.

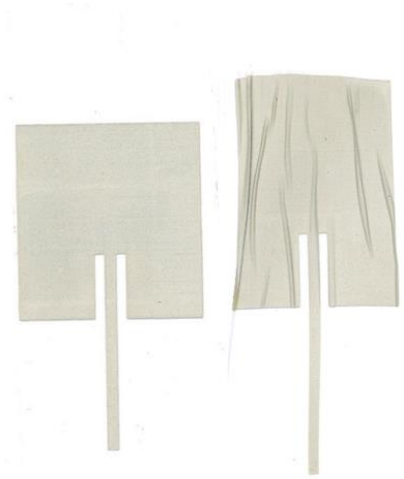

Figure 54: Left: unstretched right: 30 % stretched patch antenna

Table 8: Sheet resistance in function of elongation of ME602 on TPU1

	0 % strain [Ω/sq]	**10 % strain [Ω/sq]**	**15 % strain [Ω/sq]**	**20 % strain [Ω/sq]**	**25 % strain [Ω/sq]**	**30 % strain [Ω/sq]**
1	0,283	0,350	0,572	0,659	1,73	8,06
2	0,338	0,490	0,532	0,711	2,96	4,93
3	0,317	0,787	0,805	0,753	1,72	21,8
4	0,314	0,619	0,739	0,704	1,63	/
5	0,302	0,706	0,610	0,612	2,23	/
Average	0,311	0,590	0,652	0,688	2,054	11,597

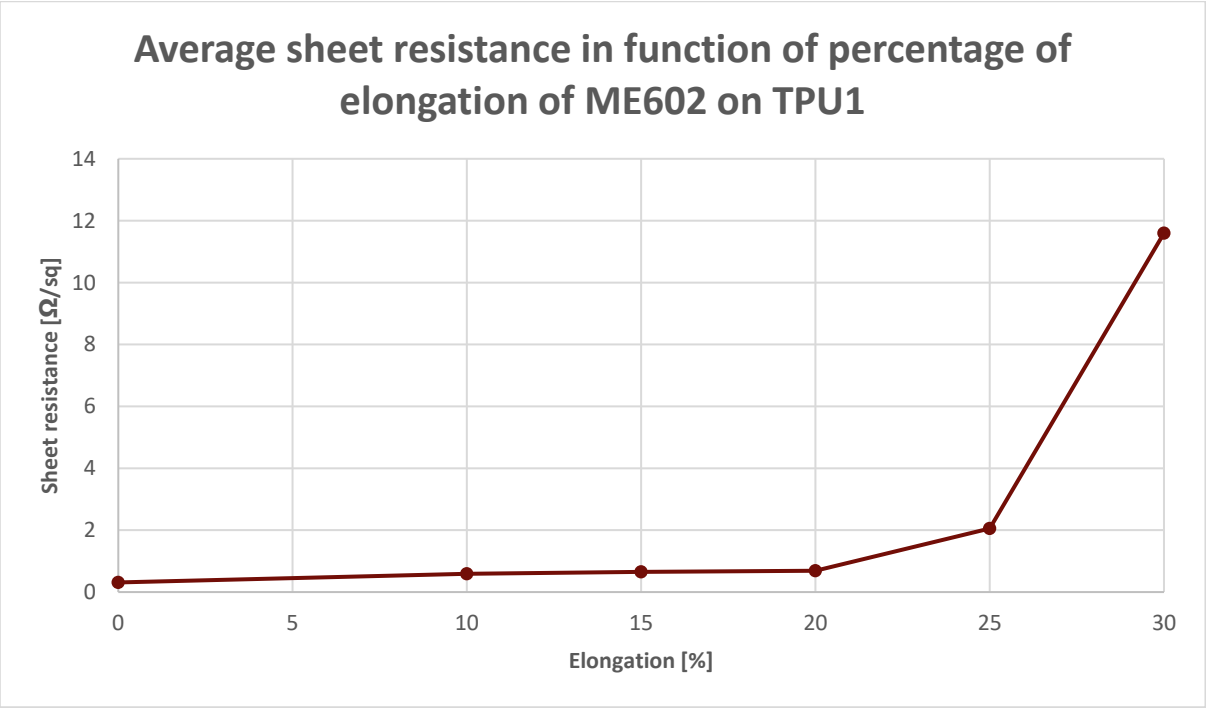

Figure 55: Average sheet resistance in function of elongation of ME602 on TPU1

It is visible that the combination of ME602 and TPU1 gives almost no change in sheet resistance up to 20 % elongation. At 25 %, the results start to differ. The resistance has increased by ±1 Ω/sq but it remains relatively consistent over all samples. At 30 %, the measurements start drifting apart. By this test, it appears that this ink-substrate combination can be used for stretching up to 20 – 25 %.

These tests are repeated on the TPU2 film to test the influence of the substrate. Before testing the TPU2 samples with Van der Pauw, it is already observed that this combination seems to be less compatible than the first. Samples already show more cracks and appear to have a higher resistance when measured with an Ohm meter. These samples were only stretched up to 15 % due to time constraints. The results from the Van der Pauw measurements are shown in Table 9 and Figure 56.

Table 9: sheet resistance in function of elongation of ME602 on TPU2

	0 % Strain [Ω/sq]	**10 % strain [Ω/sq]**	**15 % strain [Ω/sq]**
1	1,21	0,808	4,51
2	2,85	2,02	1,03
3	1,15	0,663	1,47
4	2,21	0,850	/
5	0,453	0,720	/

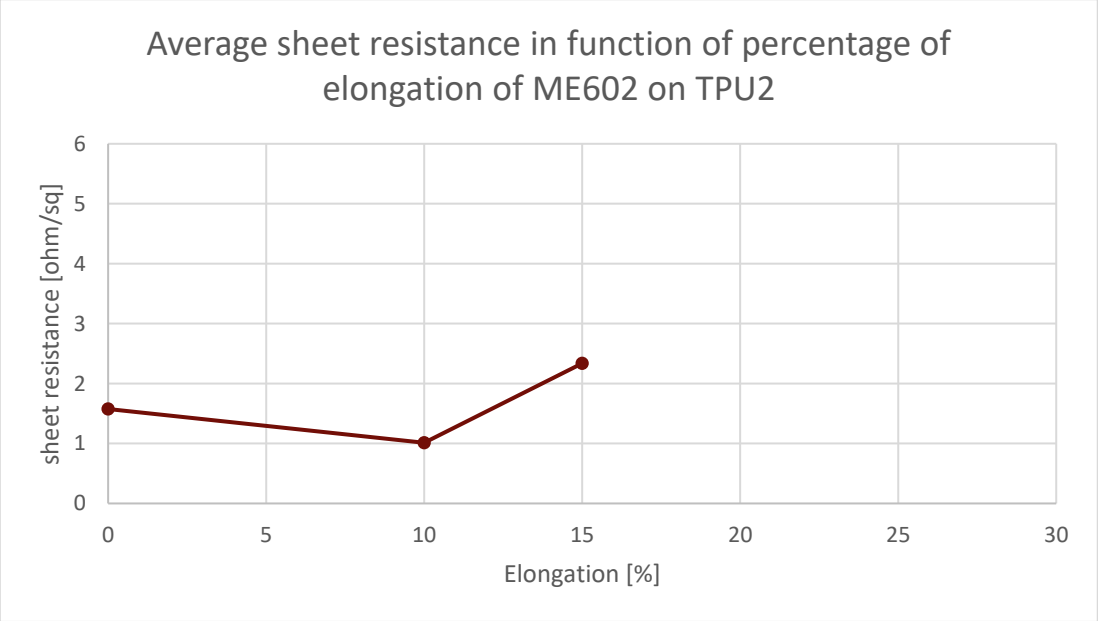

Figure 56: Average sheet resistance in function of elongation of ME602 on TPU2

5.3 Conclusion

The substrate material shows to be an important influencing factor on the resistivity of the printed layer. It is not yet possible to conclude which substrate material would be the best for the substrate combination tests on the RFID. Further tests are needed with more samples and where the resistivity is measured with a Van der Pauw measurement. However it can be noted that without any extra adaptations PET shows to be less compatible with the ME602 ink and more compatible with the SI-P2000 ink.

The importance of the ink-substrate compatibility can also be derived from the crack formation of the nano-silver inks after they are cured. It is expected that these nano silver inks shrink a bit and do not adhere well with the substrate during the curing process, which results in cracks in the RFID paths. That is why it is expected that the silver micro flake ME602 ink shows a higher potential. Although it does not achieve the lowest resistance compared with the nano silver inks, it does remain functional after curing.

The experiments further show that lower resistance values can be achieved with the micro flake ink by printing multiple layers on top of each other. These experiments show that after three layers, the decrease of the resistance becomes negligable. It is uncertain however how this thicker printing layer would react when stretched. It might start cracking faster than a single layer print. Further tests are needed to check this influence.

From the tests with the Clevios SV4 Heraeus ink, PEDOT:PSS does not seem like a viable ink option. This might be due to the design of the antenna. Nevertheless, PEDOT:PSS has a very high resistance value that will make it difficult to utilise for antenna purposes. Because of the high stretchability of PEDOT:PSS, however, it is not ruled out for further experiments.

The tests where the sheet resistance is measured in function of the stretch of the ink show that the ME602 ink on TPU1 was stretchable to approximately 20 – 25 %. It is not possible to determine to which stretch percentage the resistance of the ME602 on TPU2 remains constant. More samples and tests are needed for this. However it can be concluded that the resistivity of the ME602 is higher on TPU2 than on TPU1. When these results are combined with the knowledge of chapter 4.2, this can be explained. Because the results with TPU1 are better, it is expected that this TPU variant has a better wettability and thus a higher surface free energy than TPU2, making the printed silver ink layer stick better to the surface and form a more uniform layer. Further tests on the wettability of the substrate would be needed to validate this conclusion.

6 Antenna simulation in Sonnet Lite

As the required equipment (anechoic chamber etc) is not available, making physical prototypes and demonstrators is not worthwhile. To gain in depth knowledge and results of the proposed antenna designs and to study their behaviour under elongation, the antennas are modelled and simulated using Sonnet Lite. As explained in 5.1, Sonnet is an electronics simulation software with a free lite version that can be used to do virtual tests. The amount of features that can be utilised is limited without a paying license. An additional limitation is that the file size of the simulation model cannot be larger than 32 Mb. With the Sonnet simulations, information on the resonant frequency, S11 parameter and VSWR of the antenna can be found.

The first step when using Sonnet is to define the dielectric material that is used as the substrate material. TPU is chosen to stay as close to the physical experiments as possible. The data required for this is found in [76]. As it is unknown what type of TPU is used in the physical experiments, the average of the parameters of the different types of TPU BASF offers is used. The parameters that should be used in sonnet are the relative permittivity (ε_{rel}) and the dielectric loss tangent (loss). The values used for these parameters are shown in Table 10.

Table 10: Average values of important dielectric parameters of TPU

Parameter	Value
ε_{rel}	5,57
Loss	0,0790

PET will also be used as the dielectric material. This material is included in Sonnet's database and can be used immediately. The dielectric parameters of PET are shown in Table 11.

Table 11: values of important dielectric parameters of PET as given by Sonnet

Parameter	Value
ε_{rel}	3,37
Loss	0,0208

After the dielectric material, the ink should also be defined. The goal here is again to stay as close to the physical experiments as possible by trying to mimic the DuPont ME602 ink in Sonnet. For this, only the layer thickness and sheet resistance are required. The sheet resistance can be found in Table 8. By simulating the antenna with the given sheet resistance with different substrate thicknesses, it is attempted to find the substrate thickness at which the antenna will work optimally. Next, by simulating the antenna with different thicknesses for the ink layer, it is examined if there is an optimal ink layer thickness for the antenna.

6.1 Simulation setup

6.1.1 Inset fed patch antenna

As mentioned, the file size of the model cannot be larger than 32 Mb. This poses no problem for the inset fed patch antenna design. Thanks to its simple, square geometry, the antenna is easy to mesh with square mesh elements as depicted in Figure 57. This keeps the amount of elements low, allowing a file size that remains under the 32 Mb limit.

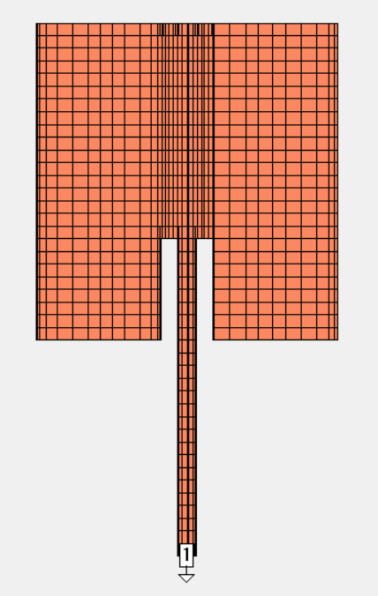

Figure 57: Mesh of inset fed patch design in Sonnet

Before looking at the different levels of elongation, it is interesting to look at the effect of the thickness of the ink layer and the substrate layer. As it is unknown what the exact thicknesses are, it is useful to simulate what the effect would be.

To start, the influence of the ink layer thickness is tested. This is done by simulating the inset fed patch design and only changing the value of the layer thickness in between simulations. The results of these tests are shown in Table 12. These results are also shown in form of a graph in Figure 58. The graph is only given for a thickness of 5 µm as the results show little to no difference when the layer thickness increases. This indicates that because the ink layer is sufficiently thin, the layer thickness of the ink does not influence the working of the antenna.

Table 12: Influence of ink layer thickness on inset fed patch

Thickness [µm]	Res freq [GHz]	S11 [dB]
5	2,34	-4,06
10	2,34	-4,06
15	2,34	-4,15
20	2,34	-4,18
25	2,28	-4,20
30	2,28	-4,19

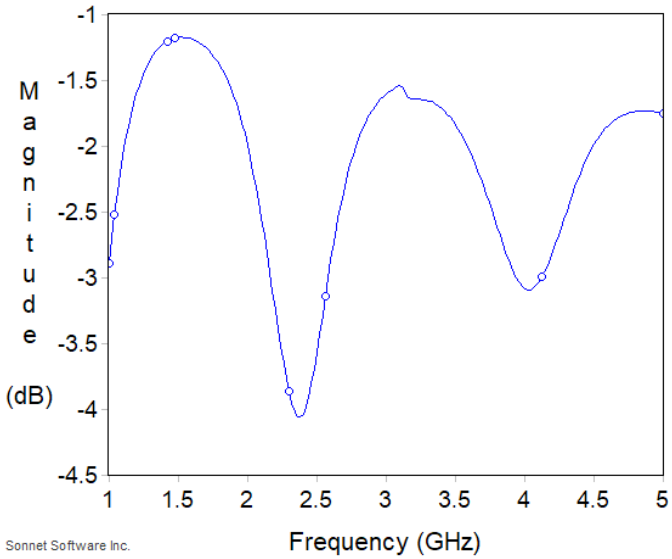

Figure 58: S11 in function of frequency for a 5 µm ink layer and 100 µm dielectric layer for patch

Next, the thickness of the substrate material is tested. This is done in a similar fashion as the ink layer thickness. In between simulations, only the thickness of the substrate material will be changed. This is done for both TPU and PET to find if there is an optimal thickness for each material and if the thickness influences the resonant frequency of the antenna.

The results for TPU are shown in Table 13. When the thickness of the substrate increases, the resonant frequency will shift to a higher frequency (Figure 59). From 100 to 200 µm, the frequency will increase less each time. After 200 µm the increase shows a linear behaviour. When looking at the VSWR and reflected power, it can be observed that there is a minimum at 320 µm (Figure 60). At this point, no power gets reflected back from the antenna. This means that the input impedance of the antenna matches the output impedance of the transmitter. In sonnet, the value of the output impedance of the port is set to 50 Ω.

Table 13: Results of varying substrate thickness on resonant frequency and reflected power using TPU for patch

Thickness [mm]	Resonant freq. [GHz]	S11 [dB]	VSWR	Reflected power [%]
0,100	2,34	-4,06	4,38	39,47
0,150	2,42	-7,28	2,54	18,92
0,200	2,46	-11,31	1,75	7,44
0,250	2,48	-17,06	1,33	1,97
0,260	2,48	-18,61	1,27	1,37
0,270	2,49	-20,33	1,21	0,93
0,280	2,49	-22,56	1,16	0,55
0,290	2,5	-25,02	1,12	0,31
0,300	2,5	-29,15	1,07	0,12
0,310	2,51	-33,93	1,04	0,04
0,320	**2,51**	**-54,42**	**1,00**	**0,00**
0,330	2,51	-33,57	1,04	0,04
0,340	2,52	-29,00	1,07	0,13
0,350	2,52	-25,82	1,11	0,26
0,400	2,54	-18,24	1,28	1,50
0,450	2,56	-14,88	1,44	3,25
0,500	2,58	-12,94	1,58	5,09

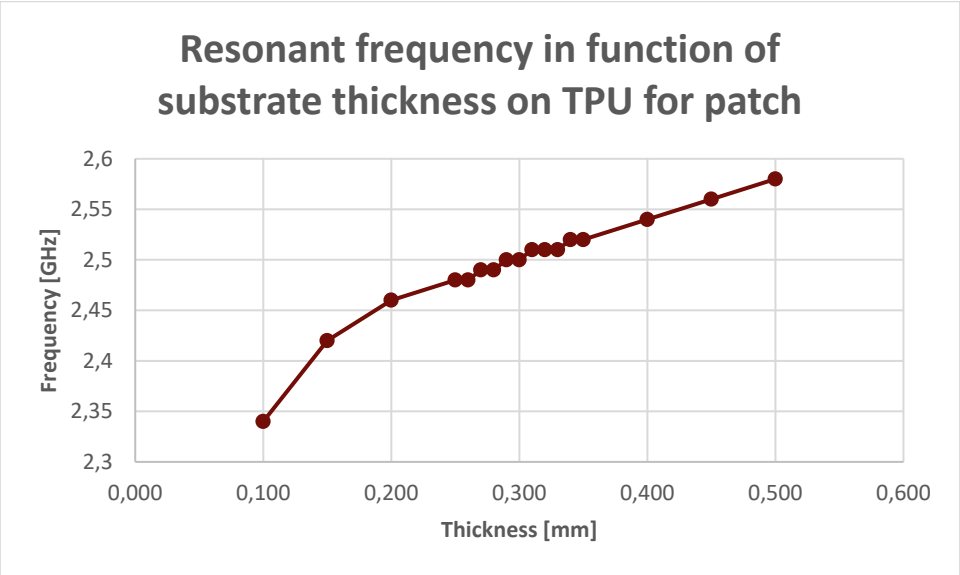

Figure 59: Resonant frequency in function of substrate thickness on TPU for patch

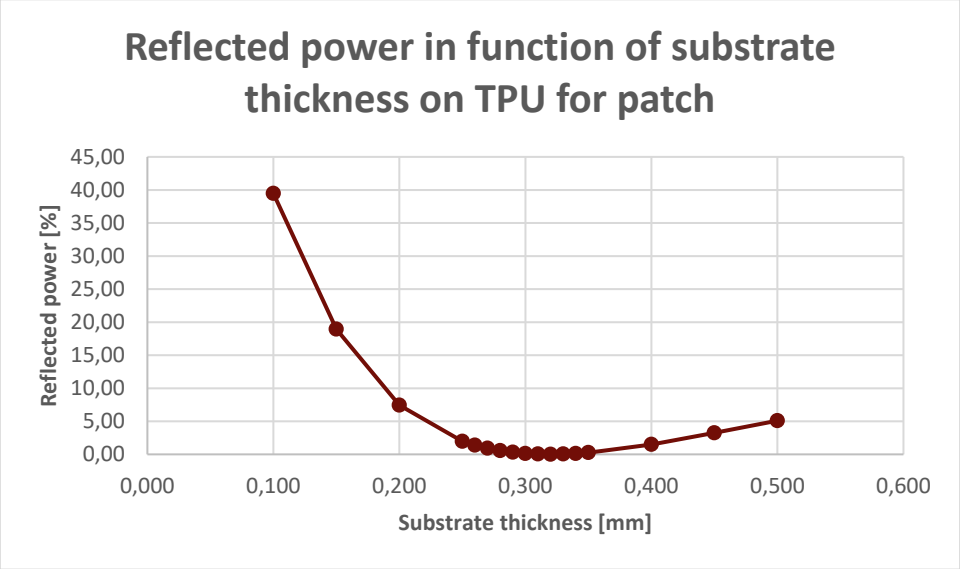

Figure 60: Reflected power in function of the substrate thickness on TPU for patch

It is known that the TPU film used in the practical experiments is manufactured by *Grafityp*. From their website it is found that they offer TPU film with a thickness of 100, 150 or 200 µm. In this case, using the 200 µm variant would give the closest results. Other suppliers might offer more different thicknesses.

The same simulations are done using PET instead of TPU. The results are depicted in Table 14. The resonant frequency immediately shows a linear increase as the thickness increases, unlike on TPU (Figure 61). Looking at Figure 62, for PET there is also a minimum at which the reflected power is close to 0 %. This indicates that the optimal thickness for PET in this case would be 170 µm.

Table 14: Results of varying substrate thickness on resonant frequency and reflected power using PET for patch

Thickness [mm]	Resonant freq. [GHz]	S11 [dB]	VSWR	Reflected power [%]
0,100	3,06	-8,34	2,24	14,65
0,110	3,05	-9,53	2,00	11,14
0,120	3,06	-11,33	1,75	7,37
0,130	3,07	-13,43	1,54	4,54
0,140	3,08	-16,09	1,37	2,46
0,150	3,08	-19,34	1,24	1,16
0,160	3,10	-25,07	1,12	0,31
0,170	**3,10**	**-37,63**	**1,03**	**0,02**
0,180	3,11	-30,06	1,06	0,10
0,190	3,12	-23,59	1,14	0,44
0,200	3,12	-19,35	1,24	1,16
0,250	3,14	-11,59	1,71	6,93
0,300	3,18	-8,56	2,19	13,93

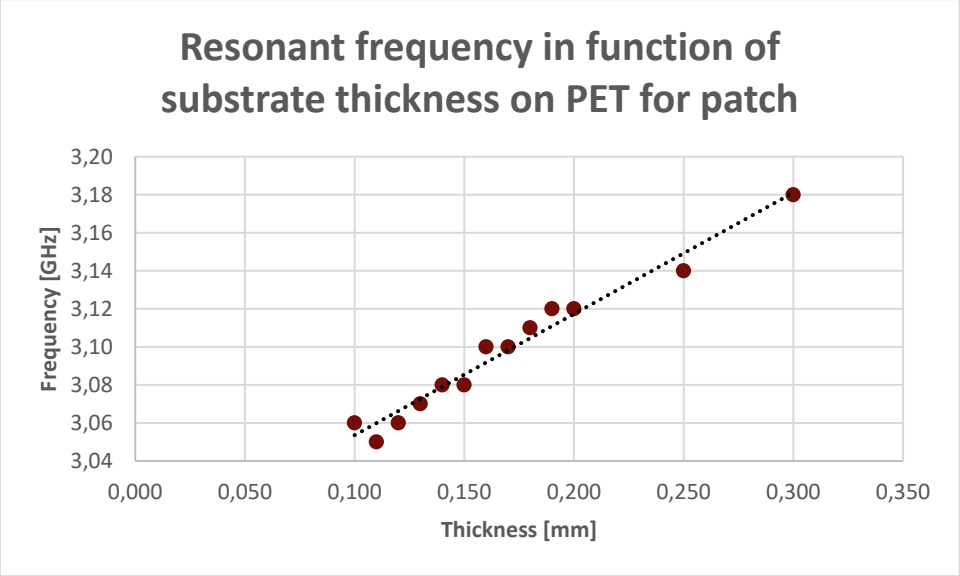

Figure 61: Resonant frequency in function of substrate thickness on PET for patch

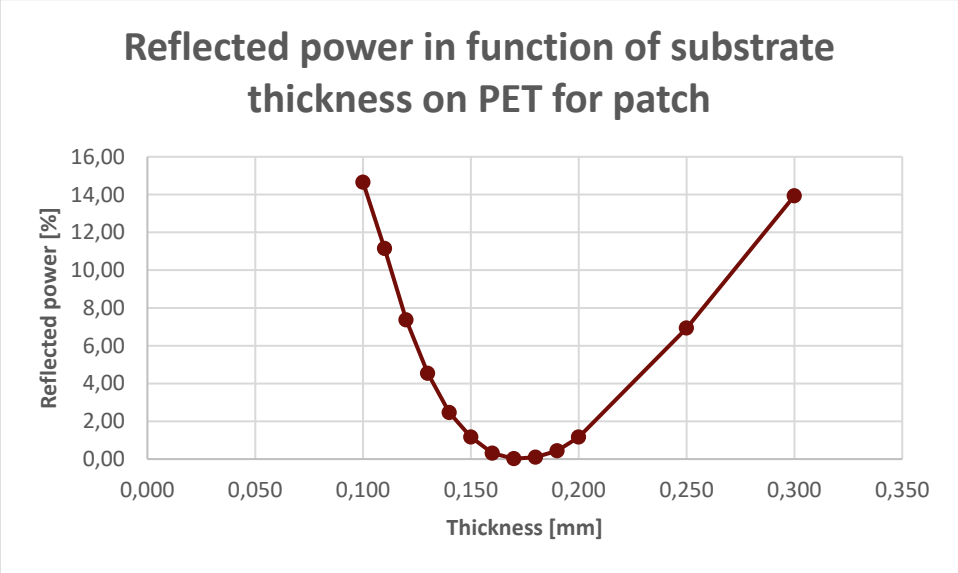

Figure 62: Reflected power in function of substrate thickness on PET for patch

Thirdly, it is interesting to look at the impact of the conductivity of the ink on how the antenna functions. To achieve this, in the next set of simulations, only the conductivity of the ink is changed by lowering the value of the sheet resistance with each simulation. For TPU the thickness is set to 320 µm as found in Table 13 and for PET the thickness is set to 170 µm as shown in Table 14. These are the optimal thicknesses found via simulations and might not be directly available from suppliers. The closest available thickness should be chosen.

The results of the simulations on TPU are shown in Table 15. The resonant frequency shows no difference at different levels of conductivity (Figure 63). When looking at the reflected power, it can be observed that when the thickness is set to 320 µm, the amount of reflected power will be close to 0 % from 0,250 to 0,350 Ω/sq (Figure 64). This means that small changes in the sheet resistance of the ink will have no effect on the working of the antenna. As stated earlier, this is due to the impedance matching of the antenna to the port.

Table 15: Influence of conductivity of ink on TPU for patch

sheet resistance [ohm/sq]	Resonant freq. [GHz]	S11 [dB]	VSWR	Reflected power [%]
0,100	2,56	-15,23	1,42	3,00
0,150	2,56	-18,38	1,27	1,45
0,200	2,56	-22,66	1,16	0,55
0,250	2,56	-29,67	1,07	0,11
0,280	2,56	-39,09	1,02	0,01
0,290	2,56	-44,68	1,01	0,00
0,295	2,56	-45,45	1,01	0,00
0,297	2,56	-44,77	1,01	0,00
0,300	2,56	-43,19	1,01	0,00
0,350	2,56	-28,30	1,08	0,15
0,400	2,56	-23,38	1,15	0,46
0,500	2,54	-18,68	1,26	1,36
0,600	2,54	-15,97	1,38	2,53
0,700	2,54	-14,19	1,49	3,81
0,800	2,52	-12,94	1,58	5,09

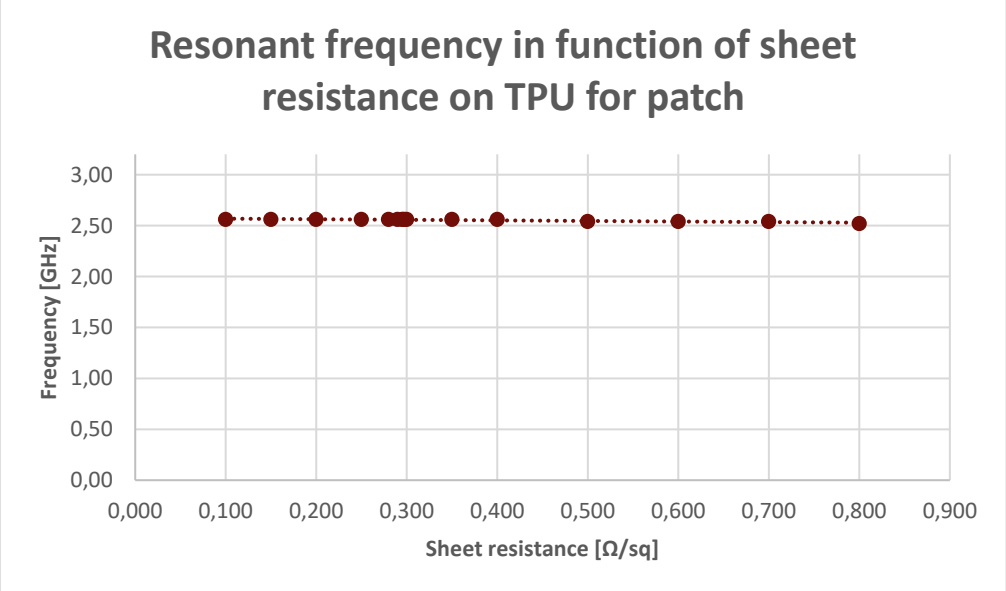

Figure 63: Resonant frequency in function of the sheet resistance on TPU for patch

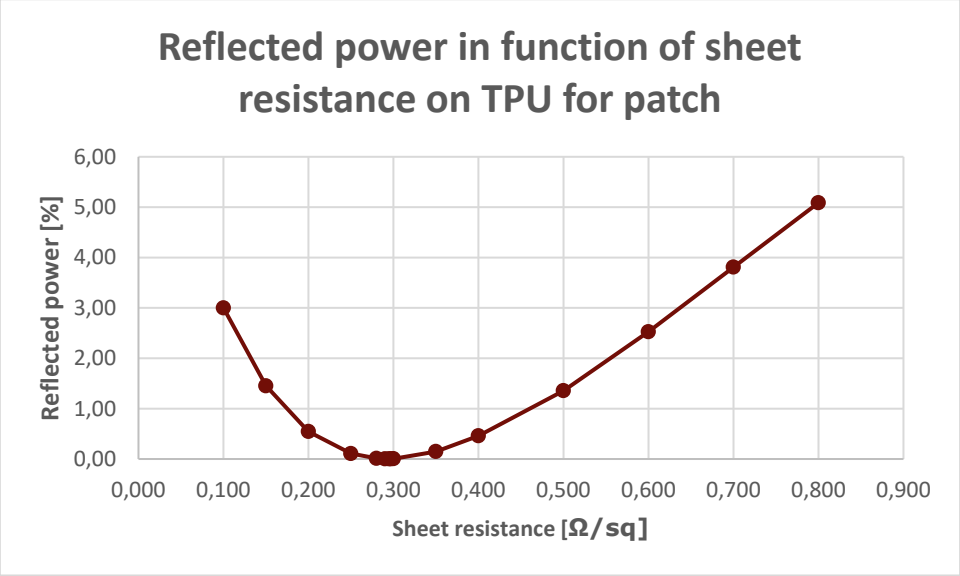

Figure 64: Reflected power in function of the sheet resistance on TPU for patch

The results of the conductivity tests on PET are shown in Table 16. The resonant frequency again shows no change with the change of the ink conductivity (Figure 65). The amount of reflected power also shows close to no change from 0,250 to 0,350 Ω/sq. When the conductivity changes more than this range, the impact on the reflected power is more significant on PET than on TPU.

Table 16: Influence of conductivity of ink on PET for patch

sheet resistance [ohm/sq]	Resonant freq. [GHz]	S11 [dB]	VSWR	Reflected power [%]
0,100	3,18	-8,90	2,12	12,89
0,150	3,18	-12,58	1,67	6,30
0,200	3,18	-16,84	1,34	2,11
0,250	3,18	-23,45	1,14	0,43
0,280	3,16	-32,46	1,08	0,15
0,290	3,16	-36,69	1,03	0,02
0,295	3,16	-37,73	1,03	0,02
0,297	3,16	-37,60	1,03	0,02
0,300	3,16	-36,87	1,03	0,02
0,350	3,16	-23,62	1,14	0,43
0,400	3,16	-18,73	1,26	1,32
0,500	3,16	-13,88	1,51	4,13
0,600	3,14	-11,70	1,70	6,72
0,700	3,14	-10,17	1,90	9,63
0,800	3,12	-9,13	2,07	12,15

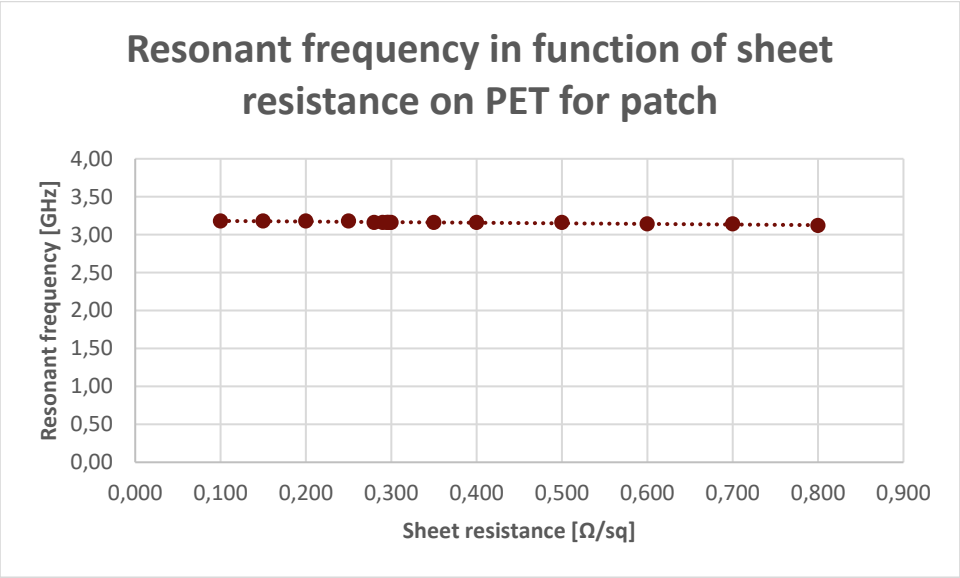

Figure 65: Resonant frequency in function of sheet resistance on PET for patch

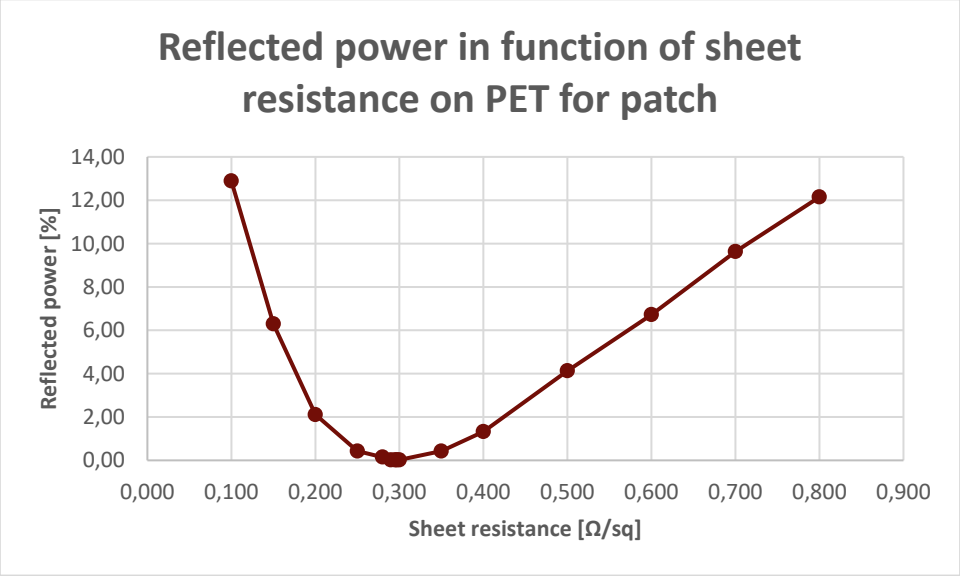

Figure 66: Reflected power in function of sheet resistance on PET for patch

Simulations were also carried out in which the conductive layers consisted of PEDOT:PSS ink. The results of these experiments are shown in Figure 67 and Figure 68. The upper experiment is a simulation of a five layer inkjet ink of 45 ohm/sq. The lower experiment is a simulation of the ME801 screenprint ink of DuPont which achieved an average sheet resistivity of 9608 ohm/sq. Immediately it can be seen that there is no resonant frequency and the antenna will not work with these PEDOT:PSS inks. In the literature study a PEDOT:PSS antenna was shown, but this antenna uses a non-resonant design because just like these experiments showed, the resistivity of PEDOT:PSS is too high to get a functioning resonant antenna. A brief consultation of [77] shows that when the PEDOT:PSS is chemically treated to increase its conductivity, it becomes possible to obtain a functioning resonant antenna.

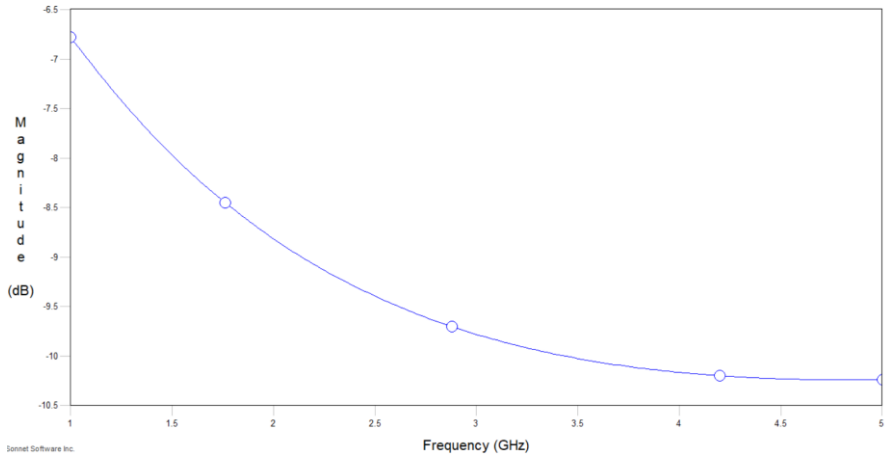

Figure 67: S11 in function of the frequency for a PEDOT:PSS inkjet ink for patch

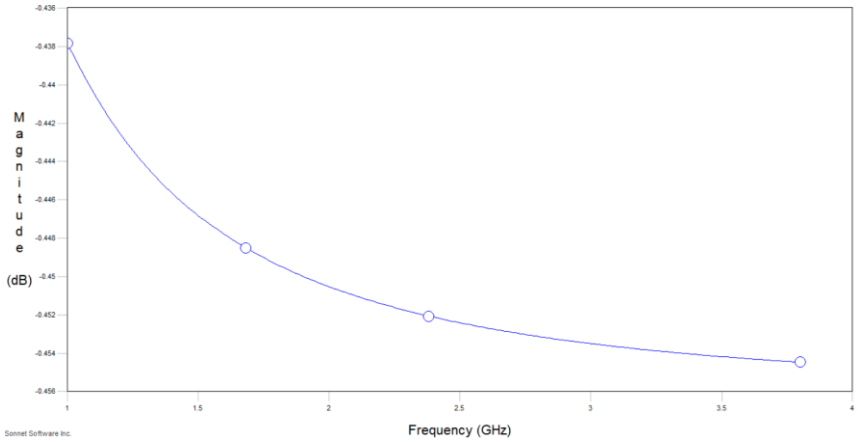

Figure 68: S11 in function of the frequency for a PEDOT:PSS screen print ink (DuPont ME801) for patch

The last step before the simulations with elongation can be started is to draw the desired antenna shape. To test how the antenna would behave under different levels and orientations of elongation, it is required to redraw the antenna with the dimensions as if it was stretched. To find these dimensions, Poisson's ratio is used:

$$\nu = -\frac{d\varepsilon_y}{d\varepsilon_x} = -\frac{d\varepsilon_z}{d\varepsilon_x} \tag{18}$$

With ε being the elongations in x, y and z direction respectively. (15) shows that when an object is elongated in the x-direction, the dimensions of the y- and z- axis (being perpendicular to x) are decreased. Moreover, the ratio of this decrease to elongation is a constant known as Poisson's constant. Reference [78] shows that for TPU it can be assumed that $\nu = 0{,}5$, and according to [79], for PET it can be assumed that $\nu = 0{,}4$. In other words, when the length of an object is increased by 5 %, the width and thickness of the object will decrease by 2,5 % when $\nu = 0{,}5$.

It should be noted that normally, Poisson's ratio is only used for elastic deformation. According to Figure 69 TPU has a linear elastic behaviour from 0 % to ±35 % strain. Seeing as the following simulations will be performed up to 30 % elongation, the Poisson ratio approach can be assumed as valid. This elastic limit could vary between different TPU variants.

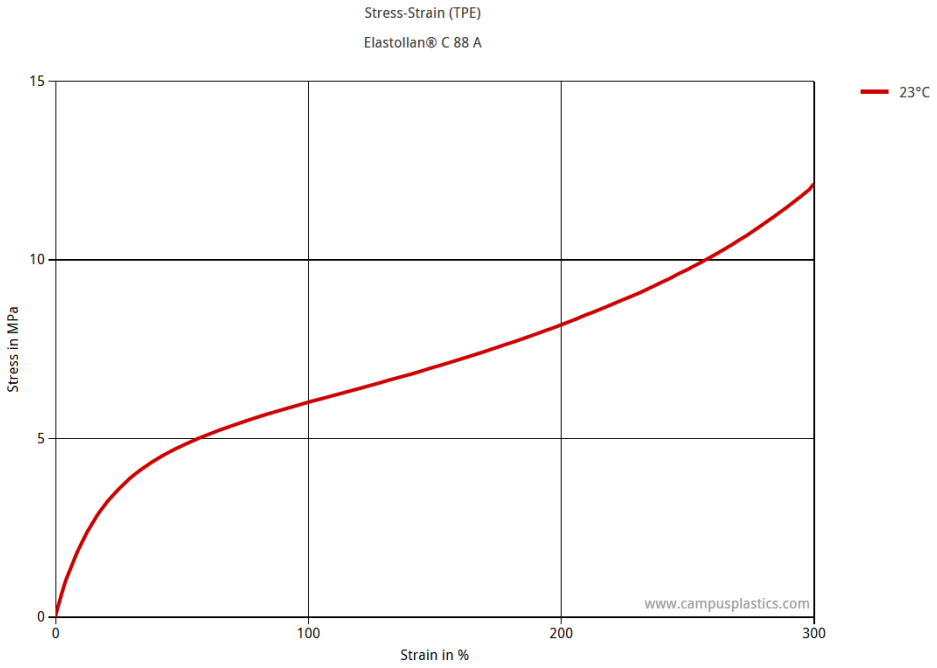

Figure 69: Stress-Strain characteristic of Elastollan C88 A TPU [80]

With this method. The new dimensions of the design are determined for a vertical and a horizontal elongation of the antenna as shown in Figure 70. Each will be tested at different levels of strain going from 0 % up to 30 % with steps of 5 %.

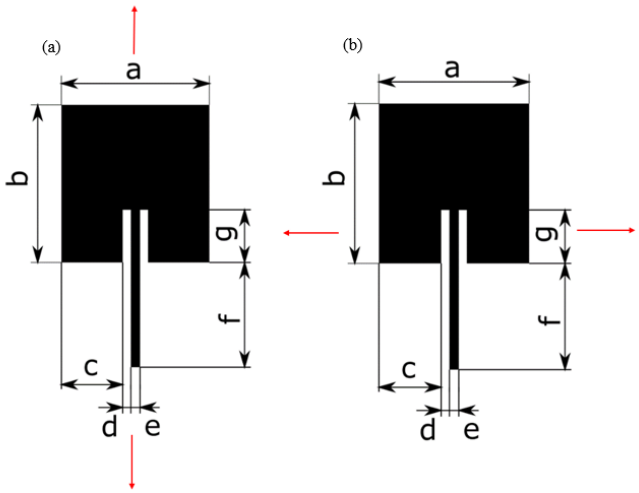

Figure 70: (a) Vertical elongation of inset fed patch (b) Horizontal elongation of inset fed patch

6.1.2 RFID antenna

The RFID antenna is also simulated similar to the inset fed patch. In order for the RFID antenna design to meet the 32 Mb restriction, the design has to be altered. This is because the rounded corners of the conductive path of the antenna have to be approximated by rectangular mesh elements for the simulation. These elements of the mesh have to be sufficiently small for them to give a close approximation of the curve. This drives up the file size. Figure 71 shows the reworked antenna design where the rounded corners have been taken out. This might cause the antenna to operate at a different frequency than it was originally designed for. However, the general behaviour of the antenna can still be studied.

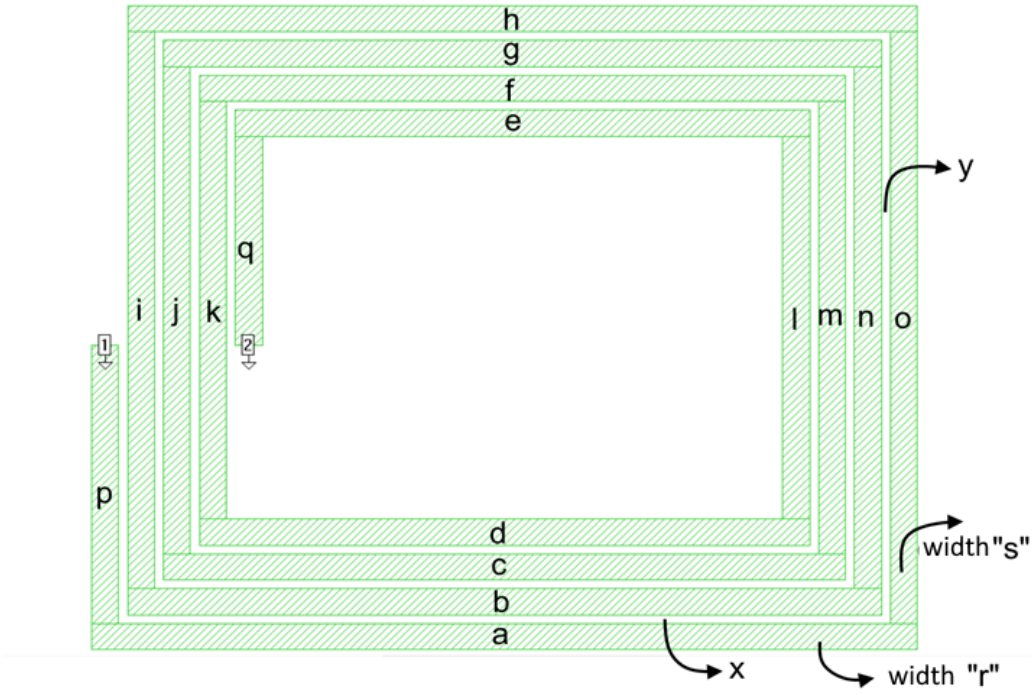

Figure 71: Reworked RFID antenna design in sonnet lite

A quick check shows that the ink layer thickness also has no influence on the RFID antenna, as the layer is sufficiently thin. This is shown in Table 17. The S11-frequency graph is shown in Figure 72.

Table 17: Influence of ink layer thickness on RFID

Thickness [µm]	**Res. Freq [MHz]**	**S11 [dB]**
5	50	-8,96
40	50	-9,05

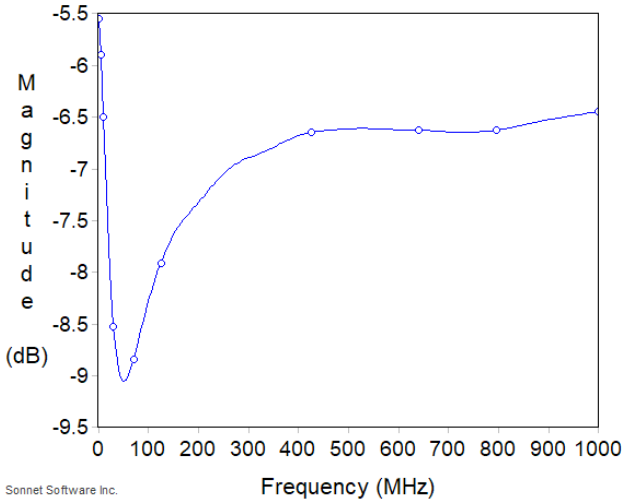

Figure 72: S11 in function of frequency for a 5 µm ink layer and 200 µm dielectric layer for RFID

Next, simulations to find the optimal substrate layer thickness are performed. As the design and therefore the impedance of the antenna is different than for the patch antenna, it is expected that the RFID design will require a different substrate thickness for optimal performance. The results of these tests are shown in Table 18. The resonant frequency in function of the substrate thickness is shown in Figure 74 and the reflected power percentage in function of the substrate thickness is shown in Figure 75. Unlike the inset fed patch design, the RFID does not show an optimal substrate thickness. The resonant frequency increases and the VSWR decreases as the substrate becomes thicker. On first sight, a thick substrate appears to be ideal as the VSWR becomes lower than 2. However, the use of an RFID antenna is to wirelessly identify a certain object. This means that the antenna has to operate at a very specific resonant frequency. When the substrate becomes thicker than 400 µm, the resonant frequency is completely lost (Figure 73).

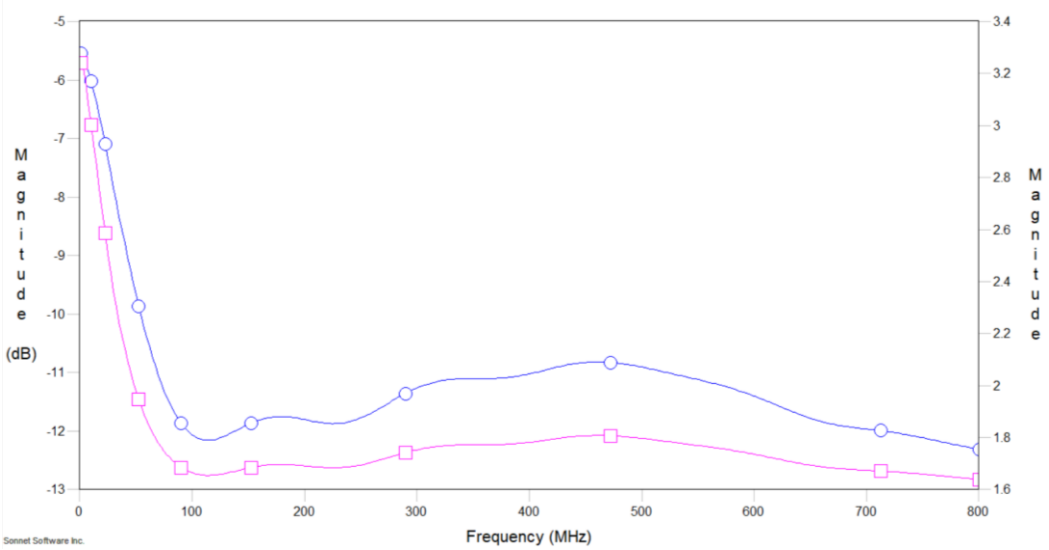

Figure 73: S11(blue) and VSWR(pink) for RFID antenna with a 400 µm substrate layer

The authors of [41] shows that the design frequency for this RFID is supposed to be 13,56 MHz. At 60 µm, the resonant frequency of the antenna is closest to this design frequency. This is why the elongation tests will be performed with a substrate thickness of 60 µm.

Table 18: Results of varying substrate thickness on resonant frequency and reflected power using TPU for RFID

Thickness [µm]	Res. freq. [MHz]	S11 [dB]	VSWR	Reflected power [%]
0,010	/	/	/	/
0,020	5,0	-7,80	2,37	16,53
0,030	5,0	-7,81	2,37	16,53
0,035	10,0	-7,71	2,40	16,96
0,040	10,0	-7,84	2,36	16,38
0,045	10,0	-7,91	2,35	16,24
0,050	10,0	-7,93	2,34	16,10
0,055	10,0	-7,92	2,34	16,10
0,060	**15,0**	**-7,93**	**2,34**	**16,10**
0,070	15,0	-8,02	2,32	15,81
0,080	15,0	-8,02	2,32	15,81
0,090	20,0	-8,10	2,30	15,52
0,100	20,0	-8,17	2,28	15,23
0,150	35,0	-8,52	2,20	14,06
0,200	50,0	-9,05	2,09	12,44
0,250	70,0	-9,74	1,97	10,67
0,300	90,0	-10,58	1,84	8,75
0,350	100,0	-11,54	1,72	7,01
0,400	/	/	/	/

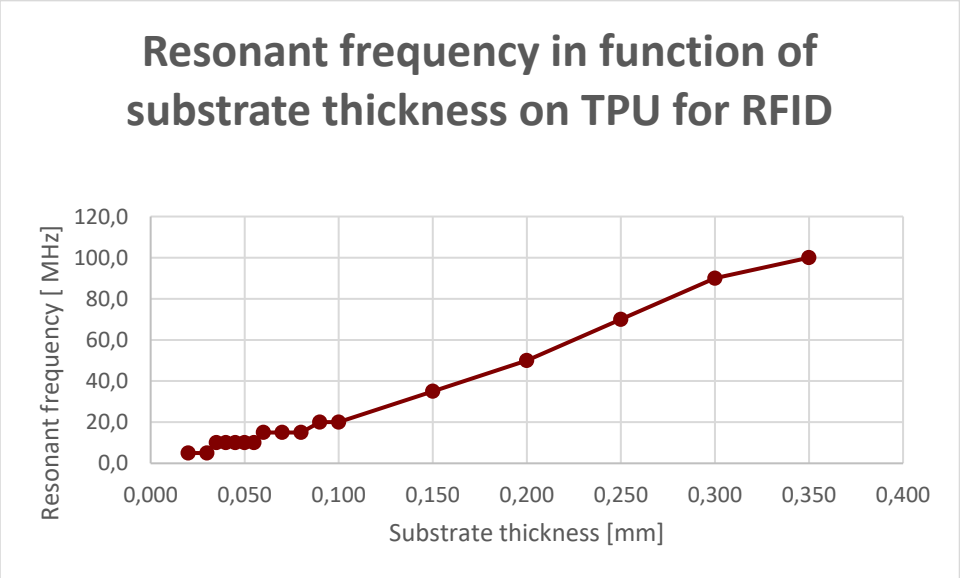

Figure 74: Resonant frequency in function of substrate thickness on TPU for RFID

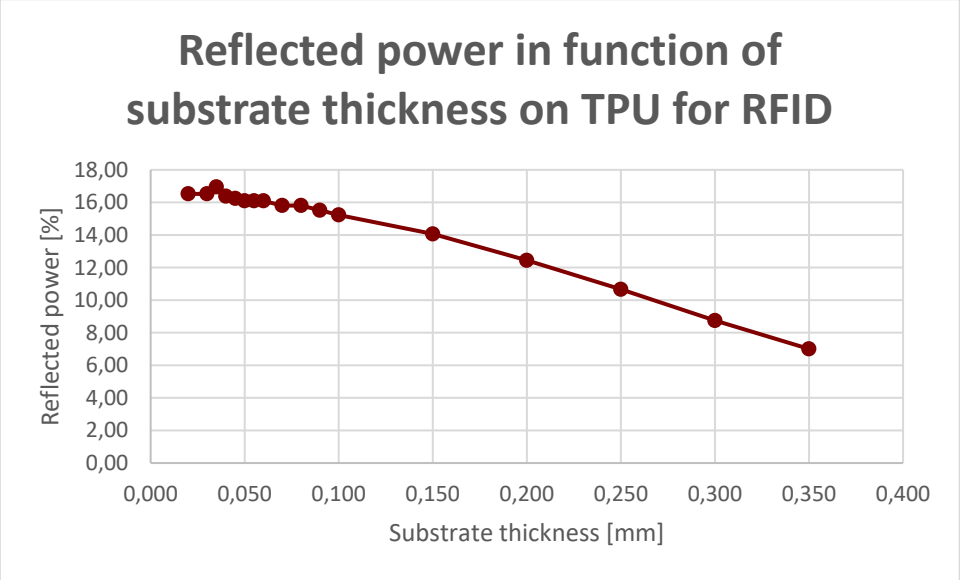

Figure 75: Reflected power in function of substrate thickness on TPU for RFID

When looking at the results of varying PET substrate thicknesses (Table 19), they look similar to the results on TPU. The resonant frequency on PET is higher than on TPU, but the S11, VSWR and reflected power stay in the same range. The thickness at which the resonant frequency is closest to the design frequency for PET is 35 µm.

Table 19: Results of varying substrate thickness on resonant frequency and reflected power using PET for RFID

Thickness [µm]	**Res. freq. [MHz]**	**S11 [dB]**	**VSWR**	**Reflected power [%]**
0,010	5,00	-7,28	2,52	18,65
0,020	5,00	-7,32	2,51	18,51
0,030	10,00	-7,53	2,45	17,66
0,035	**15,00**	**-7,50**	**2,46**	**17,81**
0,040	15,00	-7,55	2,44	17,52
0,045	15,00	-7,50	2,46	17,81
0,050	20,00	-7,58	2,44	17,52
0,055	20,00	-7,56	2,44	17,52
0,060	25,00	-7,67	2,41	17,10
0,070	25,00	-7,81	2,37	16,53
0,080	30,00	-7,90	2,35	16,24
0,090	35,00	-7,96	2,33	15,95
0,100	40,00	-8,03	2,31	15,66
0,150	70,00	-8,69	2,16	13,48
0,200	100,00	-9,72	1,97	10,67
0,250	/	/	/	/

Lastly, the influence of the conductivity of the ink is inspected. The substrate thickness is kept at 60 µm for each simulation for TPU and at 35 µm for PET. The results of the simulations are shown in Table 20 for TPU and in Table 21 for PET. These results show little to no difference between TPU and PET. When the resistance becomes too low, no resonant frequency can be observed. Because the resonant frequency decreases as the resistance decreases, the resonant frequency of the antenna becomes close to zero. This is shown in the table with a forward slash.

Table 20: Influence of conductivity of ink on TPU for RFID

Sheet resistance [Ω/sq]	Resonant freq. [MHz]	S11 [dB]	VSWR	Reflected power [%]
0,10	/	/	/	/
0,15	/	/	/	/
0,20	5,00	-7,82	2,37	16,53
0,25	10,00	-7,72	2,40	16,96
0,30	15,00	-7,87	2,36	16,38
0,35	15,00	-8,12	2,30	15,52
0,40	15,00	-8,24	2,27	15,08
0,45	15,00	-8,25	2,26	14,94
0,50	15,00	-8,23	2,27	15,08
0,55	20,00	-8,25	2,26	14,94
0,60	20,00	-8,27	2,26	14,94

Table 21: Influence of conductivity of ink on PET for RFID

Sheet resistance [Ω/sq]	Resonant freq. [GHz]	S11 [dB]	VSWR	Reflected power [%]
0,10	/	/	/	/
0,15	/	/	/	/
0,20	/	/	/	/
0,25	10,00	-7,26	2,53	18,79
0,30	10,00	-7,54	2,45	17,66
0,35	15,00	-7,66	2,41	17,10
0,40	15,00	-7,79	2,38	16,67
0,45	15,00	-7,85	2,36	16,38
0,50	15,00	-7,86	2,36	16,38
0,55	20,00	-7,87	2,36	16,38
0,60	20,00	-7,86	2,36	16,38

As the influence of substrate thickness and conductivity on TPU and PET for the RFID design show close to no difference, the elongation tests will only be performed on TPU.

PEDOT:PSS is also investigated as a possible material for the RFID antenna. This is again done with a simulation of a five layer inkjet printed PEDOT:PSS layer with a sheet resistance of 45 ohm/sq. According to the simulation results (Figure 76) the RFID antenna does not show a resonant frequency and thus will not function as the sheet resistance is too high. As PEDOT:PSS is not functional for both the inset fed patch and the RFID antenna, it is not examined further.

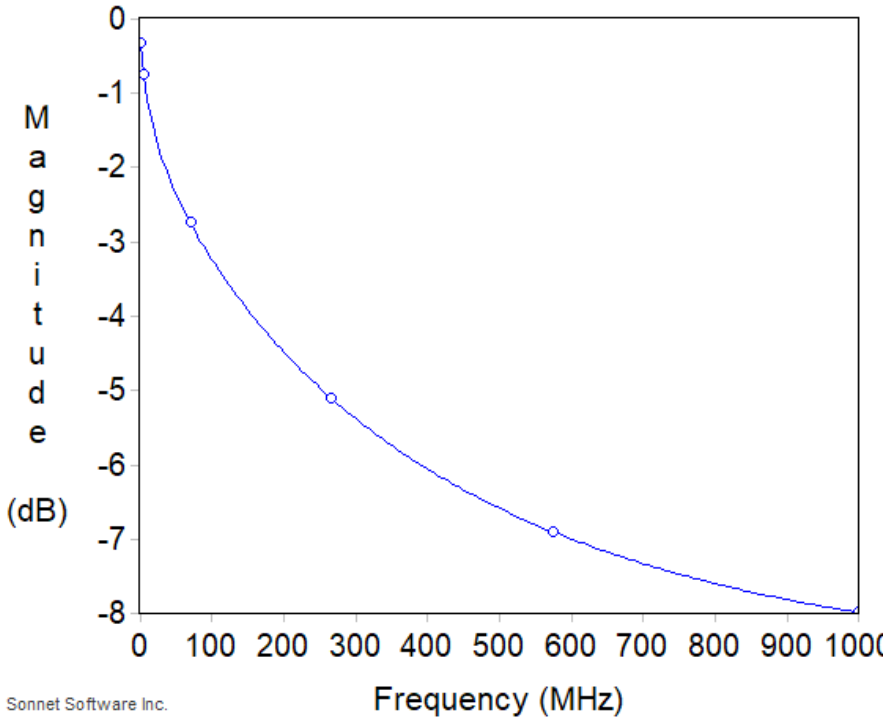

Figure 76: S11 in function of the frequency for a PEDOT:PSS inkjet ink for RFID

The deformation of the RFID is determined using the same approach as the inset fed patch using Poisson's ratio.

6.2 *Inset fed patch antenna simulations*

To start, the inset fed patch antenna design is simulated with elongation in its vertical, horizontal and in both directions. These simulations go from 0 % to 30 % elongation with 5 % increase with each step, and are performed on a TPU and a PET substrate.

6.2.1 Elongation in vertical direction

To simulate the antenna at different levels of vertical elongation, each simulation is run with an altered version of the antenna design using the dimensions shown in Table 22. Figure 77 shows the used patch antenna designs at 0 % and 30 % strain. The thickness of the substrate will decrease at each level of elongation according to its Poisson coefficient.

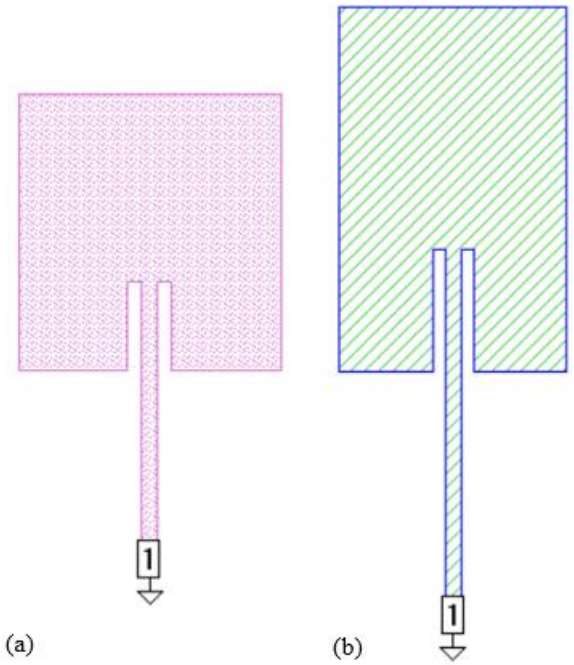

Figure 77: Inset fed patch antenna at (a) 0 % vertical elongation (b) 30 % vertical elongation

Using (18), the new dimensions of the design are determined with the different levels of vertical elongation. A summary of all new dimensions on TPU is shown in Table 22. Table 23 gives a summary of the dimensions on PET. The dimensions of the antenna are shown in Figure 70.

Table 22: New dimensions of inset fed patch after vertical elongation in mm on TPU

	0 %	**5 %**	**10 %**	**15 %**	**20 %**	**25 %**	**30 %**
a	36,850	35,929	35,008	34,086	33,165	32,244	31,323
b	39,150	41,108	43,065	45,023	46,980	48,938	50,895
c	15,270	14,888	14,507	14,125	13,743	13,361	12,980
d	2,000	1,950	1,900	1,850	1,800	1,750	1,700
e	2,300	2,243	2,185	2,128	2,070	2,013	1,955
f	26,050	27,353	28,655	29,958	31,260	32,563	33,865
g	13,100	13,755	14,410	15,065	15,720	16,375	17,030

Table 23: New dimensions of inset fed patch after vertical elongation in mm on PET

	0 %	5 %	10 %	15 %	20 %	25 %	30 %
a	36,850	36,113	35,376	34,639	33,902	33,165	32,428
b	39,150	41,108	43,065	45,023	46,980	48,938	50,895
c	15,270	14,965	14,659	14,354	14,048	13,743	13,438
d	2,000	1,960	1,920	1,880	1,840	1,800	1,760
e	2,300	2,254	2,208	2,162	2,116	2,070	2,024
f	26,050	27,353	28,655	29,958	31,260	32,563	33,865
g	13,100	13,755	14,410	15,065	15,720	16,375	17,030

First, a simulation on TPU is made. The substrate thickness is set to 320 µm as found in Table 13. The results are shown in Table 24 varying from 0 % to 30 %. From these results it is clear that the resonant frequency shifts to a lower frequency, and the value of the VSWR increases when the strain is increased. This is also visualised in Figure 78. As discussed in chapter 3, the operating area of the antenna is the range of frequencies around the resonant frequency where the VSWR is lower than 2. This is shown as the bandwidth 2:1 VSWR in Table 24. When looking at the VSWR of the antenna, it appears as the antenna will remain functional up to 20 % strain as the VSWR at 20 % is 1,68. However if the antenna has to remain functional on its original resonant frequency (2,5 GHz in this case), it becomes clear that the antenna loses its functionality after 10 % elongation, as the original resonant frequency is no longer part of the bandwidth of the antenna. For 25 %, the antenna will no longer be functional regardless as the VSWR does not go below 2. For 30 %, no resonant frequency was found anymore.

Table 24: Results of vertical elongation simulations from 0 % to 30 % on TPU

Elongation [%]	Sheet resistance [Ω/sq]	Resonant freq. [GHz]	S11 [dB]	VSWR	Reflected power [%]	Bandwidth 2:1 VSWR [GHz]
0 %	0,311	2,50	-32,55	1,05	0,1	2,36 - 2,66
5 %	0,451	2,33	-18,96	1,25	1,2	2,17 - 2,52
10 %	0,590	2,33	-15,68	1,39	2,7	2,16 - 2,50
15 %	0,652	2,18	-13,63	1,53	4,4	2,03 - 2,32
20 %	0,688	2,10	-11,92	1,68	6,4	1,96 - 2,23
25 %	2,054	1,79	-7,23	2,54	18,9	/
30 %	11,597	No Resonant frequency	/	/	/	/

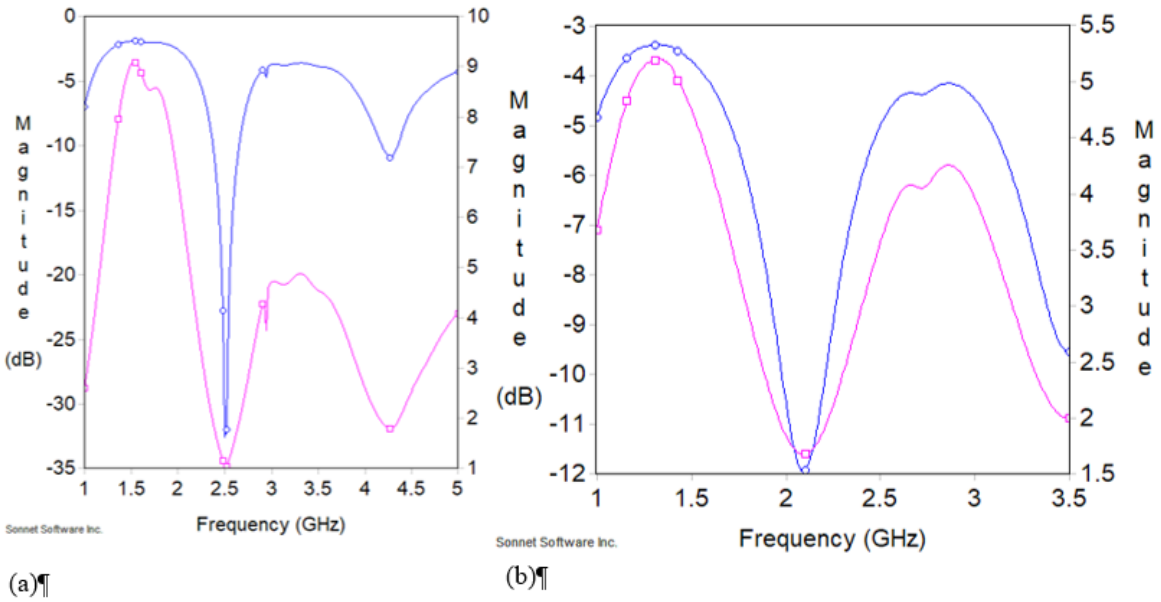

(a)¶ (b)¶

Figure 78: S11(blue) and VSWR(pink) in function of the frequency for (a) 0 % vertical elongation (b) 20 % vertical elongation on TPU

In Figure 79 and Figure 80 the resonant frequency and the VSWR are plotted in function of the elongation.

When looking at the resonant frequency, it appears it decreases in a linear fashion. The VSWR also appears to be linear up to 20 %, but will increase as the amount of strain is increased. After 20 %, the increase of the VSWR becomes steeper.

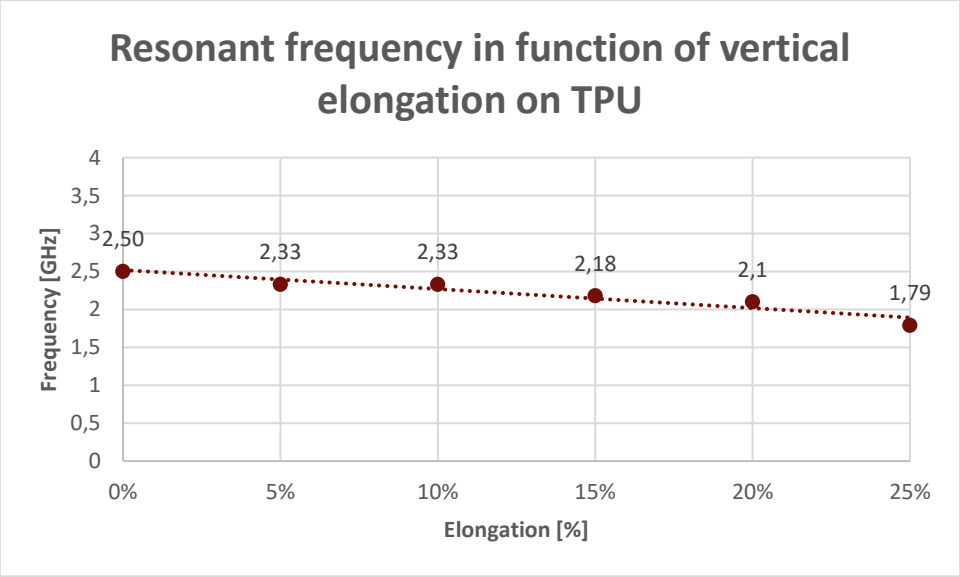

Figure 79: Resonant frequency in function of vertical elongation on TPU

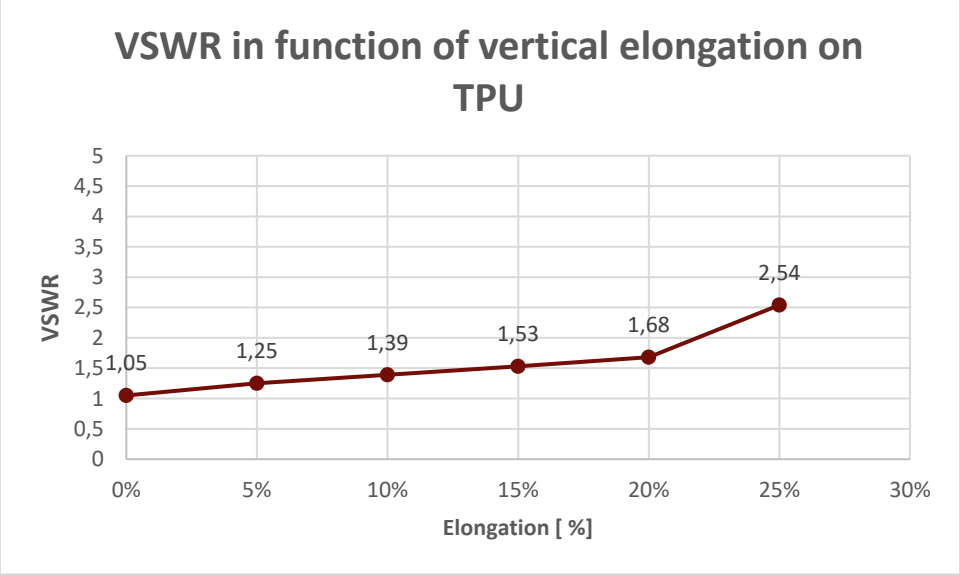

Figure 80: VSWR in function of vertical elongation on TPU

The S11, VSWR and reflected power are different notations for the same parameter. Because of this, the plot of the value of S11 and the reflected power in function of the vertical elongation will show the same curve shape as shown in Figure 80. Therefore only the plot of the VSWR is shown.

The same simulations of vertical elongation are now performed using PET as the dielectric material. The designs of the antenna at each level of stretch is adapted using the data found in Table 23. The layer thickness is set to 170 µm as found in Table 14. This value will decrease according to its Poisson coefficient of 0,4. The sheet resistance at each level of strain is kept the same as on TPU. This will not be the case in a practical situation because of the difference in surface free energy of the two materials, but as explained in 5.2.1, this can be remedied by using a corona treatment.

The simulation results are shown in Table 25. The same effects can be observed as for the simulations on TPU. As the amount of elongation increases, the resonant frequency will shift to a lower frequency and the VSWR will increase resulting in more reflected power. The change in material does have an effect on the value of these parameters. While the antenna resonated at 2,50 GHz on TPU, on PET it appears to resonate at 3 GHz. The VSWR also appears to change more drastically than on TPU. The VSWR of the resonant frequency remains below 2 up to 10 % strain, whereas on TPU this could go up to 20 %. Moreover when looking at the bandwidth, it can be seen that the original resonant frequency falls outside of the bandwidth at 5 % elongation, indicating that on PET, the antenna will not be functional anymore on the original resonant frequency after at 5 % vertical elongation. Figure 81 visualises the S11 and VSWR parameters in function of the frequency for 0 % and 20 % elongation.

Table 25: Results of vertical elongation simulations from 0 % to 30 % on PET

Elongation [%]	**Sheet resistance [Ω/sq]**	**Resonant freq. [GHz]**	**S11 [dB]**	**VSWR**	**Reflected power [%]**	**Bandwidth 2:1 VSWR [GHz]**
0 %	0,311	3,04	-34,77	1,04	0,0	2,92 - 3,18
5 %	0,451	2,90	-11,09	1,79	8,0	2,78 - 3,00
10 %	0,59	2,80	-10,74	1,82	8,5	2,70 - 2,88
15 %	0,652	2,66	-9,43	2,00	11,1	2,66
20 %	0,688	2,54	-8,65	2,17	13,6	/
25 %	2,054	No resonant frequency	/	/	/	/
30 %	11,597	No resonant frequency	/	/	/	/

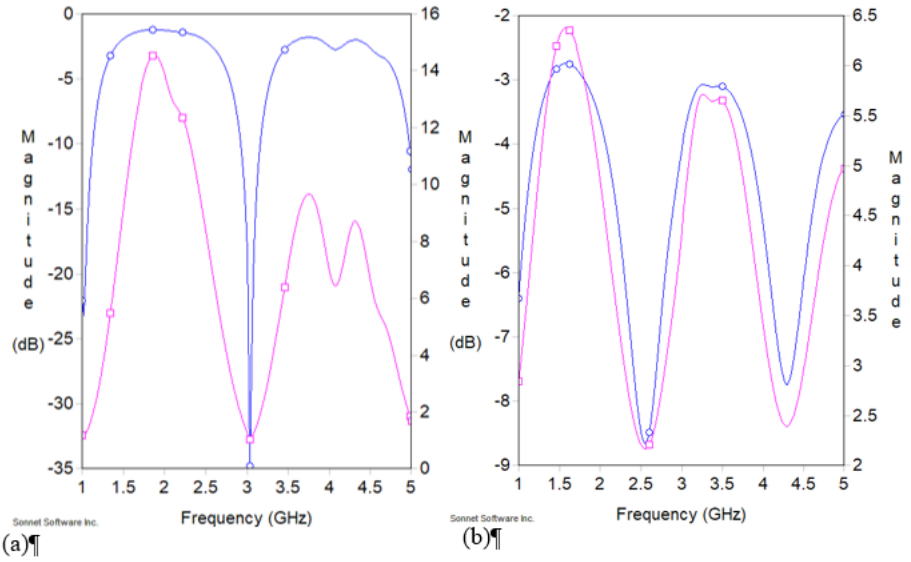

Figure 81: S11(blue) and VSWR(pink) in function of the frequency for (a) 0 % vertical elongation (b) 20 % vertical elongation on PET

As on TPU, the resonant frequency seems to decrease in a linear fashion as the vertical elongation increases. This is shown in Figure 82. Figure 83 shows a steep increase of the VSWR from 0 to 5 %. After 5 % the increase becomes more linear with a slower increase up to 20 %.

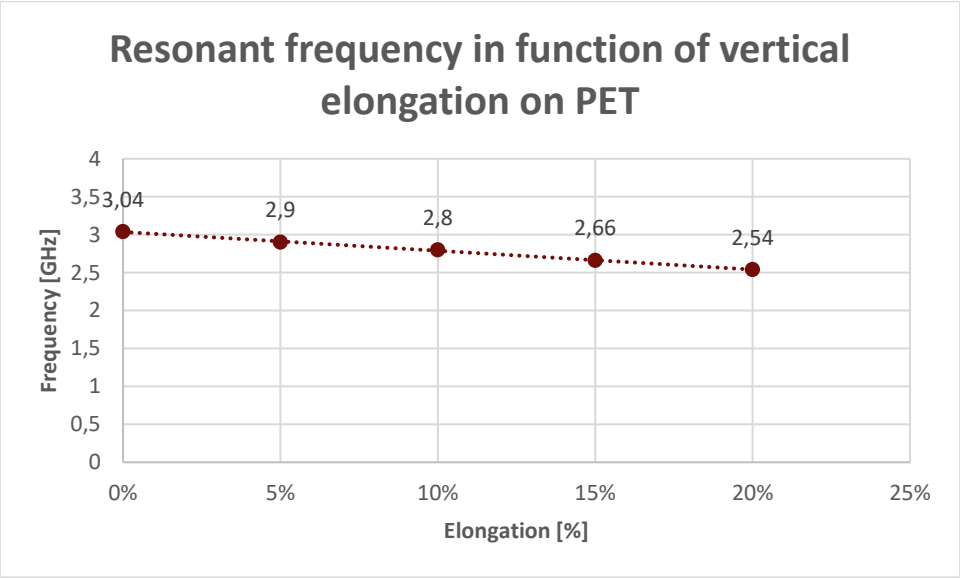

Figure 82: Resonant frequency in function of vertical elongation on PET

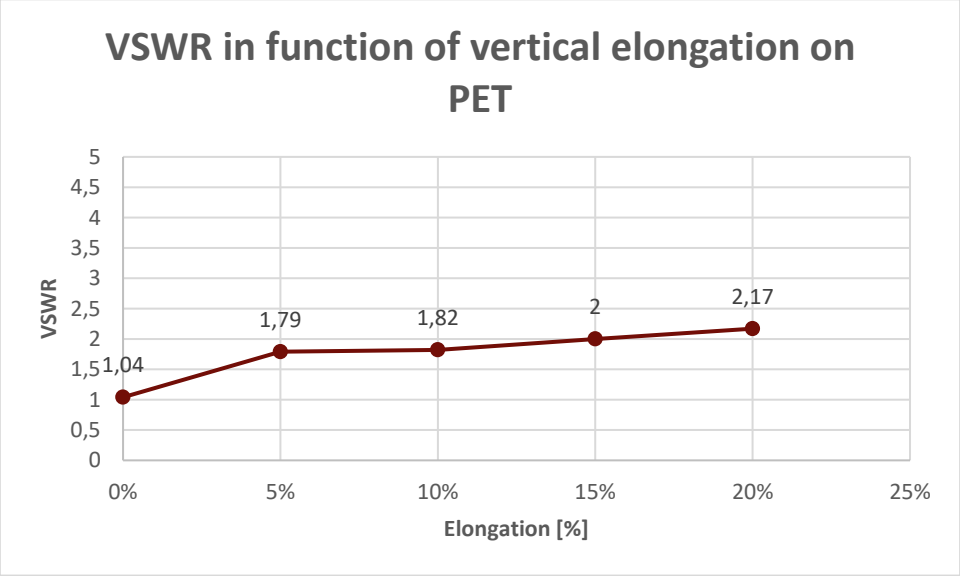

Figure 83: VSWR in function of vertical elongation on PET

6.2.2 Elongation in horizontal direction

To simulate the antenna when it is stretched horizontally, the design should again be altered. Figure 84 shows the design at 0 % and 30 % horizontal strain. The thickness decreases again according to the Poisson ratio with a starting thickness of 320 µm.

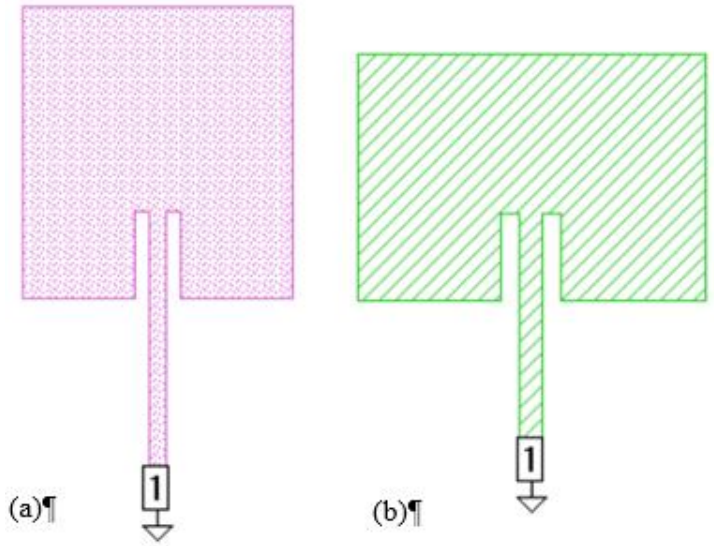

Figure 84: Inset fed patch antenna at (a) 0 % horizontal elongation (b) 30 % horizontal elongation

Using (18) again, the dimensions for horizontal elongation can also be determined. A summary of all new dimensions on TPU is shown in Table 26. Table 27 gives the new dimensions after horizontal elongation on PET.

Table 26: New dimensions of inset fed patch after horizontal elongation in mm on TPU

	0 %	**5 %**	**10 %**	**15 %**	**20 %**	**25 %**	**30 %**
a	36,850	38,693	40,535	42,378	44,220	46,063	47,905
b	39,150	38,171	37,193	36,214	35,235	34,256	33,278
c	15,270	16,034	16,797	17,561	18,324	19,088	19,851
d	2,000	2,100	2,200	2,300	2,400	2,500	2,600
e	2,3	2,415	2,530	2,645	2,760	2,875	2,990
f	26,050	25,399	24,748	24,096	23,445	22,794	22,143
g	13,100	12,773	12,445	12,118	11,790	11,463	11,135

Table 27: New dimensions of inset fed patch after horizontal elongation in mm on PET

	0 %	**5 %**	**10 %**	**15 %**	**20 %**	**25 %**	**30 %**
a	36,850	38,693	40,535	42,378	44,220	46,063	47,905
b	39,150	38,367	37,584	36,801	36,018	35,235	34,452
c	15,270	16,034	16,797	17,561	18,324	19,088	19,851
d	2,000	2,100	2,200	2,300	2,400	2,500	2,600
e	2,300	2,415	2,530	2,645	2,760	2,875	2,990
f	26,050	25,529	25,008	24,487	23,966	23,445	22,924
g	13,100	12,838	12,576	12,314	12,052	11,790	11,528

The results of the simulation of ME602 on TPU for horizontal elongation are shown in Table 28. When looking at these results, it can be seen that the VSWR increases as the amount of strain is increased. However, this increase is larger than the one found for vertical elongation. Furthermore, the horizontal elongation shows very little influence on the resonant frequency of the antenna. The value of the resonant frequency changes slightly in between simulations, but this seems to be due to simulation constraints. Horizontal elongation does not appear to effect the resonant frequency, unlike the vertical elongation, indicating that only the vertical dimensions of the patch antenna determine the resonant frequency. These results are solidified by [81] as it states that the vertical dimension of patch antenna designs determines the resonant frequency of the antenna, while the horizontal dimension influences the impedance and radiation pattern. When looking at the VSWR, the antenna will have a functional resonant frequency (with a VSWR lower than 2) up to 20 % horizontal elongation. At this level of elongation, the antenna will also be able to operate at its original resonant frequency as 2,50 GHz is still part of the bandwidth at 20 % horizontal elongation. The S11 and VSWR at different frequencies are shown in Figure 85.

Table 28: Results of horizontal elongation simulations from 0 % to 30 % on TPU

Elongation [%]	**Sheet resistance [Ω/sq]**	**Resonant freq. [GHz]**	**S11 [dB]**	**VSWR**	**Reflected power [%]**	**Bandwidth 2:1 VSWR [GHz]**
0 %	0,311	2,50	-32,55	1,05	0,1	2,36 - 2,66
5 %	0,451	2,52	-17,25	1,32	1,9	2,38 - 2,66
10 %	0,59	2,62	-13,3	1,57	4,9	2,48 - 2,78
15 %	0,652	2,58	-10,65	1,83	8,6	2,49 - 2,68
20 %	0,688	2,58	-9,66	1,98	10,8	2,50 -2,62
25 %	2,054	2,46	-5,58	3,22	27,7	/
30 %	11,597	No resonant frequency	/	/	/	/

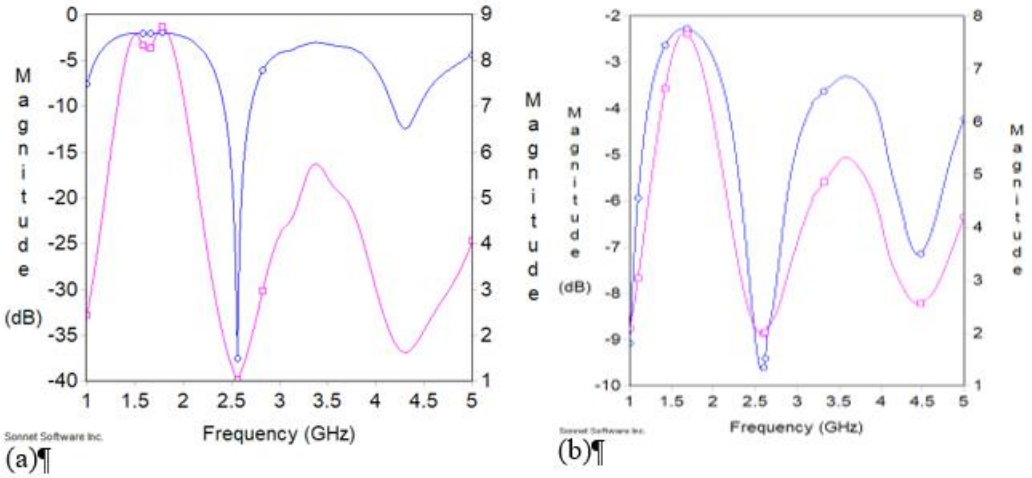

Figure 85: S11(blue) and VSWR(pink) in function of the frequency for (a) 0 % horizontal elongation (b) 20 % horizontal elongation on TPU

As stated earlier, the resonant frequency is not influenced by the horizontal strain. This is also shown in Figure 86. The VSWR shows a similar linear increase as with the vertical elongation (Figure 87), but has a slightly greater increase of its value compared to the vertical simulation. It also does not show the steep increase going from 20 to 25 % which was present with the vertical elongation.

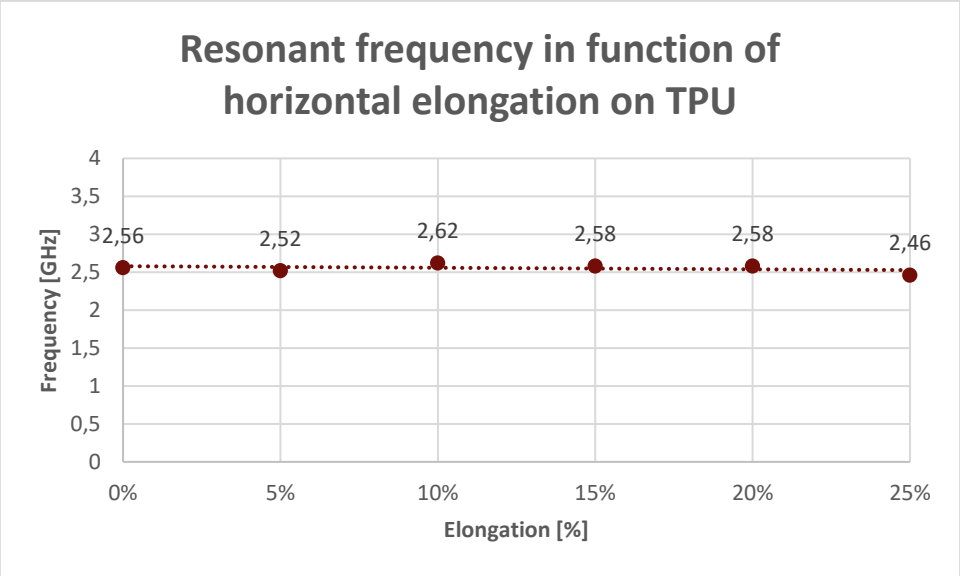

Figure 86:Resonant frequency in function of horizontal elongation on TPU

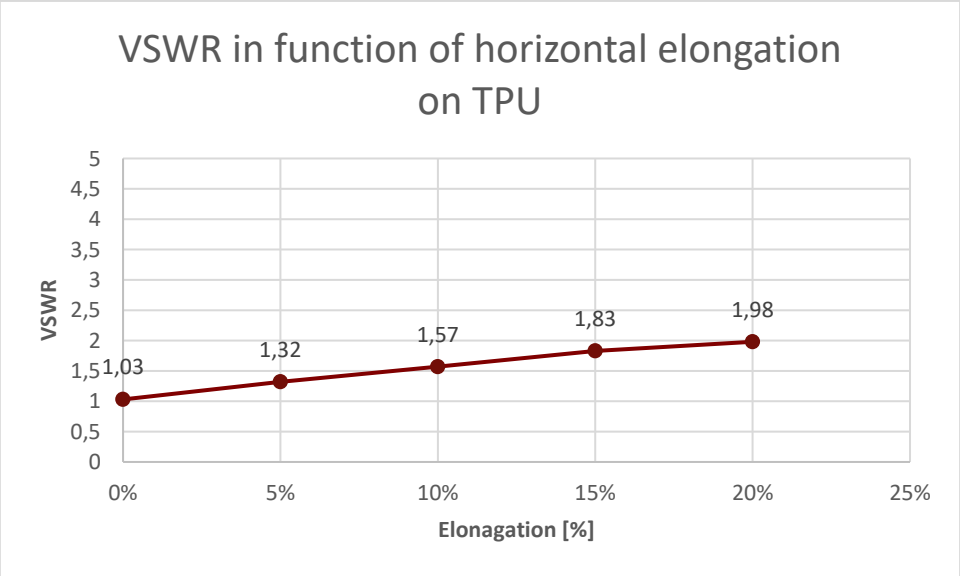

Figure 87: VSWR in function of horizontal elongation on TPU

The results for the simulations of horizontal elongation on PET are shown in Table 29. Again, the resonant frequency does not seem to be effected by the horizontal strain. Further establishing that only the vertical dimensions of the antenna have an impact on the resonant frequency. Looking at the VSWR, the antenna will show a functional resonant frequency up to 10 %. After 10 % the VSWR will be larger than 2. When looking at the bandwidth, the original resonant frequency will also be part of the bandwidth up to 10 %. This indicates that the antenna will be able to function on its original frequency with up to 10 % horizontal elongation on PET. Figure 88 shows the plot of S11 and VSWR in function of the frequency.

Table 29: Results of horizontal elongation simulations from 0 % to 30 % on PET

Elongation [%]	Sheet resistance [Ω/sq]	Resonant freq. [GHz]	S11 [dB]	VSWR	Reflected power [%]	Bandwidth 2:1 VSWR [GHz]
0 %	0,311	3,04	-34,77	1,04	0	2,92 - 3,18
5 %	0,451	3,06	-15,41	1,41	2,9	2,92 - 3,20
10 %	0,59	3,02	-9,64	1,98	10,8	2,98 - 3,08
15 %	0,652	3,24	-8,77	2,15	13,3	/
20 %	0,688	3,22	-7,95	2,33	16	/
25 %	2,054	2,94	-4,04	4,37	39,4	/
30 %	11,597	/	/	/	/	/

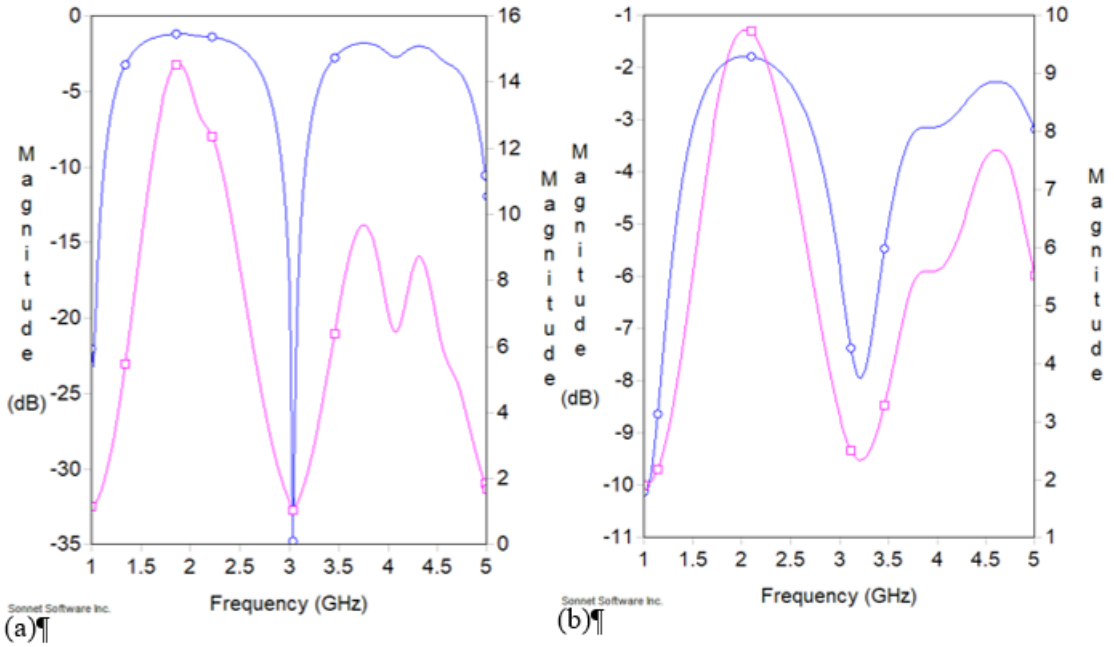

Figure 88: S11(blue) and VSWR(pink) in function of the frequency for (a) 0 % horizontal elongation (b) 20 % horizontal elongation on PET

Just as for horizontal elongation on TPU, the resonant frequency of the antenna does not change for PET (Figure 89). The VSWR increases linear up to 20 %. From 20 to 25 % the increase becomes more steep(Figure 90).

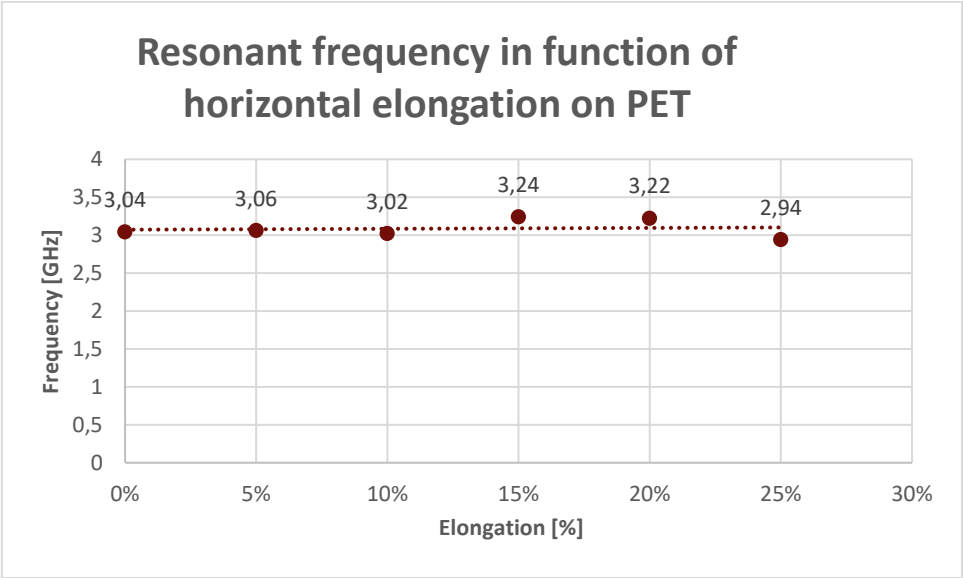

Figure 89: Resonant frequency in function of horizontal elongation on PET

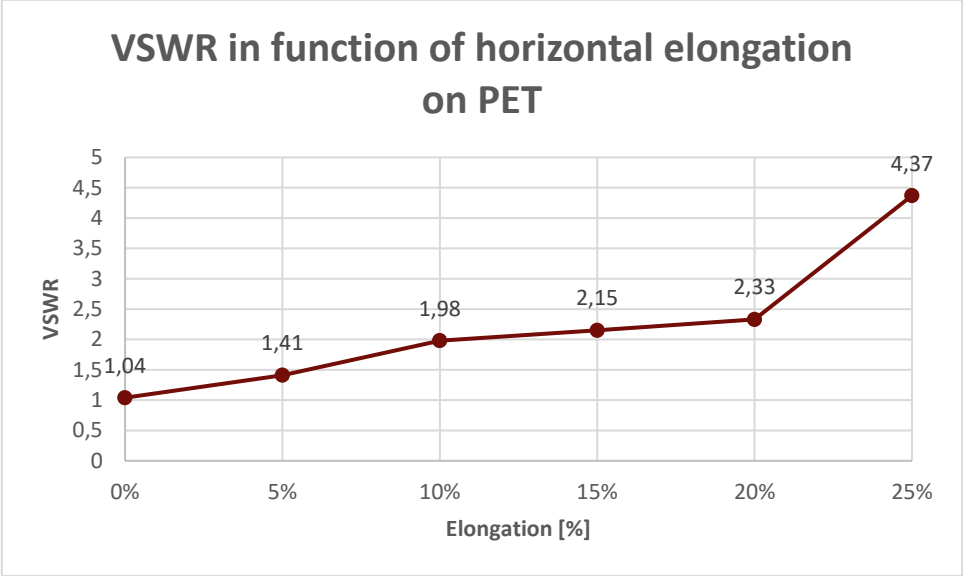

Figure 90: VSWR in function of horizontal elongation on PET

6.2.3 Elongation in both directions

It would now also be interesting to look at the how the antenna would react if it is elongated horizontally and vertically at the same time. The required dimensions for the inset fed patch antenna for both TPU and PET are shown in Table 30. The thickness will be set to 320 µm for TPU and 170 µm for PET. Each will decrease by 10 % with each level of elongation.

Table 30: New dimensions of inset fed patch after elongation in both directions in mm on TPU and PET

	0 %	5 %	10 %	15 %	20 %	25 %	30 %
a	36,850	38,693	40,535	42,378	44,220	46,063	47,905
b	39,150	41,108	43,065	45,023	46,980	48,938	50,895
c	15,270	16,034	16,797	17,561	18,324	19,088	19,851
d	2,000	2,100	2,200	2,300	2,400	2,500	2,600
e	2,300	2,415	2,530	2,645	2,760	2,875	2,990
f	26,050	27,353	28,655	29,958	31,260	32,563	33,865
g	13,100	13,755	14,410	15,065	15,720	16,375	17,030

The results of the simulations for TPU are shown in Table 31. The antenna would remain functional up to 10 % strain as the VSWR stays under the target value of 2. However, if the antenna needs to remain functional at its original resonant frequency, functionality is already lost at 5 % as the desired frequency of 2,54 GHz is no longer part of the antenna's bandwidth. The antenna shows no more bandwidth after 10 % elongation. The S11 and VSWR in function of the frequency are depicted in Figure 91.

Table 31: Results of elongation in both directions simulations from 0 % to 30 % on TPU

Elongation [%]	Sheet resistance [Ω/sq]	Resonant freq. [GHz]	S11 [dB]	VSWR	Reflected power [%]	Bandwidth 2:1 VSWR [GHz]
0 %	0,311	2,54	-36,13	1,03	0,02	2,39 - 2,68
5 %	0,451	2,35	-15,34	1,41	2,89	2,21 - 2,49
10 %	0,590	2,24	-9,50	2,01	11,26	2,24
15 %	0,652	2,09	-6,98	2,62	20,03	/
20 %	0,688	1,98	-4,98	3,58	31,73	/
25 %	2,054	/	/	/	/	/
30 %	11,597	/	/	/	/	/

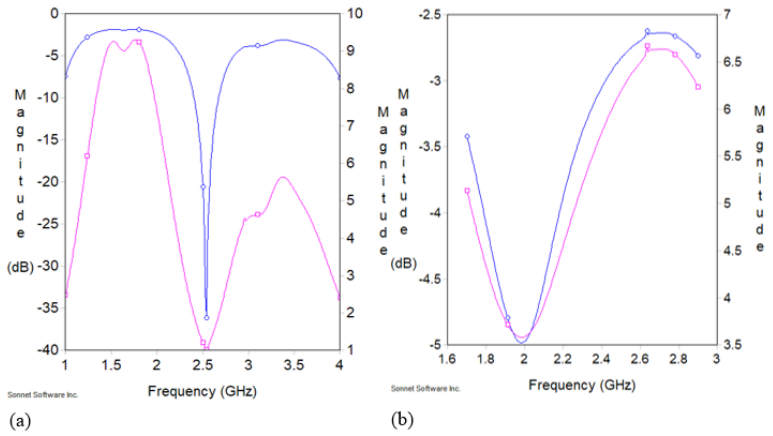

Figure 91: S11(blue) and VSWR(pink) in function of the frequency for (a) 0 % elongation (b) 20 % elongation in both directions on TPU

Figure 92 shows that the resonant frequency shifts to a lower value just as if the antenna is only stretched vertically. This further indicates that the horizontal dimensions of the antenna do not influence the antennas operating point. Figure 93 shows that when the antenna is stretched in both directions, the VSWR shows to increase following an exponential curve.

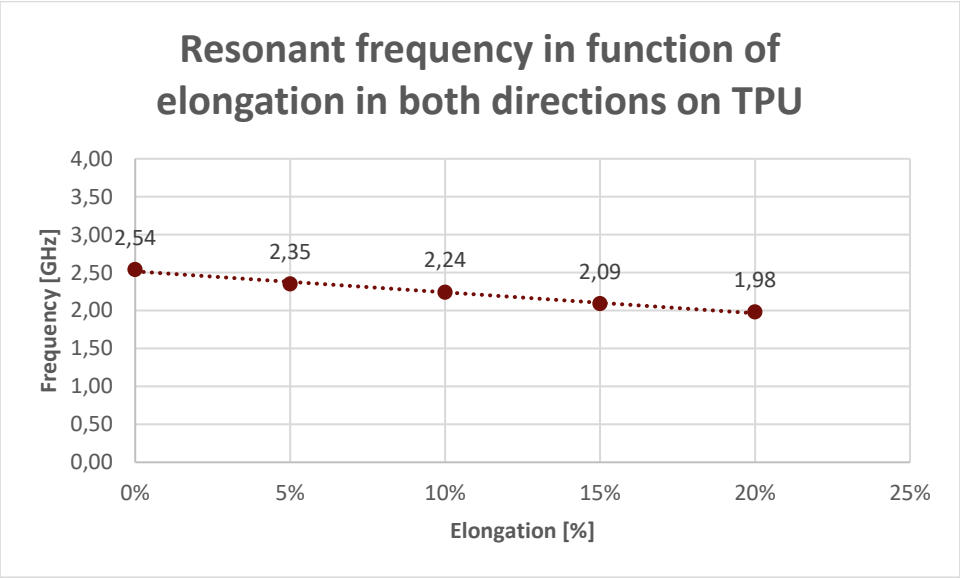

Figure 92: Resonant frequency in function of elongation in both directions on TPU

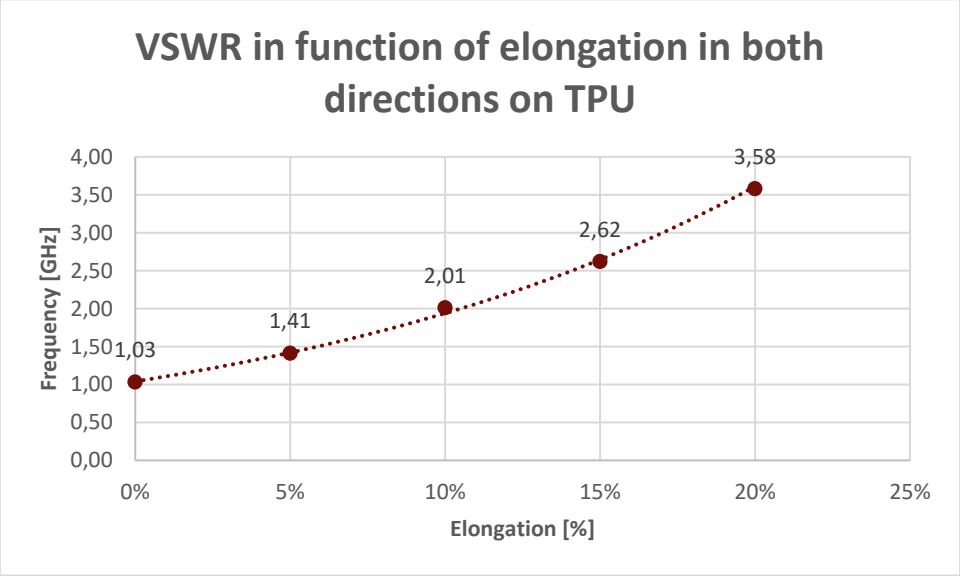

Figure 93: VSWR in function of elongation in both directions on TPU

When performing these simulations on PET, the results of Table 32 are found. In this case, the antenna would remain functional up to 5 % elongation. If the antenna is required to work at its original frequency, functionality is already lost at 5 %. At 10 % and beyond, the antenna no longer shows a bandwidth where the VSWR becomes lower than 2. The S11 and VSWR in function of the frequency is given in Figure 94.

Table 32: Results of elongation in both directions simulations from 0 % to 30 % on PET

Elongation [%]	**Sheet resistance [Ω/sq]**	**Resonant freq. [GHz]**	**S11 [dB]**	**VSWR**	**Reflected power [%]**	**Bandwidth 2:1 VSWR [GHz]**
0 %	0,311	3,14	-30,91	1,06	0,08	3,01 - 3,26
5 %	0,451	2,91	-11,53	1,73	7,15	2,82 - 3,01
10 %	0,590	2,78	-6,94	2,64	20,30	/
15 %	0,652	2,55	-4,81	3,71	33,11	/
20 %	0,688	2,45	-3,31	5,31	46,65	/
25 %	2,054	/	/	/	/	/
30 %	11,597	/	/	/	/	/

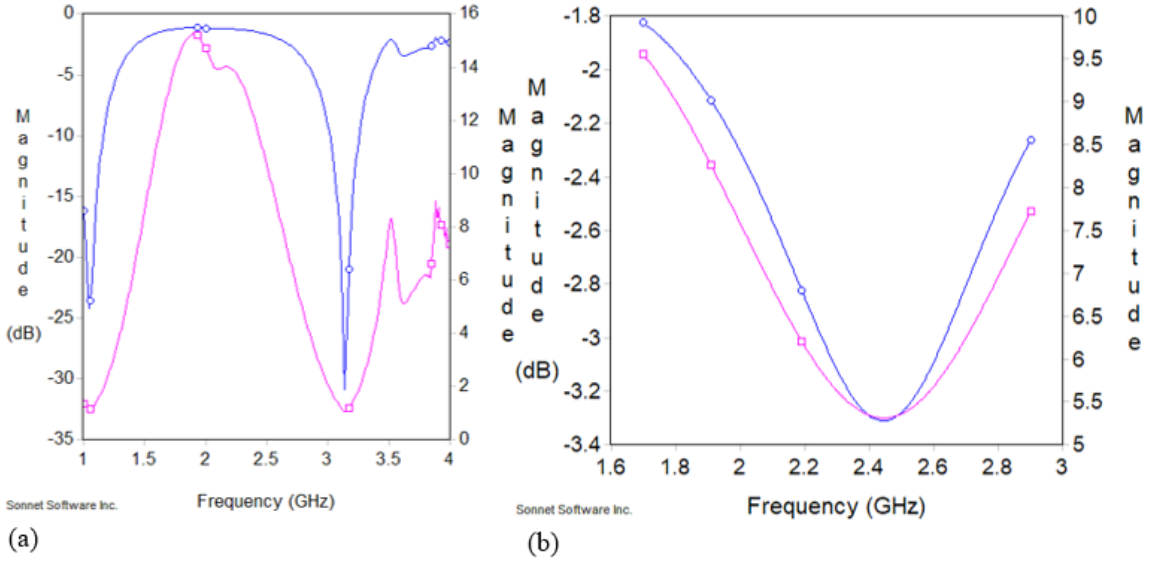

Figure 94: S11(blue) and VSWR(pink) in function of the frequency for (a) 0 % elongation (b) 20 % elongation in both directions on PET

The resonant frequency again shows a linear decrease as the elongation increases, following the results of the vertical elongation on PET (Figure 95). Just as on TPU, the VSWR increases exponentially with the increase of strain (Figure 96).

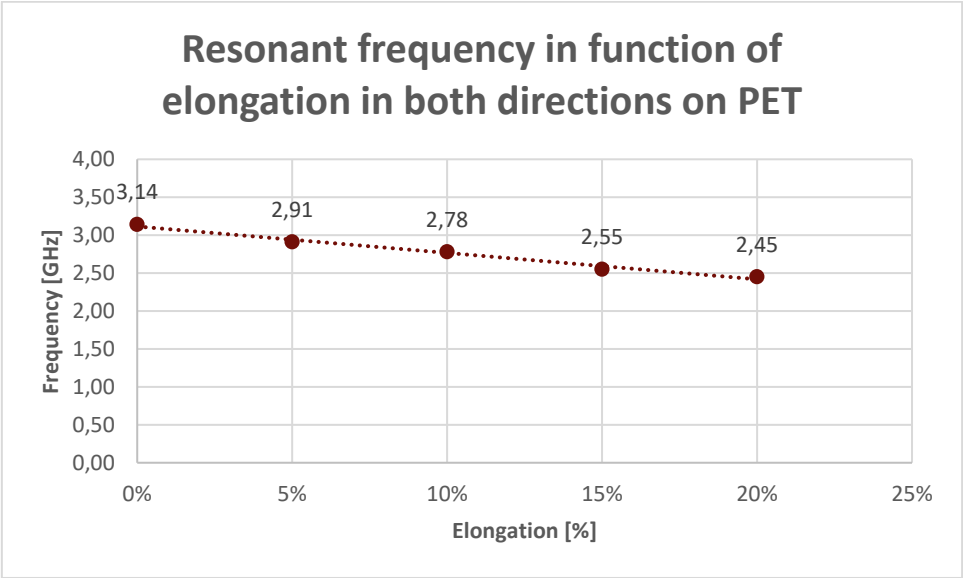

Figure 95: Resonant frequency in function of elongation in both directions on PET for patch

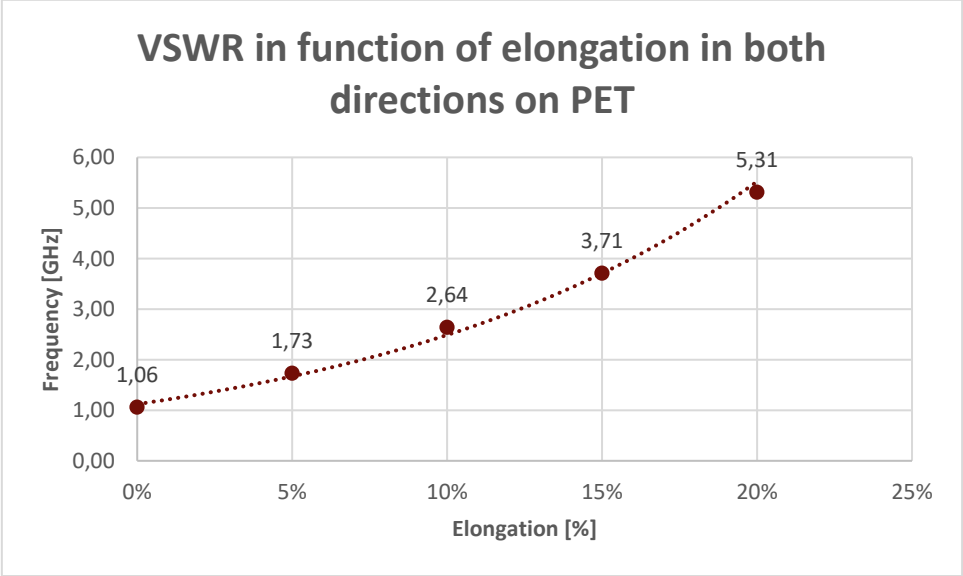

Figure 96: VSWR in function of elongation in both directions on PET for patch

6.3 RFID antenna simulations

Second, the same simulations are performed on the RFID design. The RFID is also simulated in its vertical, horizontal and in both directions going form 0 % to 30 % elongation. Each step is again a 5 % increase of strain.

6.3.1 Elongation in vertical direction

As the RFID antenna is stretched, its shape changes accordingly. The change in shape with its corresponding new dimensions is given in Figure 97 and Table 33. The annotations for the design are given in Figure 71.

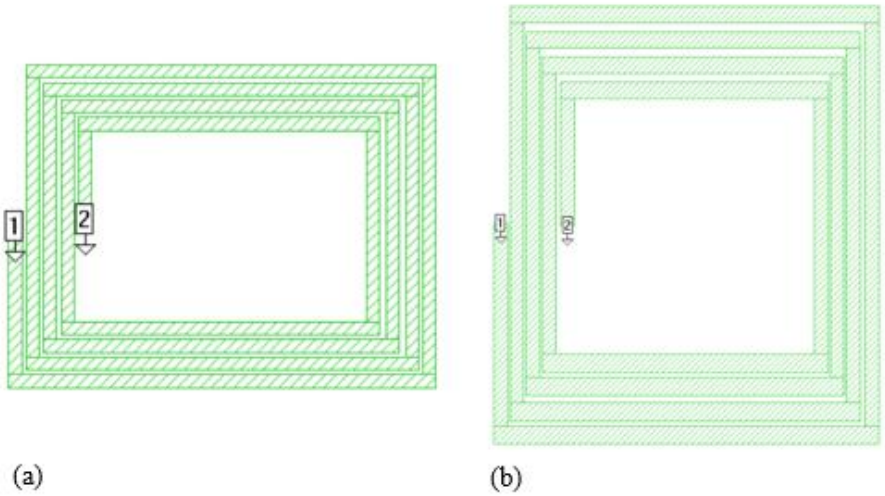

Figure 97: RFID antenna at (a) 0 % vertical elongation (b) 30 % vertical elongation

Table 33: New dimensions of RFID after vertical elongation in mm on TPU

	0%	5%	10%	15%	20%	25%	30%
a	49,020	48,040	47,059	46,079	45,098	44,118	43,138
b	44,810	43,914	43,018	42,121	41,225	40,329	39,433
c	40,640	39,827	39,014	38,202	37,389	36,576	35,763
d	36,420	35,692	34,963	34,235	33,506	32,778	32,050
e	35,050	34,349	33,648	32,947	32,246	31,545	30,844
f	39,220	38,436	37,651	36,867	36,082	35,298	34,514
g	43,420	42,552	41,683	40,815	39,946	39,078	38,210
h	47,610	46,658	45,706	44,753	43,801	42,849	41,897
i	31,680	33,264	34,848	36,432	38,016	39,600	41,184
j	27,480	28,854	30,228	31,602	32,976	34,350	35,724
k	23,290	24,455	25,619	26,784	27,948	29,113	30,277
l	21,190	22,250	23,309	24,369	25,428	26,488	27,547
m	25,380	26,649	27,918	29,187	30,456	31,725	32,994
n	29,590	31,070	32,549	34,029	35,508	36,988	38,467
o	33,780	35,469	37,158	38,847	40,536	42,225	43,914
p	16,890	17,735	18,579	19,424	20,268	21,113	21,957
q	10,570	11,099	11,627	12,156	12,684	13,213	13,741
r	1,599	1,679	1,759	1,839	1,919	1,999	2,079
s	1,599	1,567	1,535	1,503	1,471	1,439	1,407
x	0,501	0,526	0,551	0,576	0,601	0,626	0,651
y	0,501	0,491	0,481	0,471	0,461	0,451	0,441

From 0 % to 20 % vertical elongation, all measured parameters show little to no change (Table 34). The resonant frequency shifts upwards slightly going from 15 MHz to 20 MHz. From 20 % to 25 % strain, the resonant frequency jumps up to 60 MHz, while the S11, VSWR and reflected power remain the same, unlike the inset fed patch design. 20 % to 25 % is also to step where the sheet resistance increases drastically going from 0,688 to 2,054 Ω/sq. This is a first indication that the RFID antenna design is not affected by deformation, but is dependent on the resistance of the antenna. The S11 and VSWR in function of the frequency are shown in Figure 98.

Table 34: Results of vertical elongation simulations from 0 % to 30 % on TPU for RFID

Elongation [%]	Sheet resistance [Ω/sq]	Res. freq. [MHz]	S11 [dB]	VSWR	Reflected power [%]
0	0,311	15,0	-8,25	2,26	14,94
5	0,451	15,0	-8,21	2,27	15,08
10	0,590	20,0	-8,21	2,27	15,08
15	0,652	20,0	-8,23	2,27	15,08
20	0,688	20,0	-8,23	2,27	15,08
25	2,054	60,0	-8,24	2,26	14,94
30	11,597	/	/	/	/

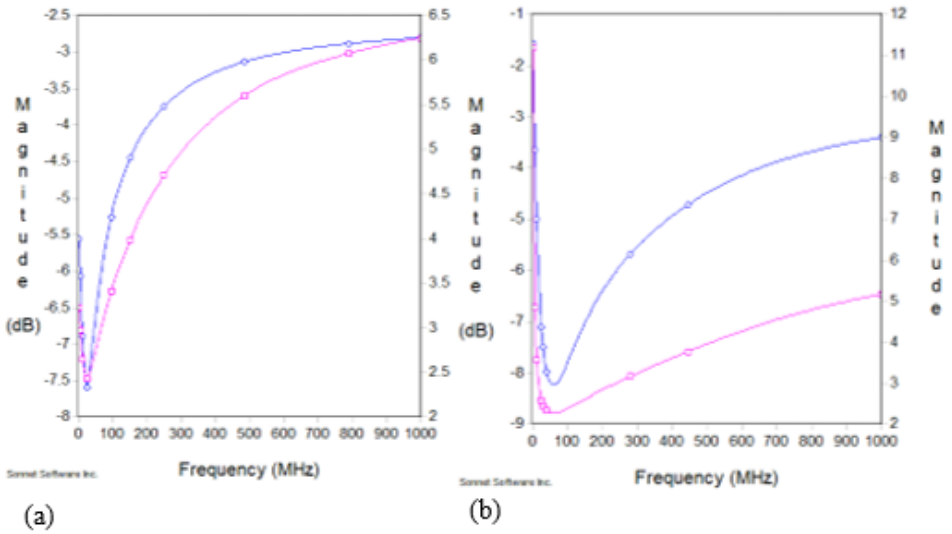

Figure 98: S11(blue) and VSWR(pink) in function of the frequency for (a) 0 % vertical elongation (b) 25 % vertical elongation on TPU for RFID

As an additional test to see if the elongation has an influence on the antenna, a new simulation is made where the sheet resistance of the antenna at 25 % is used at 0 % elongation. These results are then compared to the results at 25 % (Table 35 and Figure 98). These results show that there is no significant difference in the response, indicating further that the RFID antenna is only dependent on the resistance.

Table 35: Results of 2,054 Ω/sq at 0 % and 25 % vertical elongation for RFID

Elongation [%]	Sheet resistance [Ω/sq]	Res. freq. [MHz]	S11 [dB]	VSWR	Reflected power [%]
0	2,054	70,0	-8,24	2,26	14,94
25	2,054	60,0	-8,24	2,26	14,94

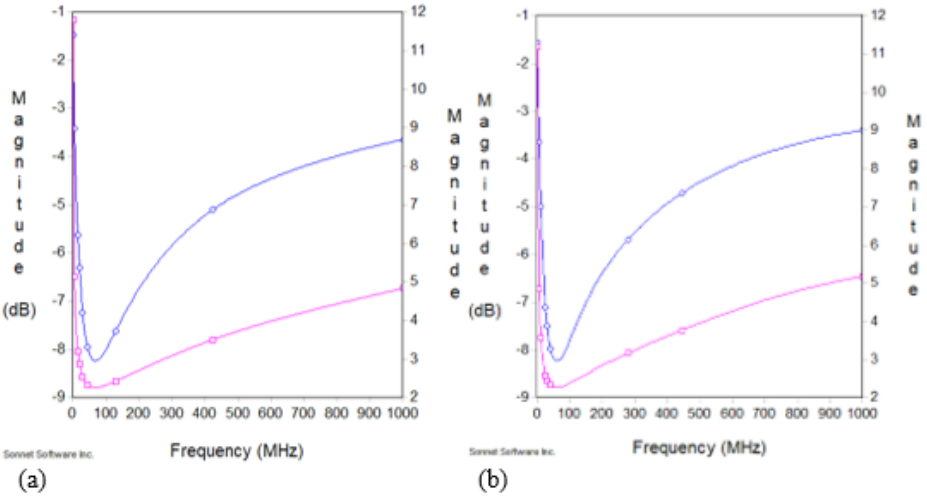

6.3.2 Elongation in horizontal direction

The horizontal elongation of the RFID antenna is depicted in Figure 99 with its new dimensions shown in Table 36.

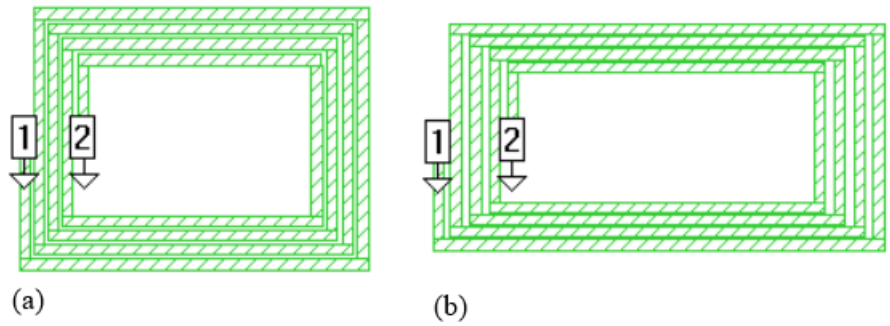

Figure 99: RFID antenna at (a) 0 % horizontal elongation (b) 30 % horizontal elongation

Table 36: New dimensions of RFID after horizontal elongation in mm on TPU

	0%	5%	10%	15%	20%	25%	30%
a	49,020	51,471	53,922	56,373	58,824	61,275	63,726
b	44,810	47,051	49,291	51,532	53,772	56,013	58,253
c	40,640	42,672	44,704	46,736	48,768	50,800	52,832
d	36,420	38,241	40,062	41,883	43,704	45,525	47,346
e	35,050	36,803	38,555	40,308	42,060	43,813	45,565
f	39,220	41,181	43,142	45,103	47,064	49,025	50,986
g	43,420	45,591	47,762	49,933	52,104	54,275	56,446
h	47,610	49,991	52,371	54,752	57,132	59,513	61,893
i	31,680	30,888	30,096	29,304	28,512	27,720	26,928
j	27,480	26,793	26,106	25,419	24,732	24,045	23,358
k	23,290	22,708	22,126	21,543	20,961	20,379	19,797
l	21,190	20,660	20,131	19,601	19,071	18,541	18,012
m	25,380	24,746	24,111	23,477	22,842	22,208	21,573
n	29,590	28,850	28,111	27,371	26,631	25,891	25,152
o	33,780	32,936	32,091	31,247	30,402	29,558	28,713
q	10,570	10,306	10,042	9,777	9,513	9,249	8,985
p	16,890	16,468	16,046	15,623	15,201	14,779	14,357
r	1,599	1,559	1,519	1,479	1,439	1,399	1,359
s	1,599	1,679	1,759	1,839	1,919	0,400	0,480
x	0,501	0,488	0,476	0,463	0,451	0,438	0,426
y	0,501	0,526	0,551	0,576	0,601	0,125	0,150

When the RFID antenna is stretched horizontally, the resonant frequency of the antenna shifts upwards (Table 37). From 0 % to 20 %, the resonant frequency only changes slightly. From 20 % to 25 % the resonant frequency suddenly jumps form 20 MHz to 60 MHz identical to the vertical elongation tests. This indicates again that the resonant frequency of the RFID is dependent on the resistance of the antenna, as the sheet resistance also shows a significant jump going from 20 % to 25 %. When comparing Table 37 to Table 34 it is clear that there is close to no difference between stretching the RFID antenna horizontally or vertically. The S11 and VSWR in function of the frequency are shown in Figure 100.

Table 37: Results of horizontal elongation simulations from 0 % to 30 % on TPU for RFID

Elongation [%]	Sheet resistance [Ω/sq]	Res. freq. [MHz]	S11 [dB]	VSWR	Reflected power [%]
0	0,311	15,0	-7,93	2,34	16,10
5	0,451	15,0	-8,24	2,26	14,94
10	0,590	20,0	-8,22	2,26	14,94
15	0,652	20,0	-8,22	2,27	15,08
20	0,688	20,0	-8,21	2,27	15,08
25	2,054	60,0	-8,21	2,27	15,08
30	11,597	/	/	/	/

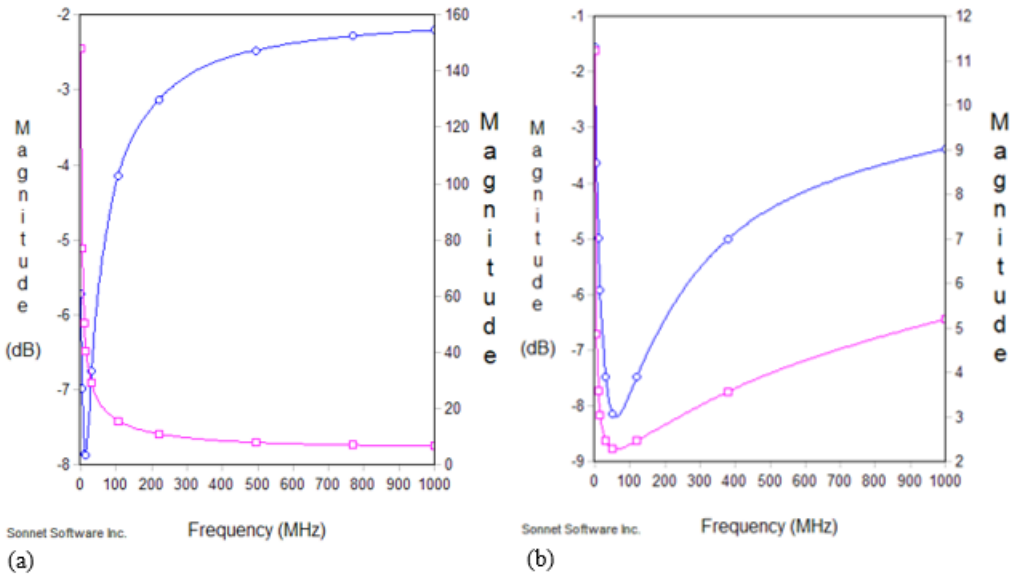

Figure 100: S11(blue) and VSWR(pink) in function of the frequency for (a) 0 % horizontal elongation (b) 25 % horizontal elongation on TPU for RFID

To further investigate if the elongation has a significant influence on the antenna behaviour or if it is mostly dependent on the sheet resistance, an additional simulation is performed. This simulation again uses the sheet resistance of 25 % elongation at 0 % to eliminate the deformation of the antenna from the test. The results are depicted in Figure 101 and Table 38 and again show no significant difference. Furthermore, the results for horizontal and vertical elongation appear to be near identical.

Table 38: Results of 2,054 Ω/sq at 0 % and 25 % horizontal elongation for RFID

Elongation [%]	Sheet resistance [Ω/sq]	Res. freq. [MHz]	S11 [dB]	VSWR	Reflected power [%]
0	2,054	70,0	-8,24	2,26	14,94
25	2,054	60,0	-8,21	2,27	15,08

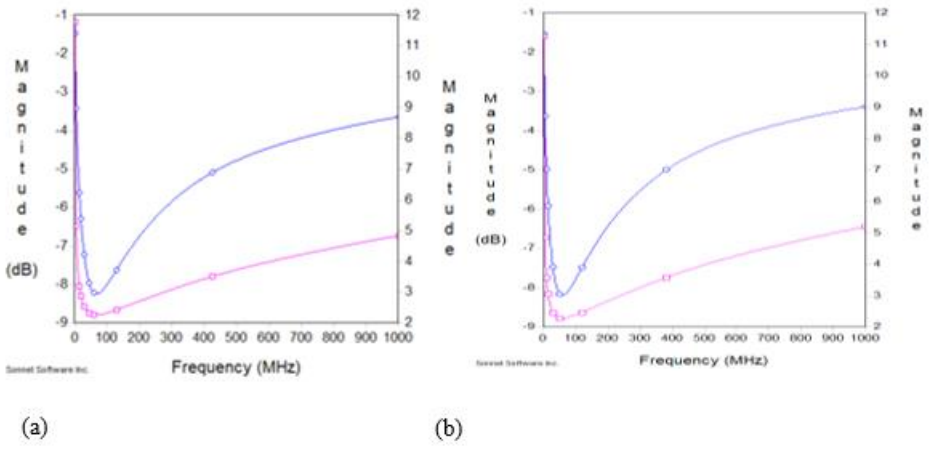

Figure 101: S11 (blue) and VSWR (pink) in function of frequency for (a) 0 % (b) 25 % horizontal elongation with 2,054 Ω/sq for RFID

6.3.3 Elongation in both directions

Finally, the RFID antenna is stretched in both its vertical and horizontal direction simultaneously. The new dimensions for the antenna at each level of elongation are given in Table 39.

Table 39: New dimensions of RFID after elongation in both directions in mm on TPU

	0%	5%	10%	15%	20%	25%	30%
a	49,020	51,471	53,922	56,373	58,824	61,275	63,726
b	44,810	47,051	49,291	51,532	53,772	56,013	58,253
c	40,640	42,672	44,704	46,736	48,768	50,800	52,832
d	36,420	38,241	40,062	41,883	43,704	45,525	47,346
e	35,050	36,803	38,555	40,308	42,060	43,813	45,565
f	39,220	41,181	43,142	45,103	47,064	49,025	50,986
g	43,420	45,591	47,762	49,933	52,104	54,275	56,446
h	47,610	49,991	52,371	54,752	57,132	59,513	61,893
i	31,680	33,264	34,848	36,432	38,016	39,600	41,184
j	27,480	28,854	30,228	31,602	32,976	34,350	35,724
k	23,290	24,455	25,619	26,784	27,948	29,113	30,277
l	21,190	22,250	23,309	24,369	25,428	26,488	27,547
m	25,380	26,649	27,918	29,187	30,456	31,725	32,994
n	29,590	31,070	32,549	34,029	35,508	36,988	38,467
o	33,780	35,469	37,158	38,847	40,536	42,225	43,914
p	16,890	17,735	18,579	19,424	20,268	21,113	21,957
q	10,570	11,099	11,627	12,156	12,684	13,213	13,741
r	1,599	1,679	1,759	1,839	1,919	1,999	2,079
s	1,599	1,679	1,759	1,839	1,919	1,999	2,079
x	0,501	0,526	0,551	0,576	0,601	0,626	0,651
y	0,501	0,526	0,551	0,576	0,601	0,626	0,651

When comparing the results of elongation in both directions to the results of the individual vertical and horizontal tests, it is clear that again there is no significant difference (Table 40). This solidifies the hypothesis that the characteristics of the RFID do not change due to deformation, but due to the change of the resistance of the antenna as it gets deformed. The graph of the S11 and VSWR in function of the frequency are given in Figure 102.

Table 40: Results of elongation in both directions from 0 % to 30 % on TPU for RFID

Elongation [%]	Sheet resistance [Ω/sq]	Res. freq. [MHz]	S11 [dB]	VSWR	Reflected power [%]
0	0,311	15,0	-7,93	2,34	16,10
5	0,451	15,0	-8,24	2,26	14,99
10	0,590	20,0	-8,19	2,28	15,16
15	0,652	20,0	-8,20	2,27	15,16
20	0,688	20,0	-8,20	2,27	15,14
25	2,054	52,0	-8,22	2,27	15,07
30	11,597	/	/	/	/

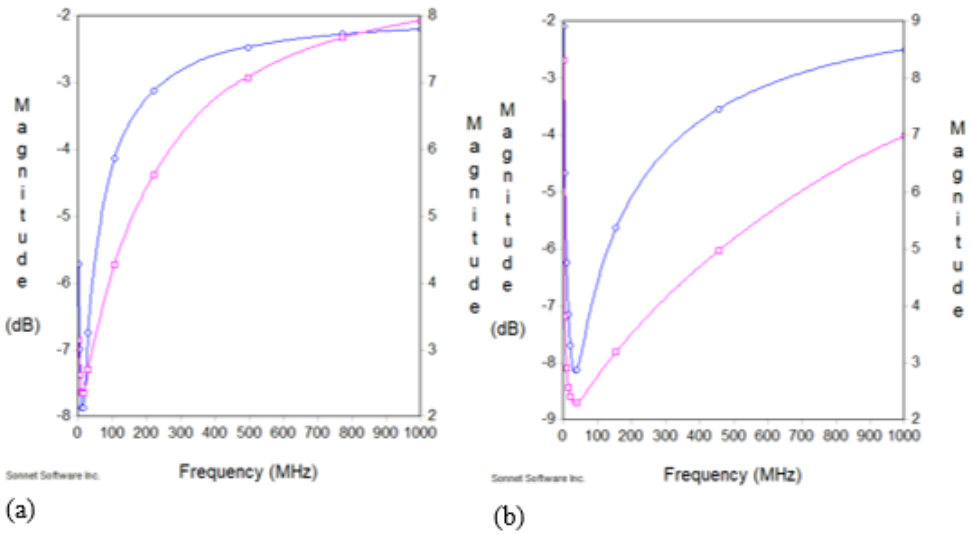

Figure 102: S11(blue) and VSWR(pink) in function of the frequency for (a) 0 % (b) 25 % elongation in both directions on TPU for RFID

The above indicates that if the VSWR can be brought down by a possible redesign of the antenna, the antenna could remain functional up to 20 % horizontal or vertical elongation, possibly even 25 % if the bandwidth remains large enough. It should also be taken into account that the model used for the simulations of the RFID antenna is a simplified version of the design (no rounded corners). This in combination with the achievable accuracy of sonnet lite (0,25 mm to keep the file size low enough) might cause the real life paperonics RFID antenna to behave differently than these simulations show. Although these software limitations might influence the exact frequency at which the antenna resonates, or the value of the VSWR, it will not affect the behaviour of the antenna as it is stretched.

6.4 Conclusion

This chapter discusses virtual antenna testing using the simulation software *Sonnet Lite*. Tests are performed on the inset fed patch antenna and the RFID antenna design. As only the lite version of the Sonnet software is available, the RFID uses a simplified redesign to keep its file size sufficiently low. The dipole antenna cannot be tested as Sonnet Lite does not offer the required feed settings. Before looking at the effects of elongation on the designs, preliminary tests are performed to see the effect of the thickness of the ink layer, the thickness of the substrate material and the conductivity of the ink. For both the inset fed patch and the RFID antenna, the thickness of the ink layer does not show an influence on the behaviour of the antenna as the layer thickness that the printers can achieve is sufficiently thin.

For the inset fed patch antenna, the substrate thickness and ink conductivity go hand in hand as the impedance of the antenna should be matched to the impedance of the port it is connected to. When using the sheet resistance of 0,311 Ω/sq as found in chapter 5, the ideal substrate thickness was found to be 320 μm when using TPU, and 170 μm when using PET. With this combination, no power is reflected back from the antenna to the port, indicating that a more conductive ink is not beneficial. If a more conductive ink is used, the thickness of the substrate has to be recalculated to ensure that the impedance is matched. For the RFID antenna, the substrate thickness does not show an ideal value. The resonant peak fades away as the thickness of the substrate increases. As the RFID antenna is used to identify objects using a specific frequency, it is decided to use the substrate thickness at which the resonant frequency would be closest to the designed frequency of 13,56 MHz. With a sheet resistance of 0,311 Ω/sq, this would be the case at a 60 μm thick substrate layer when using TPU or 35 μm when using PET. For the RFID antenna, lowering the conductivity of the ink shows that it only impacts the resonant frequency of the antenna. Using the previously stated thicknesses for TPU and PET, it can be observed that when the ink becomes too conductive (< 0,15 Ω/sq or < 0,20 Ω/sq respectively), no resonant frequency can be found as the resonant frequency becomes ±0 MHz. PEDOT:PSS was investigated as a possible ink material for both the inset fed patch and RFID antenna because of its high stretchability. However, no resonant frequency can be obtained for either one of the antenna designs as the resistance of PEDOT:PSS is too high. Therefore this ink type is not further investigated in this research. Literature shows that by chemically treating the PEDOT:PSS, the resistance could be lowered enough for it to work for resonant antennas, but this should be further investigated in future research. Another option is to use a non-resonant antenna design as these designs require less conductive materials as discussed in 2.6.2 and 6.1.

When elongating the inset fed patch antenna, it can be observed that vertical elongation lowers the resonant frequency, and increases the VSWR of the antenna. Up to 20 % vertical elongation on TPU, the VSWR remains lower than 2 indicating a functioning antenna. If however the antenna has to remain functional at its original resonant frequency of 2,50 GHz, the antenna would remain functional up to 10 % elongation as the resonant frequency after 10 % is no longer part of the bandwidth of the antenna. The results are less promising on PET as the antenna would be functional up to 10 % elongation, or 5 % if the antenna has to remain functional at 2,50 GHz. Horizontal elongation increases the VSWR, but does not affect the resonant frequency of the antenna. For this reason the antenna can remain functional and will also still work at 2,50 MHz up to 20% horizontal elongation on TPU. For PET, the antenna will be functional up to 10 % elongation. When the antenna is stretched in both directions, the VSWR will remain low enough up to 10 % elongation on TPU and 5 % elongation on PET. However for both substrate materials, the original frequency of 2,50 GHz is no longer part of the antennas bandwidth at 5 % elongation.

When elongating the RFID antenna, it can be observed that the kind of elongation does not affect how the antenna behaves. With the same sheet resistances, the results for vertical, horizontal and both directions are near identical. This is further consolidated when the antenna is simulated with the sheet resistances of 25 % elongation at 0 % elongation. In this case, the results are also near identical. These results indicate that the RFID antenna is not affected by elongation, but only by its sheet resistance.

7 Conclusion

After a consultation with Fremach and an extensive literature study, it was decided that the focus of this thesis would be put on the development of printable, stretchable antenna applications using silver nano-particle ink, silver micro flake ink and PEDOT:PSS ink on TPU and PET substrates. The antennas would be printed with both inkjet and screen printing. First, a step-by-step guide is given that depicts the antenna development process. This contains the important parameters that should be taken into account, a discussion on the material selection process and the difficulties that could occur. Next, physical and virtual testing is combined to investigate how the proposed inset fed patch, RFID and dipole antenna would behave when 2D stretch is applied.

The step-by-step guide could be used as a guide for Fremach to develop a specific antenna that would fulfil their needs. The first step is to specify the type and use case of the antenna. This in turn determines the antenna design and its parameters. The next step is to analyse the antenna with antenna simulation software. These simulations can be used to further narrow down the choice of materials and to tweak and redesign the antenna if necessary without having to produce prototypes. Finally, a physical antenna can be produced and tested to see if it functions according to the predetermined parameters from the simulations.

Experiments show a great potential for micro flake inks like the DuPont ME602, these combine a relatively low and constant resistivity up to approximately 20 – 25 %. Although the silver nano-particle ink has a higher conductivity than its micro flake counterpart, the ink is not stretchable and shows crack formation even before the antenna is stretched. The PEDOT:PSS on the other hand shows great stretchability, but suffers from high resistivity. The substrate material also shows to have a great influence on the resistance of the antenna. This however can be changed by altering the surface free energy of the substrate to obtain a higher wettability by using a corona treatment. Nevertheless, the wettability of the substrate is an important parameter on how well the antenna functions.

Simulations with Sonnet Lite demonstrate how the substrate thickness should be determined. The inset fed patch antenna printed with ME602 ink would function best with a substrate thickness of 320 µm for TPU but 170 µm of PET. The ideal substrate thicknesses for the RFID antenna could not be determined. The material and thickness of the substrate have a major influence on the functioning of the antenna, as does the conductivity of the ink. However, the thickness of the ink has no influence on the antennas performance. Simulations show that 2D elongation influences the antenna parameters of the inset fed patch antenna. The direction of elongation is important when using the inset fed patch design as the resonant frequency will lower when it is stretched vertically, but will stay constant when stretched horizontally. The antenna shows to stay functional when elongated up to 10 % vertically or 20 % horizontally on TPU and 5 % vertically or 10 % horizontally on PET, when the stretch is applied in both directions, it can be stretched up to 5 % for both substrate types. A redesign of the antenna is thus not always necessary if the applied elongation is low enough. The elongation does not have any effect on the functioning of the RFID whether it is applied vertically, horizontally or in both directions. The behaviour of the RFID only changed because the sheet resistance of the antenna increases as the elongation increases.

The next logical step after the influence of 2D deformation is to investigate the effect of 3D deformation. The antenna parameters are also expected to change even when the antenna is bent. It could be interesting for future research to investigate how much the antenna can be warped instead of stretched, and how warping and bending influences the behaviour of the antenna. Finally, experiments on thermo and vacuum forming the antenna are an interesting next step so in-mold labelling could be made possible. For realising a PEDOT:PSS antenna in future research, resonant antennas could be possible after developing a more conductive PEDOT:PSS variant using chemical treatment. Another option is to research non-resonant antenna designs as literature has proven this to be functional.

Bibliography

[1] "DuPont Microcircuit Materials Introduces Stretchable Inks for Wearable Electronics." [Online]. Available: https://www.prweb.com/releases/dupont-microcircuit/stretchable-ink/prweb12368818.htm. [Accessed: 17-Feb-2020].

[2] "In-Mold Electronics 2019-2029: Technology, Market Forecasts, Players: IDTechEx." [Online]. Available: https://www.idtechex.com/en/research-report/in-mold-electronics-2019-2029-technology-market-forecasts-players/647. [Accessed: 24-Oct-2019].

[3] "In-Mold Electronics White Paper - Sun Chemical." [Online]. Available: https://www.sunchemical.com/resource/in-mold-electronics-white-paper/. [Accessed: 26-Oct-2019].

[4] IDTechEx, "Structural Electronics 2018-2028: Applications, Technologies, Forecasts: IDTechEx." [Online]. Available: https://www.idtechex.com/en/research-report/structural-electronics-2018-2028-applications-technologies-forecasts/602. [Accessed: 18-Dec-2019].

[5] E. Macdonald *et al.*, "3D Printing for the Rapid Prototyping of Structural Electronics," *IEEE Access*, vol. 2, pp. 234–242, Dec. 2014.

[6] T. Cheng, Y. Zhang, W.-Y. Lai, and W. Huang, "Stretchable Thin-Film Electrodes for Flexible Electronics with High Deformability and Stretchability," *Adv. Mater.*, vol. 27, no. 22, pp. 3349–3376, Jun. 2015.

[7] S. Nagels, "Electronic devices which stretch like rubber bands: a holistic approach to materials and fabrication methods for stretchable electronics," 2019.

[8] J. Abu-Khalaf, L. Al-Ghussain, and A. Al-Halhouli, "Fabrication of Stretchable Circuits on Polydimethylsiloxane (PDMS) Pre-Stretched Substrates by Inkjet Printing Silver Nanoparticles," *Materials (Basel).*, vol. 11, no. 12, p. 2377, Nov. 2018.

[9] "'Linear Polydimethylsiloxanes' Joint Assessment of Commodity Chemicals, September 1994 (Report No. 26)." 1994.

[10] J. Wu *et al.*, "Inkjet-printed microelectrodes on PDMS as biosensors for functionalized microfluidic systems," *Lab Chip*, vol. 15, no. 3, pp. 690–695, Jan. 2015.

[11] Z. W. Zhong, R. W. L. Tang, S. H. Chen, and X. C. Shan, "A study of screen printing of stretchable circuits on polyurethane substrates," *Microsyst. Technol.*, vol. 25, no. 1, pp. 339–350, Jan. 2019.

[12] J. Yoon, J. Lee, and J. Hur, "Stretchable Supercapacitors Based on Carbon Nanotubes-Deposited Rubber Polymer Nanofibers Electrodes with High Tolerance against Strain," *Nanomaterials*, vol. 8, no. 7, p. 541, Jul. 2018.

[13] S. Eom and S. Lim, "Stretchable Complementary Split Ring Resonator (CSRR)-Based Radio Frequency (RF) Sensor for Strain Direction and Level Detection," *Sensors*, vol. 16, no. 10, p. 1667, Oct. 2016.

[14] J. A. Rogers, T. Someya, and Y. Huang, "Materials and Mechanics for Stretchable Electronics," *Science (80-.).*, vol. 327, no. 5973, pp. 1603–1607, Mar. 2010.

[15] A. J. Stapleton *et al.*, "Planar silver nanowire, carbon nanotube and PEDOT:PSS nanocomposite transparent electrodes.," *Sci. Technol. Adv. Mater.*, vol. 16, no. 2, p. 025002, Apr. 2015.

[16] R. Gupta and S. Peruvemba, "What's The Difference Between Silver Nanowire And ITO For Touchscreens?," *Aug 05*, 2013. [Online]. Available: https://www.electronicdesign.com/components/what-s-difference-between-silver-nanowire-and-ito-touchscreens. [Accessed: 02-Oct-2019].

[17] H. Lee, K. Lee, J. T. Park, W. C. Kim, and H. Lee, "Well-Ordered and High Density Coordination-Type Bonding to Strengthen Contact of Silver Nanowires on Highly Stretchable Polydimethylsiloxane," *Adv. Funct. Mater.*, vol. 24, no. 21, pp. 3276–3283, Jun. 2014.

[18] L. Cai and C. Wang, "Carbon Nanotube Flexible and Stretchable Electronics," *Nanoscale Res. Lett.*, vol. 10, no. 1, p. 320, Dec. 2015.

[19] Y. Khan *et al.*, "Inkjet-Printed Flexible Gold Electrode Arrays for Bioelectronic Interfaces," *Adv. Funct. Mater.*, vol. 26, no. 7, pp. 1004–1013, Feb. 2016.

[20] L. V. Kayser and D. J. Lipomi, "Stretchable Conductive Polymers and Composites Based on PEDOT and PEDOT:PSS," *Adv. Mater.*, vol. 31, no. 10, pp. 1–13, 2019.

[21] H. Jang, Y. J. Park, X. Chen, T. Das, M.-S. Kim, and J.-H. Ahn, "Graphene-Based Flexible and Stretchable Electronics," *Adv. Mater.*, vol. 28, no. 22, pp. 4184–4202, Jun. 2016.
[22] Dupont, "DuPont In-Mold Electronic Technology | Electronic Inks." [Online]. Available: https://www.dupont.com/products/in-mold-electronic-technology.html. [Accessed: 19-Oct-2019].
[23] Agfa, "Orgacon for conductive circuitry - Specialty Products." [Online]. Available: https://www.agfa.com/specialty-products/solutions/conductive-materials/orgacon-conductive-circuitry/. [Accessed: 19-Oct-2019].
[24] L. Henkel Electronic Materials, "INKS AND COATINGS PRINTED ELECTRONICS." [Online]. Available: https://dm.henkel-dam.com/is/content/henkel/Brochure_Printed_Electronics_Inks___Coatingspdf. [Accessed: 30-Oct-2019].
[25] W. J. Hyun, E. B. Secor, M. C. Hersam, C. D. Frisbie, and L. F. Francis, "High-Resolution Patterning of Graphene by Screen Printing with a Silicon Stencil for Highly Flexible Printed Electronics," *Adv. Mater.*, vol. 27, no. 1, pp. 109–115, Jan. 2015.
[26] F. Hoeng, A. Denneulin, N. Reverdy-Bruas, G. Krosnicki, and J. Bras, "Rheology of cellulose nanofibrils/silver nanowires suspension for the production of transparent and conductive electrodes by screen printing," *Appl. Surf. Sci.*, vol. 394, pp. 160–168, Feb. 2017.
[27] T. Liimatta, E. Halonen, H. Sillanpaa, J. Niittynen, and M. Mantysalo, "Inkjet printing in manufacturing of stretchable interconnects," in *2014 IEEE 64th Electronic Components and Technology Conference (ECTC)*, 2014, pp. 151–156.
[28] HELMHOLTZ-Zentrum Berlin für materialien und energie, "Inkjet printing process for kesterite solar cells | EurekAlert! Science News." [Online]. Available: https://www.eurekalert.org/pub_releases/2015-05/hbfm-ipp050615.php. [Accessed: 13-Nov-2019].
[29] Innoflex, "In-Mold Electronics - Inno-Flex," *In-Mold Electronics*, 2019. [Online]. Available: https://www.innoflexcorp.com/in-mold-electronics/. [Accessed: 30-Oct-2019].
[30] Axel Barrett, "Thermoforming With Biobased Plastics for Greater Sustainability – Bioplastics News," 2019. [Online]. Available: https://bioplasticsnews.com/2019/05/04/thermoforming-with-biobased-plastics-for-greater-sustainability/. [Accessed: 30-Oct-2019].
[31] "Difference Between Thermoforming Vacuum Forming And Pressure Forming," *What is the difference between Thermoforming, Vacuum Forming and Pressure Forming*. [Online]. Available: http://engatech.com/difference-thermoforming-vacuum-forming-pressure-forming/. [Accessed: 30-Oct-2019].
[32] T. Azdast, A. Doniavi, S. Rash Ahmadi, and E. Amiri, "Numerical and experimental analysis of wall thickness variation of a hemispherical PMMA sheet in thermoforming process."
[33] Tactotek, "Manufacturing of TactoTek IMSE – from printed electronics to hybrid integration on Vimeo." [Online]. Available: https://vimeo.com/224631203. [Accessed: 19-Oct-2019].
[34] S. Rosset and H. R. Shea, "Flexible and stretchable electrodes for dielectric elastomer actuators," *Appl. Phys. A*, vol. 110, no. 2, pp. 281–307, Feb. 2013.
[35] F. A. Mohd Ghazali, C. K. Mah, A. AbuZaiter, P. S. Chee, and M. S. Mohamed Ali, "Soft dielectric elastomer actuator micropump," *Sensors Actuators, A Phys.*, vol. 263, pp. 276–284, Aug. 2017.
[36] K. J. Son, "A nonlinear rheological model for the ultrasonically induced squeeze film effect in variable friction haptic displays," *Korea-Australia Rheol. J.*, vol. 29, no. 3, pp. 219–228, Aug. 2017.
[37] M. Mohiuddin, H.-U. Ko, H.-C. Kim, J. Kim, and S.-Y. Kim, "Transparent and flexible haptic actuator based on cellulose acetate stacked membranes," *Int. J. Precis. Eng. Manuf.*, vol. 16, no. 7, pp. 1479–1485, Jun. 2015.
[38] Q. Liu, K. L. Ford, R. Langley, A. Robinson, and S. Lacour, "Stretchable antennas," in *2012 6th European Conference on Antennas and Propagation (EUCAP)*, 2012, pp. 168–171.
[39] S. J. Chen, C. Fumeaux, P. Talemi, B. Chivers, and R. Shepherd, "Progress in conductive polymer antennas based on free-standing polypyrrole and PEDOT: PSS," in *2016 17th International Symposium on Antenna Technology and Applied Electromagnetics, ANTEM 2016*, 2016, pp. 1–4.
[40] F. Declercq, H. Rogier, and C. Hertleer, "Permittivity and loss tangent characterization for garment antennas based on a new matrix-pencil two-line method," *IEEE Trans. Antennas*

Propag., vol. 56, no. 8 II, pp. 2548–2554, 2008.
[41] W. Deferme, "Paperonics antennas," Diepenbeek, 2019.
[42] P. Bevelacqua, "Dielectric Constant." [Online]. Available: http://www.antenna-theory.com/definitions/dielectric-constant.php. [Accessed: 16-Mar-2020].
[43] P. Bevelacqua, "Radiation Pattern." [Online]. Available: http://www.antenna-theory.com/basics/radpattern.php. [Accessed: 16-Mar-2020].
[44] "Solved: 3-D and 2-D radiation patterns of a Hertzian dipole. In... | Chegg.com." [Online]. Available: https://www.chegg.com/homework-help/3-d-2-d-radiation-patterns-hertzian-dipole-matlab-plot-3-d-p-chapter-12-problem-17me-solution-9780132857949-exc. [Accessed: 30-Mar-2020].
[45] P. Bevelacqua, "Antenna Efficiency." [Online]. Available: http://www.antenna-theory.com/basics/efficiency.php. [Accessed: 16-Mar-2020].
[46] P. Bevelacqua, "S-Parameters for Antennas (S11, S12, ...)." [Online]. Available: http://www.antenna-theory.com/definitions/sparameters.php. [Accessed: 16-Mar-2020].
[47] "How Do You Specify The Bandwidth Of An Antenna? - MobileMark." [Online]. Available: https://www.mobilemark.com/about/faq/how-do-you-specify-the-bandwidth-of-an-antenna/. [Accessed: 18-Apr-2020].
[48] P. Bevelacqua, "VSWR." [Online]. Available: http://www.antenna-theory.com/definitions/vswr.php. [Accessed: 15-Apr-2020].
[49] P. Bevelacqua, "Impedance of an Antenna." [Online]. Available: http://www.antenna-theory.com/basics/impedance.php. [Accessed: 29-Mar-2020].
[50] C. A. Balanis, *Antenna theory : analysis and design*, 4th ed. New Jersey: John Wiley & Sons, Incorporated, 2016.
[51] P. Bevelacqua, "Antenna Theory - Baluns." [Online]. Available: http://www.antenna-theory.com/definitions/balun.php. [Accessed: 16-Mar-2020].
[52] P. Crilly, "The visual dipole - A key to understanding antenna theory," in *Proceedings - Frontiers in Education Conference, FIE*, 2016, vol. 2016-November.
[53] "Do You Remember Rabbit Ears? | Geezer Guff." [Online]. Available: https://geezerguff.com/do-you-remember-rabbit-ears/. [Accessed: 23-Apr-2020].
[54] P. Bevelacqua, "Monopole Antenna." [Online]. Available: http://www.antenna-theory.com/antennas/monopole.php. [Accessed: 29-Mar-2020].
[55] "Mobile Phones Before 2000 : HardwareZone's 10th Anniversary: The 1998 - 1999 Era - HardwareZone.com.sg." [Online]. Available: https://www.hardwarezone.com.sg/feature-hardwarezones-10th-anniversary-1998-1999-era/mobile-phones-2000. [Accessed: 29-Mar-2020].
[56] H. Talleb, S. Faci, D. Lautru, V. F. Hanna, and J. Wiart, "Investigation on an RFID planar coil for a wireless communicative aortic stent," *C. R. Phys.*, vol. 14, pp. 438–446, 2013.
[57] A. Sharif and V. Potdar, "A critical analysis of RFID security protocols," in *Proceedings - International Conference on Advanced Information Networking and Applications, AINA*, 2008, pp. 1357–1362.
[58] "u.fl-ipex-connector-ufl-sma-size-comparison.jpg (JPEG-afbeelding, 1000 × 750 pixels)." [Online]. Available: https://oscarliang.com/ctt/uploads/2016/09/u.fl-ipex-connector-ufl-sma-size-comparison.jpg. [Accessed: 21-Mar-2020].
[59] F. Hirtenfelder, "Effective Antenna Simulations using CST MICROWAVE STUDIO®," 2007, pp. 239–239.
[60] "(PDF) Simulation Comparison between HFSS and CST for Design of Conical Horn Antenna." [Online]. Available: https://www.researchgate.net/publication/277875165_Simulation_Comparison_between_HFSS_and_CST_for_Design_of_Conical_Horn_Antenna. [Accessed: 01-Apr-2020].
[61] S. Koziel and A. Bekasiewicz, *Multi-objective design of antennas using surrogate models*. World Scientific Publishing Co. Pte. Ltd., 2017.
[62] "Accuracy in Simulation with CST STUDIO SUITE 2016 | 2016-01-15 | Microwave Journal." [Online]. Available: https://www.microwavejournal.com/articles/25734-accuracy-in-simulation-with-cst-studio-suite-2016. [Accessed: 01-Apr-2020].

[63] “Automatictriangulation.” [Online]. Available: http://www.visualfea.com/manual-normal/html/4-1-1.htm. [Accessed: 08-Apr-2020].
[64] “Antenna Pattern Display - Sonnet Software.” [Online]. Available: https://www.sonnetsoftware.com/products/sonnet-suites/ef_antpat.html. [Accessed: 01-Apr-2020].
[65] “Wettability - an overview | ScienceDirect Topics.” [Online]. Available: https://www.sciencedirect.com/topics/materials-science/wettability. [Accessed: 04-Apr-2020].
[66] “What is Corona Treatment – By the inventors of Corona.” [Online]. Available: https://www.vetaphone.com/our-offering/corona-treatment/. [Accessed: 04-Apr-2020].
[67] D. Andreescu, C. Eastman, K. Balantrapu, and D. V. Goia, “A simple route for manufacturing highly dispersed silver nanoparticles,” *J. Mater. Res.*, vol. 22, no. 9, pp. 2488–2496, Sep. 2007.
[68] E. Oblike *et al.*, “SCREEN-PRINTED ELECTRICALLY CONDUCTIVE FUNCTIONALITIES IN PAPER SUBSTRATES.”
[69] “(PDF) supporting information for ‘Semi-metallic, Strong and Stretchable Wet-spun Conjugated Polymer Microfibers.’” [Online]. Available: https://www.researchgate.net/publication/279176306_supporting_information_for_Semi-metallic_Strong_and_Stretchable_Wet-spun_Conjugated_Polymer_Microfibers. [Accessed: 09-May-2020].
[70] “BMT Services BMT-NI Blow Moulding Technologies.” [Online]. Available: https://www.bmt-ni.com/services. [Accessed: 24-Mar-2020].
[71] “Siglent SVA1075X 7.5GHz spectrum & vector network analyzer | siglent.eu.” [Online]. Available: https://www.siglent.eu/product/1291825/siglent-sva1075x-7-5ghz-spectrum-vector-network-analyzer. [Accessed: 04-Apr-2020].
[72] “Measuring VSWR and Gain in Wireless Systems | Analog Devices.” [Online]. Available: https://www.analog.com/en/technical-articles/measuring-vswr-and-gain-in-wireless-systems.html. [Accessed: 04-Apr-2020].
[73] “Radiated efficiency: A true measure of antenna performance | EE Times.” [Online]. Available: https://www.eetimes.com/radiated-efficiency-a-true-measure-of-antenna-performance/#. [Accessed: 08-Apr-2020].
[74] “What is an Anechoic Chamber? Find Out How It Works And Why We Use Them.” [Online]. Available: https://antennatestlab.com/antenna-education-tutorials/what-is-an-anechoic-chamber. [Accessed: 08-Apr-2020].
[75] “Van der Pauw Measurements.” [Online]. Available: https://www.microwaves101.com/encyclopedias/van-der-pauw-measurements. [Accessed: 13-May-2020].
[76] BASF, “Thermoplastic Polyurethane elastomers (TPU),” pp. 1–12, 2011.
[77] S. J. Chen *et al.*, “A Compact, Highly Efficient and Flexible Polymer Ultra-Wideband Antenna,” *IEEE Antennas Wirel. Propag. Lett.*, vol. 14, pp. 1207–1210, 2015.
[78] H. J. Qi and M. C. Boyce, “Stress-Strain Behavior of Thermoplastic Polyurethane Stress-Strain Behavior of Thermoplastic,” no. July, pp. 1–51, 2004.
[79] Phoenix Technologies International LLC, “Polyethylene terephthalate key properties,” p. 1, 2008.
[80] “CAMPUSplastics | datasheet Elastollan® C 88 A.” [Online]. Available: https://www.campusplastics.com/campus/en/datasheet/Elastollan®+C+88+A/BASF+PU/59/e77d2e9c/SI?pos=134. [Accessed: 13-May-2020].
[81] P. Bevelacqua, “Antenna-Theory.com - Rectangular Microstrip (Patch) Antenna - Design and Tradeoffs.” [Online]. Available: http://www.antenna-theory.com/antennas/patches/patch4.php. [Accessed: 13-May-2020].